Republic of Iraq
Ministry of Higher Education and Scientific Research
University of Babylon
College of Materials Engineering
Department of Ceramics and Building Materials

Improving the Thermal Properties of Solar Collector Using Ceramic Coating Materials

A Thesis

Submitted to the Department of ceramic and building Materials at College of Materials Engineering / University of Babylon in Partial Fulfillment of the Requirement for the Master Degree in Materials Engineering / Ceramic

By

Ahmed Zeki Hasheem Hamazah

(B.Sc. In Materials Engineering) 2002.

Supervised by

Prof. Dr. Elham Abd Al-Majeed

prof. Dr. Hayder Kraidi Rashid

2022A.D

1444H

بسم الله الرحمن الرحيم

(ولقد اتينا داوود وسليمان علما وقالا الحمد لله الذي فضلنا على كثير من عباده المؤمنين) .

صدق الله العلي العظيم.

سورة النمل اية ١٥

Supervisors Certification

We certify that this thesis, entitled (***Improving the Thermal Properties of Solar Collector Using Ceramic Coating Materials.*)** was prepared by the student (Ahmed Zeki Hasheem), under our supervision, in partial fulfillment of the requirements for the degree of Sciences in Materials Engineering / Ceramic , at the Department of Materials Engineering / Ceramic.

Signature

Supervisor

Prof. Dr. Elham Abd Al-Majeed

Date / / 2022

Signature

Supervisors

prof. Dr. Hayder Kraidi Rashid

Date / / 2022

Signature

Prof.Dr. Mohsin Abbas Aswad

Head of ceramic and building material department

Date / / 2022

Certification of the Examining Committee

We certify that we have read the thesis entitled " ***Improving the Thermal Properties of Solar Collector Using Ceramic Coating Materials..***", and as an examining committee, examined the student (**Ahmed Zeki Hasheem**), in its contents and that in what is connected with it, and that in our opinion it meets the standard of a thesis for the degree of Sciences in Materials Engineering / Ceramic.

Signature
Prof. Dr. Mohsin Abbas Aswad
University of Babylon
Date : / / 2022
Chairman

Signature
Dr. Sabah. M. Thahab
(Member)
Date / / 2022

Signature
Dr.Aseel Hadi Hamazah
(Member)
Date / / 2022

Signature
Prof. Dr. Elham Abd Al-Majeed
(Supervisor)
Date / / 2022

Signature
prof. Dr. Hayder Kraidi Rashid
(Supervisor)
Date / / 2022

Signature
Prof.Dr. Mohsin Abbas Aswad
Head of ceramic and building material department
Date / / 2022

Signature
Prof.Dr.Imad Ali Disher
Dean of material engineering collage
Date / / 2022

DEDICATION

TO THE SOUL OF MY DEAR FATHER....MAY GOD HAVE MERCY ON HIM.

TO MY DEAR MOTHER..... GOD GRANT HER HEALTH AND WELLNESS.

TO MY FAMILY AND BROTHERS...

I DEDICATE MY SIMPLE EFFORT.

Acknowledgments

Praise and thanks be to God first and foremost.

I would like to extend my sincere thanks, appreciation, and thanks to my supervisor, Prof. Dr. Elham Abd Al Majeed, for her efforts and for following up on my work in my thesis step by step, providing all scientific guidance and solutions and her continuous encouragement to complete the research of a thesis of the highest scientific value.

I would like to express my pride and appreciation to my supervisor, Professor Dr. Haider Kreidi Rasheed, who was prejudiced against himself and supported me in providing treatments and solutions to the problems I faced in preparing the thesis.

I would also like to thank the University of Babylon and the College of Materials Engineering for giving me the opportunity to complete my master's study. I would also like to express my thanks and appreciation to the professors of the Department of Ceramics and Building Materials Engineering and the staff of the laboratories of the Department of Ceramics and Building Materials Engineering and the laboratories of the Polymers and Petrochemicals Engineering Department for their assistance and cooperation with me. Finally, I would like to thank all of my study helper friends for their support in completing this letter.

Abstract

Saving energy and reducing pollution one of the most important goals of the developed world through the use of alternative energy sources for traditional (fossil) fuels, which are considered a cause of pollution when consumed. Solar energy, as a clean and renewable source of energy, one of the most important solutions and remedies for environmental pollution and increasing production costs.

One of the devices that exploit solar energy is flat plate solar collectors (FPSCs). It consists of the transparent cover, absorbent plate, heat exchanger tube and frame.

The absorber plate is made of aluminum metal plate with thickness (0.5mm), as well as the pipe of the heat exchanger from aluminum metal with thickness (1.3mm). Using the method of (spray air brush) in (FPSC) coating, which is one of the simplest and cheapest methods of spraying.

In this research, the graphite was used with percentages of copper powder as a coating to increase the thermal conductivity. From the thermal conductivity test showed when using graphite as a coating only as in sample (G1), the thermal conductivity increased about (60%), and when adding percentage of copper powder about (4%) with graphite as in sample (G5); it is increased to about (80%). In the case of insulating coatings, Mullite and Titanium dioxide were used, where using a percentage of Mullite (0.75%) with Titanium dioxide (0.25%) as in sample (S2) increased the insulation to (48%), while by increasing the percentage of Mullite to (3.75%) and Titanium dioxide (1.25%) as in sample (S4), the percentage of insulation increased to (57%).

The adhesion strength of the sample coated to increase the thermal conductivity (G1) was (19.06 MPa) containing only graphite, while the adhesion strength of the sample (G5) was (19.82 MPa), which contained graphite and percentage of copper powder while the adhesion strength of the sample coated to increase the thermal insulation (S1) (coated polystyrene only) was (17.31 MPa), which contains polystyrene material only. While the adhesion strength of the sample (S4) was (17.73 MPa), which contains 5% coating materials (Mullite and Titanium dioxide).

The achieved porosity percentage from the measurement of the cross-sectional porosity of the conduction coating is (4.62 %), while the porosity ratio in the cross-section of the insulation samples coating is (68.28 %).

The average coating thickness of the conduction samples is (405 μm), while the average thickness of the insulation samples is (715 μm).

The numerical analysis validates the improvements in thermal conductivity that increase the efficiency of the solar collector using ANSYS 16.1 software to simulate the 3D geometry of fluid flow through heat exchanger tubes.

Building a mathematical model by (ANSYS-FLUENT 16.1) using the semicircular cross section instead of the circular section of the heat exchanger tube and placing it in real dimensions to simulate the transfer of heat from the absorber plate to the heat exchanger tube by solar radiation via fixing the latitude and longitude of the Babylon city site with the number of hours (13) per day.

Simulation results ANSYS16.1 software showed the inlet and outlet temperature difference of the heat exchanger tube of the flat plate solar collector without coating was (23˚C) while after coating with ceramic materials the inlet and outlet temperature difference was (57˚C).

Contents

Chapter Three

Experimental Part and Numerical Analysis

Chapter Four

The Results and the Discussion

List of Figures

List of Tables

List of Abbreviations

Symbol	Definition
Al_2O_3	Alumina
ASHRAE	American Society of Heating, Refrigerating, and Air-Conditioning Engineers
Al	Aluminum
$3Al_2O_3.2SiO_2$	Mullite
Acheson	Primary synthetic graphite >100 nm
AFM	Atomic force microscope
Ar	Argon gas
ABRO	Symbol for a commercial black spray coat product
CMC	Carboxymethyl cellulose
Cu	Copper
CVD	Chemical Vapor Deposition
C	Carbon , Graphite
Cr	Chrome
CeO_2	Cerium oxide
COP	Charging and Discharging Operation Mode
CNT	Carbon nano tube
CG	Cryptocrystalline graphite
CB	Carbon black
CTE	Coefficient of Thermal expansion
CFD	Computational Fluid Dynamic.
DMF	Dimethyle floramide
DDW	Double distilled water
DC	Direct current
EPS	Expanded polystyrene
EPD	Electrophoretic Deposition
FTIR	Fourier transform infrared spectrophotometer
FPSCs	Flat plate solar collectors
FEM	Finite Element Method
FDM	Finite Difference Method
FVM	Finite Volume Method
Fe	Iron
f-GNPs	functionalized carbon nanoplatelets
GPPS	General purpose polystyrene
HVOF	High-Velocity Oxy-Fuel method
HGMs	Hollow glass microspheres

IPS or HIPS	High impact polystyrene
KIc	Fracture toughness
$La_2Zr_2O_7$	lanthianum zirconate
MAO	Micro-Arc Oxidation
Mo	Molybdenum
MWCNTs	Multiwall carbon nanotubes
Mn	Manganese
Ni	Nickel
NPDS	NanoParticle Deposition System
N_2	Nitrogen
NPs	Nanoparticles
O	Oxygen
Ps	Polystyrene
PVD	Physical Vapor Deposition
PAA	Poly(acrylic acide)
PEMah	poly(ethylene alt maleice anhydride
PvPA	poly(vinyl phosphonice acid)
PMMA	Poly(methyl methacrylate)
PDEs	Partial Differential Equations
R.T	Room temperature
R-value	Thermal resistance
RGC	Primary synthetic graphite 40 nm
Si	Silicon
SiO_2	Silica
SEM	Scanning electron microscope
TC	Thermal conductivity
Ti	Titanium
TiO_2	Titanium dioxide
TBC	Thermal barrier coating
UGF	ultrathin graphite foams
UV	Ultra-violent
XPS	X-ray Photoelectron Spectroscopy
XRD	X-Ray Diffraction
Yb_2SiO_5	ytterbium-silicate
YSZ	yttriua stabilized zirconia
ZrO2	Zirconia

List of Symbols

Symbols	Definitions
ºC	degrees Celsius
Cp	Specific heat (J/kg K)
c	Light velocity
cm^3	Cubic centimeter
E	Energy
h	Blanck constant
K	Thermal conductivity symbol
k	Kelvin
L/m	liters per minute
MPa	Mica Pascal
mbar	Millibar
$\dot{m}$	air mass flow rate (kg/s)
Nu	Nusselt number
Pr	Prandtl number
Re	Reynolds number

Greek Symbols

Symbols	Definitions
θ	The diffraction angle
ʎ	Wavelength
μ	Viscosity
μm	Micrometer
ρ	Density
v	Frequency
η	efficiency

CHAPTER ONE

INTRODUCTION

Chapter one

Introduction

1.1 overview

Renewable energies, which include solar and wind energy, are available and cheap energy sources and do not cause environmental damage. Renewable energies have grown rapidly around the world because they are the cleanest, cheapest, and available energy sources. Solar energy has been used in various fields such as heating, chemical treatment and mechanical applications. A solar collector is a device that transforms solar energy into thermal energy by absorbing sun rays that are transferred through a fluid. The efficiency of the solar collector depends on the energy converted through optical properties and thermal losses. The efficiency of solar rays retention depends on the type of collector used[1]. All types of solar collectors are designed to absorb short wavelengths of solar radiation, as they receive solar radiation ranging from (0.3-2) μm, but it maintains thermal wavelengths from (2-10) μm, using the warming effect, radiant energy is prevented from exiting and is then delivered either direct or indirect toward a hot water tank[2] .

The heat transfer is due to the conduction, convection and radiation processes with the environment; also depends on the local sun radiation conditions and the solar collector optical features [3]. Solar collector used in water heating, and among the most important and simplest types is flat plate solar collector (FPSC) used in buildings, swimming pools, and factories, in the exploitation of solar energy to heat water. FPSC consists of transparency cover, absorber plate, heat exchanger pipes, and frames (housing)[4]. Using various strategies, the researchers are working to enhance the achievement of the solar flat plate collectors. One of these strategies uses selective coatings to improve absorptivity, thermal conductivity, and minimize reflection by putting various coatings on absorber plate from the side exposed to sunbeams, such as selective ceramic coatings [1] and antireflection coatings are applied[5]. On the other side of the absorber plate,

ceramic coating materials boost thermal insulation and lower emissivity, reducing heat loss and increasing collector performance efficiency. Selective coatings considered from cheaper and easier methods to improve collector efficiency [1][6]. Using cermet which consists of a mixture of ceramic and metal as a coating material used to increase the efficiency of the solar collector [6]. The best selective ceramic coating materials that used to increase thermal conductivity are carbon family (graphene, carbon nanotube, graphite) [7][8],aluminum nitride and boron nitride [9].The use of insulating materials that contain large proportions of gaps and pores leads to a very large increase in insulation, as is the use of porous Mullite, the thermal conductivity value reaches to (0.09 w/m.k) [10]. The best selective coating ceramic materials that used to increase thermal insulation are (Al_2O_3, $3Al_2O_3.2SiO_2$, SiO_2, ZrO_2, YSZ, TiO_2, CeO_2, $La_2Zr_2O_7$ ...etc.) [11][12]. The filler formation, alignment, scattering, and interlayer thermal resistance all affect the coating mixture's thermal conductivity [7]. The substrate properties that used as absorber plate most common important factors that are effect on efficiency the solar collector such as thermal absorption, and heat storage [13].Substrate hardness effects on the extent of fragmentation and also interlayer separation in deposition graphite film [14]. When the substrate's surface roughness is increased, heat transfer and thermal absorption are improved. [15].The substrate preparation must be done at high level to increase the surface roughness to ensure the higher adhesion strength between the coating layers and substrate material [16].The coating method determines the coating surface texture such as coating roughness and thickness [17][4].

The placement of the heat exchanger pipe shape has an impact on the improvement of the solar collector's performance, as does the use of the spiral design leads to saving materials , increasing the thermal efficiency and the efficiency of exergy over the conventional design[18].

Most researchers tend to use simulation programs for engineering analysis and study the effect of changes in new designs for ease of use and accuracy of their work and to give detailed information on the distribution of loads in areas affected by temperature, pressure, fluid flow velocity…etc., through the introduction of sufficient data and experimental results[19]. One of the most important programs used in the field of thermal analysis is the ANSYS software[19]. Mathematical equations are solved with defining nodes by making a mesh of the drawn geometry[20][21]. It shows the effect of each surrounding group of nodes on an

element that is a small part of the geometry and from a large group of elements shows the total effect of the distribution of temperatures or the pressure[20].

1.2 Statement of the Problem

Electric energy is constantly and massively consumed, which is generated from fossil fuels, that produce toxic emissions to the environment, as it is vulnerable to exhaustion and requires high extraction costs, for the purpose of reducing consumption electric energy in the field of water heating for domestic uses, swimming pools and industrial fields used Flat Plate Solar Collectors (FPSCs) which works on solar energy, that is one of the most important renewable and clean energies and for the purpose of making the most of solar energy by raising the performance efficiency of (FPSCs) with using ceramic coatings to increase thermal conductivity and raise absorption from the side facing to the sun, while from the opposite side, using insulating ceramic coatings to reduce the loss of heat energy gained from sunlight, and as a result, raising the efficiency of (FPSCs) via increasing the temperature gradient between the input and output for the heat exchanger tube. In addition to modifying the cross-section of the heat exchanger tube from the traditional circular shape to the semicircle shape for the purpose of increasing the contact area between the absorber plate and the heat exchanger tube of the solar collector and generating turbulent flow which results in an increase in heat energy transfer and, in the end, an increase in efficiency (FPSCs).

1.3 Research Aims

The thesis presents experimental study and numerical analysis for new ceramic coating materials used to increase performance flat plate solar collector, is summarized in following:

1- Exploitation of solar energy which is one of the cheapest renewable energy sources; it is produced to save consumption of fossil energy sources, that are expensive and difficult to produce.

2- Reducing the cost of producing a solar collector by using cheap and available ceramic materials as well as using simple coating methods to manufacture a solar collector with high heating efficiency.

3- Ensuring the continuity of water heating in domestic uses and avoiding problems and interruptions of electrical power. Additionally avoiding the use of

electric energy produced from power plants that run on fossil fuels, leads to a reduction in toxic emissions and pollution resulting from burning fuels.

4- Increasing the performance of solar thermal collector by increase thermal conductivity and thermal insulation due to using selective ceramic coatings and manufacturing flat plate solar collector by using simple design and cheapest ceramic materials coatings, furthermore studying the effect of adding new ceramic materials on thermal conductivity

5- Understanding and analyzing the relationship between heat transfer behavior and properties of ceramic materials used as coatings on absorber plate.

6- Optimizing the dimensions of the heat exchanger tube and modifying the design of its cross-sectional area to give the highest thermal transfer efficiency of the fluid running in the tube with the absorber plate by using ANSYS (16.1) software to simulate all results via comparing the temperature distribution.

1.4 Thesis Structure

The thesis is divided into five chapters explaining the efforts made in the thesis and the results obtained and conclusions.

The first chapter includes the introduction, the statement of the problem and research aims. The second chapter shows the theoretical field in the thesis of classifications of solar collectors, methods for their development, materials used and the method of coating to improve the efficiency of the performance of the flat plate solar collector. The second chapter also included previous research studies in developing the performance of solar collectors using coatings, research studies on ceramic coating materials used to improve thermal conduction and insulation, coating methods and studies on the use of numerical analyzes of the obtained results, and finally the Summary.

The third chapter included the experimental work by containing the work plan , the definition of the materials used, methods and proportions of mixing, the method of preparing the surfaces of the samples before coating and the methods of work of the examination devices for the tests used. The third chapter also contains numerical calculations and equations used in thermal analyzes obtained from the results of experimental work.

The fourth chapter included explanations and practical analyzes of the results of the examinations carried out in the research. Initially interpret the results of examinations of materials used for coating prior to mixing. As well as the

interpretation of all the tests carried out on the mixture of coatings or layer of coat, which include: structural properties tests (XRD, SEM, AFM and FTIR), Thermal properties test (thermal conductivity test), Mechanical properties test (adhesion strength), Physical properties tests (density, viscosity, porosity, coating thickness and U.V). The fourth chapter also includes simulating the results through the (ANSYS 16.1) software and representing the reigns of concentration of the obtained heat. Conclusions, recommendations and suggestions are included in chapter Five.

CHAPTER TWO

THEORITICAL PART

Chapter Two
The Theoretical Part

2.1 Introduction

The second chapter discusses several theoretical facets of the current investigation, including the following: definition solar collectors and classification, mechanism and definition of thermal conductivity, description and mechanism of thermal insulation, materials used for increase thermal conductivity, materials used for increase thermal insulation, the definition of coating process, spray coating (spray airbrush), substrate material used as absorber plate, numerical analysis introduction and literature reviews.

2.2. Solar Collector

There are multiple classifications of solar collectors [1][2],one of these classifications is in the figure (2.1).

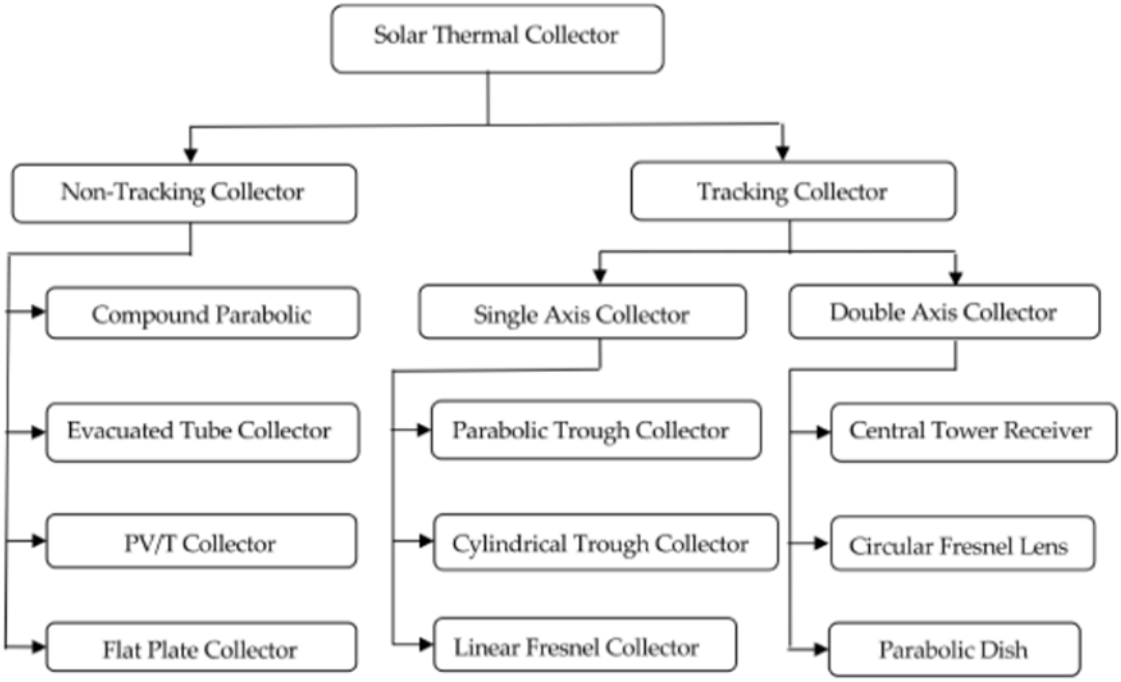

Figure (2 .1) Types the solar collectors by tracking arrangements [1].

Flat plate solar collector (FPSC) is simplest design and the most widespread among the types of solar collectors. (FPSC) consist of: transparency cover, the

absorber plate, heat exchanger tubes and frame (housing) [1][2], illustrated in figure (2.2).

- **Transparent Cover:** Transparent cover functions as an infrared (thermal) heat trap. As a result, it minimizes radiation losses and convectional heat transfer to the atmosphere. The cover, in conjunction with the frame, protects the absorber plate from inclement weather. (Glazing materials) such as (glass) must have a few irons (Fe) content and is resistant to UV radiation. Among the several classes of tempered plate glass that be contain of low-iron glass has the highest transmission and the smallest reflection of sun radiation [2].
- **Absorber Plate:** The main part of the solar flat plate collector. It absorbs the sun radiation and transform to thermal energy that transferred by work fluid inside the heat exchanger tubes. Absorber plate can developing by applied selective coatings to increasing solar collector efficiency[1]. The most common materials that made the absorber plate are copper, aluminum, iron, and stainless steel[13].
- **Heat Exchanger Tubes:** The heat exchanger tubes work to transfer the work fluid that role to loading obtained heat and conducted to storage tank. The materials that made the tubes are copper, aluminum and stainless steel[22].
- **Frame:** All components the solar collector are encased in the frame (housing). The frame plays as protector for the absorber plate and other parts for the solar collector[4].

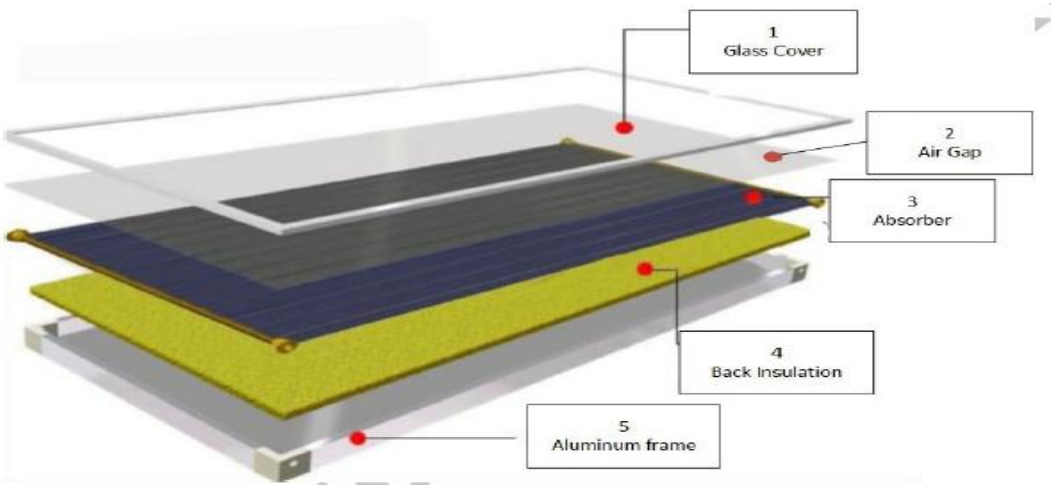

Figure (2.2) FPSC sketch parts and layers [4].

Improving performance and increasing the efficiency of the flat plate solar collector by the one the methods in figure (2.3)[1].

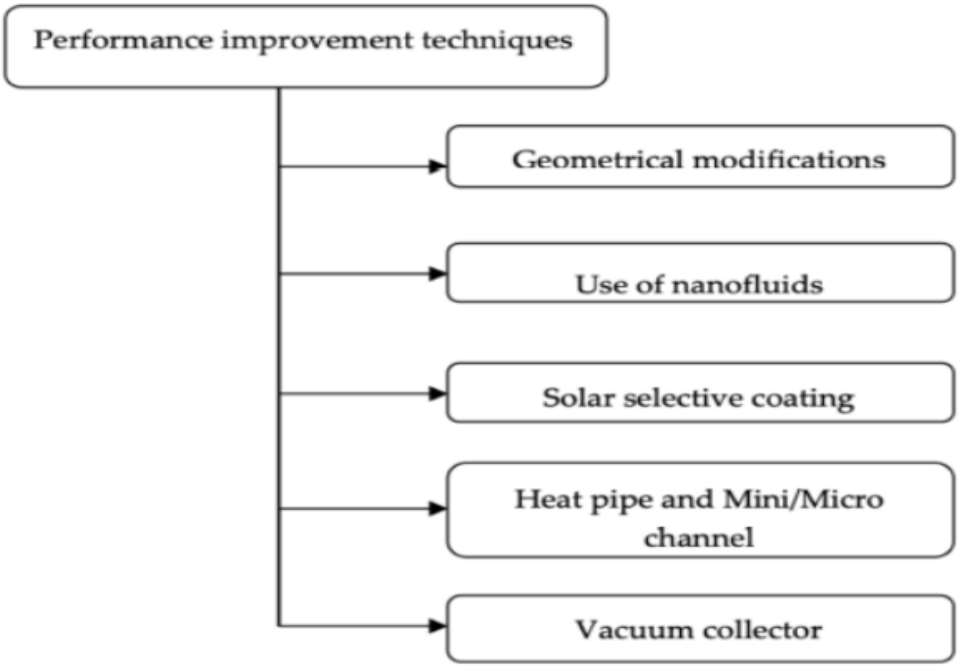

Figure (2.3) Performance enhancement methods of FPSCs [1].

2.3 Definition of Thermal Conductivity

According to the definition of thermal conductivity, it is the time rate of steady state heat flow (W) through a unit area of homogeneous material that is (1m) thick in direction perpendicular to isothermal planes, caused by a unit (1k) temperature difference from across specimen. A material's capabilities to transfer heat are determined by its thermal conductivity [23].

2.3.1 Description Thermal Conduction Mechanism

Heat is transferred from areas with high temperatures to areas with low temperatures according to the second law of thermodynamics. Thermal conductivity is one of the properties of a material that is influenced by elements such as: (size, thickness, aspect ratio, alignment, and ambient temperature)[7]. Thermal conductivity is measured in watts per meter kelvin ($w.m^{-1}.k^{-1}$) and is indicated by the letter K. The mobility of (electrons) and (phonons) produces thermal conductivity in solid materials. In metals, electrons govern thermal conduction, whereas phonons control heat conduction in polymer composites and ceramics. A (phonon) is described as quantized lattice vibrational energy that may be used to achieve heat diffusion within materials by vibrating the lattice[7]. The dispersion of phonons causes a reduction in thermal conductivity. Scattering of

phonons, which can be generated by defects, impurities, or pores, includes scattering between phonons and scattering among phonons and interfaces. When crystallinity is increased, the defects and internal interfaces are reduced resulting in an increase in thermal conductivity because phonon scattering is reduced. Graphene, graphite, carbon nanotubes, diamonds, and boron nitride particles provide straight pathways as the mechanism for heat conductivity in crystalline particles[7].

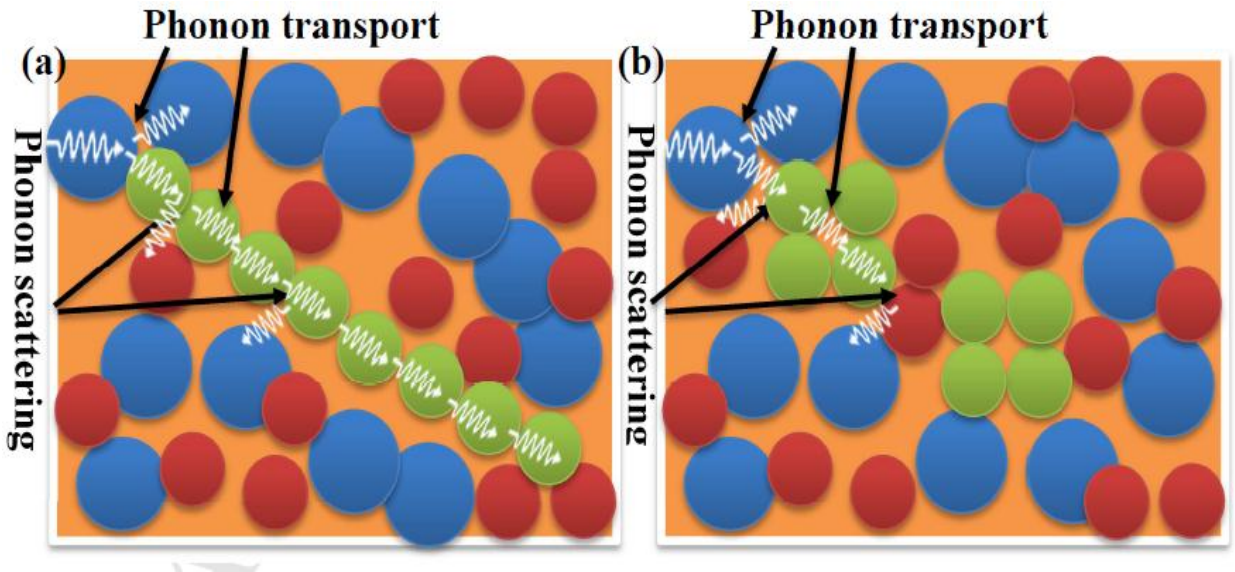

Figure (2.4) (a) Thermal conduction mechanism in crystalline filler/polymer composites with a continuous filler network, and (b) thermal conduction mechanism in crystalline filler/polymer composites with a discontinuous filler network. The green balls represent crystalline filler; the others represent polymer atoms[7].

2.4 Definition Thermal Insulation

Thermal insulation is a term that refers to a material or combination of materials used to slow the flow of heat into or out of a region via conduction, convection, or radiation [24].It is a highly efficient method of lowering the amount of energy used to heat and cool buildings. The resistance to heat transfer (impedance) engendered by limiting conduction, convection, and radiation is described by thermal resistance (R-Value). It is decided by the heat transfer, width, and density of the material. Thermal resistance, R-value is expressed in (m^2.k/w) [24].

2.4.1 Description Thermal Insulation Mechanism

Fine pores in thermal insulating materials reduce heat transfer performance via stopping air from flowing, resulting in heat flow resistance. In other words, the heat resistance is given by the material's entrapped air instead of the material directly [24].

When temperature variations are little, creating small pores (closed pores) inside thermal insulating material lowers the effects of radiation. This arrangement causes infrared radiation routes to be broken into small gaps, as well as the insulation material absorbing or scattering long waves. Conduction, on the other hand, increases when density rises, and indicates that cell size reduces [24].

Generally, air-based insulation materials cannot surpass the R-value of constant air. As a result, plastic foams like (polystyrene and polyurethane) use a gas heavy than air, like (fluorocarbon), to fill the insulation pockets instead of air, resulting in a higher (R-value). As a result of the interaction of the three types of heat transfer, the effectiveness of insulation materials with thermal conductivity can really be evaluated (convection, conduction, and radiation) [24].

2.5 The Used Materials

2.5.1 Materials Used for Increase Thermal Conductivity

2.5.1.1 Graphite

Graphite is a ceramic material produced from a coke and pitch mixtures that have been created and heated to develop a graphite crystal structure[25]. Graphite material is frequently used as a (solid lubricant) to reduce wear and abrasion, but it may additionally scattered in water and organic solvents to form a fluid lubricant. Graphite material is a soft, smooth material that is non-flammable and non-toxic. It is also inert in ambient air and has a low friction. It has a melting temperature of (3800) ˚C, and a thermal conductivity approximately (1500) w⁄m.k [26].

Graphite crystallizes in two phases: (a) hexagonal and (b) rhombohedral. In-plane bonds are completely covalent, whereas inter-planar bonds are weak van der Waals [26]. The properties of the resulting graphite are strongly dependent on the details of the structure. (Cryptocrystalline graphite) (CG) with (carbon black) (CB) have identical in elemental composition, with carbon as the predominant component. CG was found to have a layered graphitic structure distinct from the basic spherical particles found in CB [27]. Graphite possesses both metal-like characteristics including thermal and electrical conductivity as well as non-metal

characteristics including chemical stability, high thermal resistance, as well as lubricity [26]. Graphite material is composed of polycrystalline particles or granules, with very few exceptions, despite of whether it is artificial or natural. That is to say, every particle is composed of a large number of individual crystals. Natural flake graphite has a preferred orientation, but manufactured graphite has a more random orientation [26][28]. Parallel sheets of hexagonal rings can then be used to characterize the crystalline structure of graphite figure (2.5). Most of the layers are arranged in a hexagonal structure using the stacking order ABAB. ABCABC is the layer order of a rhombohedral shape. The figure (2.6) illustrates classification of graphite.

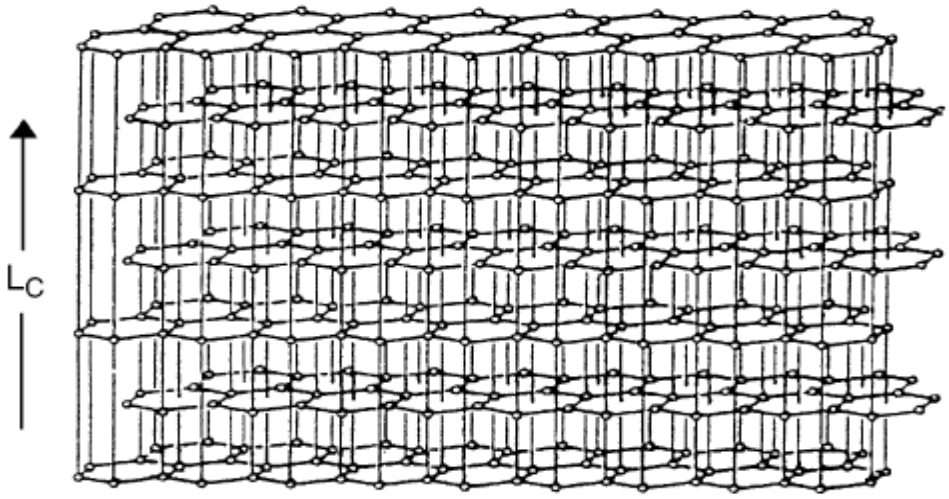

Figure (2.5) Graphite material has a crystalline structure., (hexagonal) shape with the slab series (ABAB) [28].

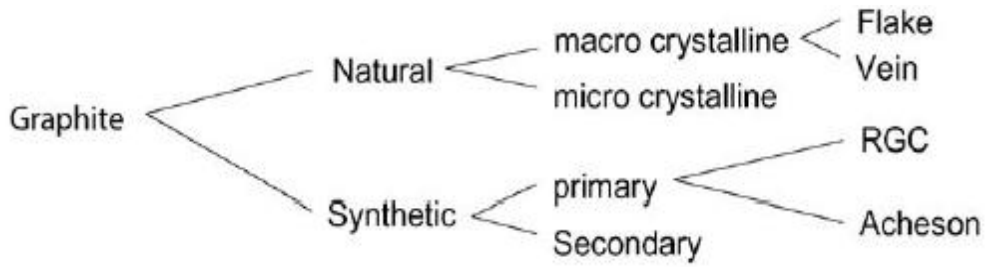

Classification of graphites.

Figure (2.6) shows classification the graphite material[28].

2.5.1.2 Carboxymethyl Cellulose (CMC)

Carboxymethyl Cellulose is Cellulose derivatives in aqueous solutions are mainly used in applications that exploit for their specific properties as thickeners, binding agents, emulsifiers and stabilizers [29]. (CMC) is utilized as a coating agent in the textile business, as well as in resin emulsion paints, adhesives, and printing inks, as well as in coating colors for the pulp and paper sector[30][31].

The repeating units are connected bonds. At the molecular level, the major difference between CMC and cellulose is only some anionic carboxymethyl groups (i.e., –CH2COOH) in the CMC structure that replaces the hydrogen atoms from some hydroxyl groups present in the pristine cellulose infrastructure figure (2.7) [30]. CMC is an excellent material for enhancing viscosity, regulating mud fluid loss, and ensuring suitable flow characteristics at elevated temperatures, salinity, and pressure. CMC is a cellulose byproduct having a wide range of applications in a variety of industries. Preliminary testing indicated that preparing (CMC) solutions required the least amount of time possible to completely dissolve the (CMC) powder. This time period is dependent on the concentration of the CMC and the temperature. Exceptionally, the solutions with high (CMC) concentrations, ranging from (4 % to 7 %) by weight, were created using water heated to (50˚C) [30][31].

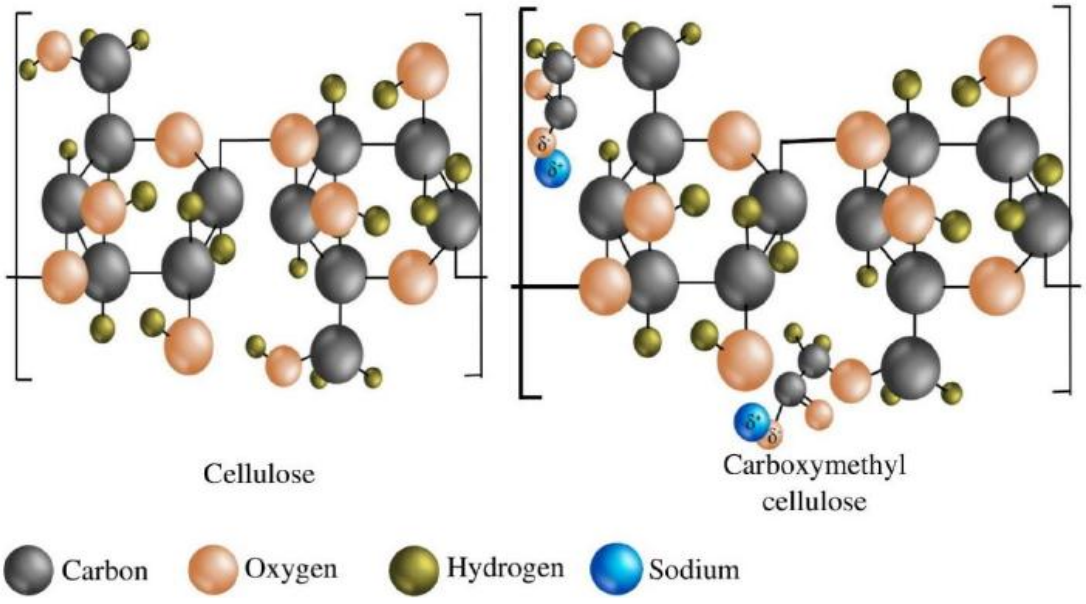

Figure (2.7) The primary structural distinction among cellulose and carboxymethyl cellulose (CMC)[30].

2.5.1.3 Copper Powder (Cu)

Copper metal has a red hue and a cubic crystalline structure that is centered on the face. It has a wonderful reddish tint because of its band gap, which reveals red and orange light while absorbing other visible spectrum frequency range. It is ductile and malleable, as well as an outstanding heat and electricity conductor. Copper metal has a density of approximately (8.9) g/cm³ at (20) °C, a melting point of (1083 ˚C), a thermal conductivity of (400) w⁄m.k, and a specific heat of 385 J/kg.k [2] . It is discovered that mixing metal powders significantly increases the deposition efficiency of the component powders. The inclusion of copper and zinc resulted in significantly increased deposition efficiencies[33]. The copper powder that added to mixture of the coating increase thermal conductivity, adhesion strength, improving stability and structure the mixture coatings [33].

Copper–graphene composites produced enhancement the hardness and thermal conductivity [34].

2.5.1.4 Polyester Resin

A covalently bonded polymer with a chain structure known as polyester resin is a (thermosetting) polymer which is frequently used like binders and topcoat resins for fibrous reinforcing agent in a wide range of applications, from (ships) to (brake linings). In order to create (thermosetting) composite materials, it is combined with other materials [35][36].

The properties of polyester resin are[37]:

1. Environment resistance.
2. Ultra-violet resistance.
3. Impact resistance and strong.
4. Adhesion strength.
5. Light weight.
6. Cheap and available.

Polyester resin is used as a liquid intermediate in conjunction with hardeners or catalysts to cure and obtain the finished product.

2.6.2 Materials Used for Increase Thermal Insulation

2.6.2.1 Mullite $3Al_2O_3.2SiO_2$

Mullite is an aluminosilicate with exceptional physical properties, making it a valuable ceramic material [38].

Mullite is often used in refractory applications but regarded as an important material for both conventional and modern ceramics relatively good mechanical and heat characteristics. Mullite is a common component of traditional ceramic products because clay and silica are frequently used as starting materials [39].

Mullite seems to have a lower thermal conductivity and thermal expansion coefficient, higher creep resistance, higher-heating resistance, and excellent chemical stability. Its configuration governed by the manner of mixing (alumina and silica-containing) materials and the temperature at which the reaction results in the creation of Mullite[40].

Mullite has been utilized in the metalworking industry for roofs of electric furnaces and hot metal mixers. It is used in the glass industry in the construction of molten glass tanks, as well as in glass drawing chambers. Table (2.1) summarizes various Mullite features[40].

Table 2.1 Traditional Mullite properties [40].

Property	Value
Density g/cm³	(3.16 - 3.22)
(Hardness)(GPa) at R.T	(13 - 15)
(Fracture toughness KIc) (MPa.m½)	(1.5 - 3)
(Young modulus) (Gpa)	(140 - 250)
(Bending strength) (MPa)	(150 - 500)
(Thermal expansion coefficient) (k^{-1}) at (300-900 ˚C)	(3.1 - $4.1*10^{-6}$)
(Thermal conductivity) (w/m.k) at (100 ˚C)	(6.07)

The producing coating from Mullite for insulation purposes must the coating structure contain on high percentages of porosity that result to raising thermal insulation[41]. Porous Mullite ceramic has lower thermal conductivity (as low as 0.05 w⁄m.k). The porosity for porous Mullite in the range (73% to 86% vol) by controlled on the solid loading in the suspension and sintering temperature[10].

Mullite and Sillimanite both have crystal structures that are composed of chains of distorted Al–O octahedra that share edges and run parallel to the c–axis at the corners and centers of each unit cell. SiO and AlO corner-sharing tetrahedra link the chains together. A mixture of solid solution compounds known as Mullite ranges in constituents from alumina-rich (2Al2O3.SiO2) (2:1 Mullite) to silica-rich (3Al2O3.2SiO2) (3:2 Mullite). The crystal structure of Mullite is depicted in figure (2.8) [38].

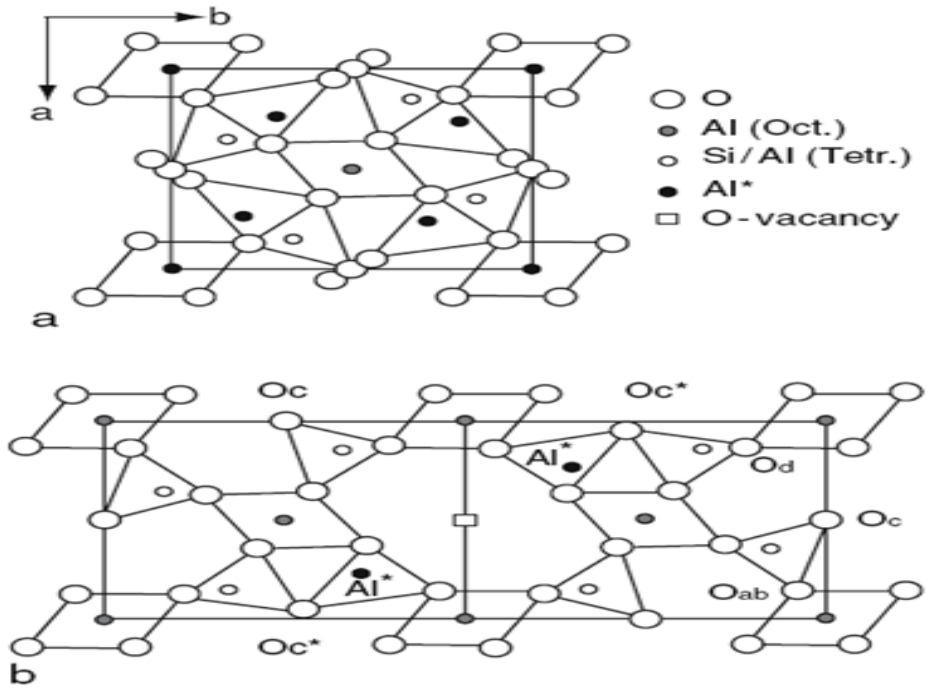

Figure (2.8) Mullite configuration (a) Typical structure. (b) Atomic displacements in the vicinity of an oxygen vacancy [38].

The composite materials from Mullite and other ceramic materials to improve the microstructure, mechanical properties, and thermal insulation such as Ytterbium-Silicate-Mullite composites [42].

Figure (2.9) Illustrates the phase diagram of Mullite, which has a limited phase field[38].

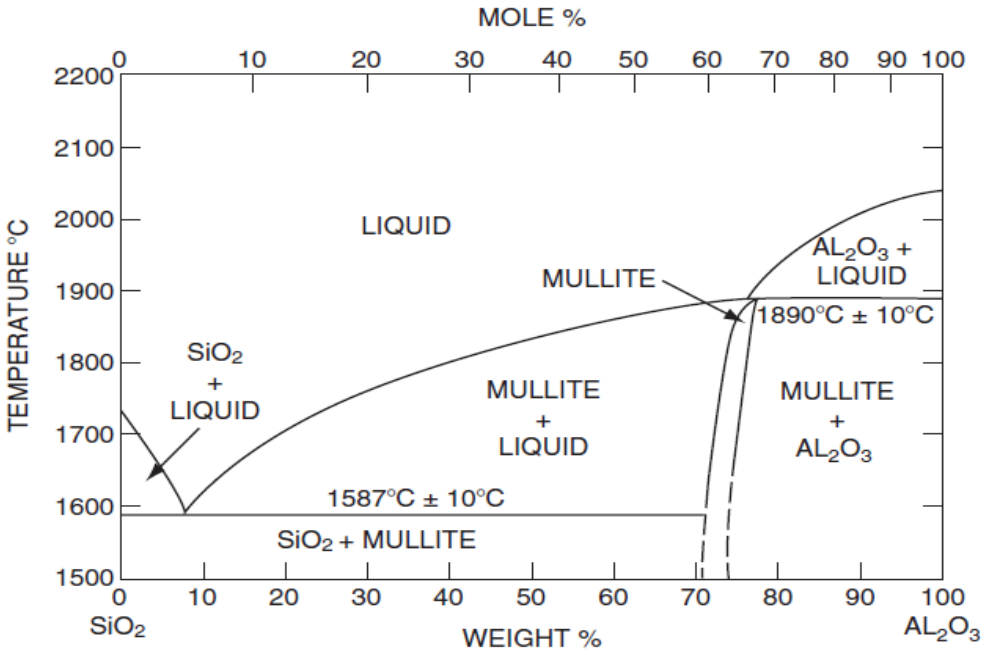

Figure (2.9) Mullite Phase Diagram [38].

2.6.2.2 Titanium Dioxide (TiO2)

Titanium dioxide, alternatively, referred to as titania, is a found in nature titanium oxide. It is a versatile material that can be used for a variety of purposes [43]. (TiO2) is being used as a photocatalyst relatively low cost, non-toxicity, and chemical inertness[43][44]. TiO2 is used in many industry sectors, such as airplane, sporting events, paint (to impart a glossy finish and rich intensity of color and as a replacement for metal lead), cosmetics (UV) safety in sunscreens and a group of industries [45]. Due to its sterilizing and anti-fouling properties, (TiO2) is utilized to cover glazing. Through a vigorous catalytic reaction, the (TiO2) will degrade and destroy organic dirt. Additionally, it is hydrophilic, allowing water to flow uniformly across its surfaces [46][47]. Titanium oxide nanoparticles are employed as a white pigment for outstanding reflective coatings or as a sterilizing agent in paints, cements, and windows. Titanium dioxide utilizes intense photocatalytic processes to degrade organic pollutants, volatile organic compounds, and bacterial membranes, thereby lowering air pollution when applied to outdoor surfaces [44][48] [30].

The titanium dioxide polymorphs are as follows[49][50].

1- Rutile structure consists of a tetragonal mineral with titanium (Ti) atoms in its corners and center. Every titanium atom is surrounding via an octahedron of oxygen atoms, and every oxygen atom is encircled by an equilateral triangle of titanium atoms. The unit cell of rutile is depicted in Figure (2.10a).

2- Anatase is always found in small, isolated, and well-developed crystals and is composed of a tetragonal mineral with an octahedral habit. Its increased photoactivity, the anatase polymorph of TiO2 looks to be an even more effective catalyst than rutile. The unit cell of anatase is seen in Fig. (2.10b).

3-Brookite is an orthorhombic mineral with tabular, elongated, and striated crystals that run parallel to their length. Brookite, like all orthorhombic minerals, is doubly refracting. The refractive indices are extremely high, exceeding (2.5) which is higher than diamond's value of (2.42). The unit cell of brookite is depicted in Figure (2.10c). Table (2.2) shows the properties of various polymorphs TiO2.

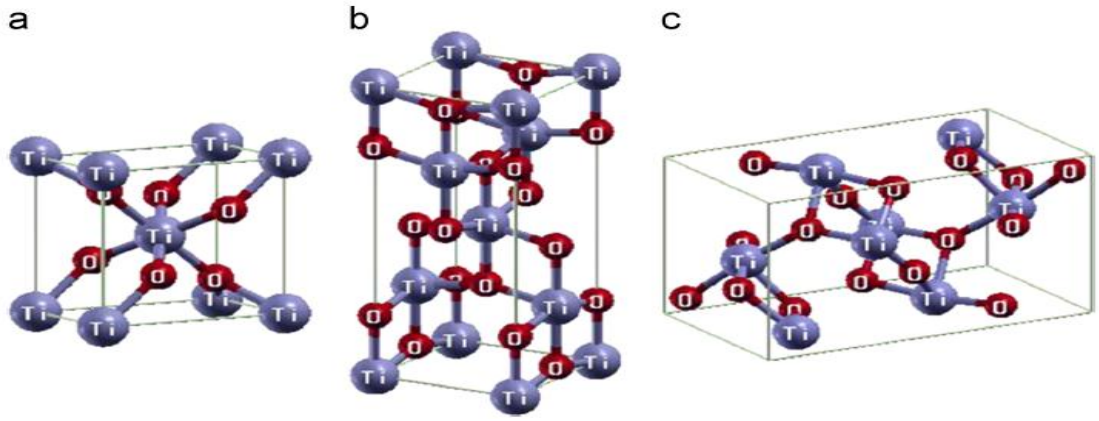

Figure (2.10) shows Titanium dioxide polymorphs(a) Rutile ,(b) Anatase (c) Brookite[50].

Table (2.2) illustrate physical properties of various polymorphs TiO2[49].

	value		
Property	**Anatase**	**Rutile**	**Brookite**
Density(g cm^{-3})	3.84	4.26	4.26
Melting point(˚C)	---	1843	---
Refraction index	2.49	2.903	2.705 2.583
Electrical resistivity(Ω.cm, RT)	10^3-10^5		
Energy gap(e.V)	3.23		

2.6.2.3 Polystyrene

Electrospinning or electrospraying has been used to create polystyrene (PS) surfaces with a variety of morphologies, including beads of varying sizes and shapes and fibers of different diameters and shapes [51].

Polystyrene is a well-known (thermoplastic) polymer that is obtained from the aromatic monomer styrene. Because of its amorphous structure (linear polymer) and relatively low heat conductivity, it is an inert, hard material that is pure white and transparent[51].

Polystyrene is broadly used in auto parts, electrical and electronic connector systems, constructing, the food processing industry, packaging, and transportation. The polystyrene microstructure can be seen in figure (2.11) [52][53].

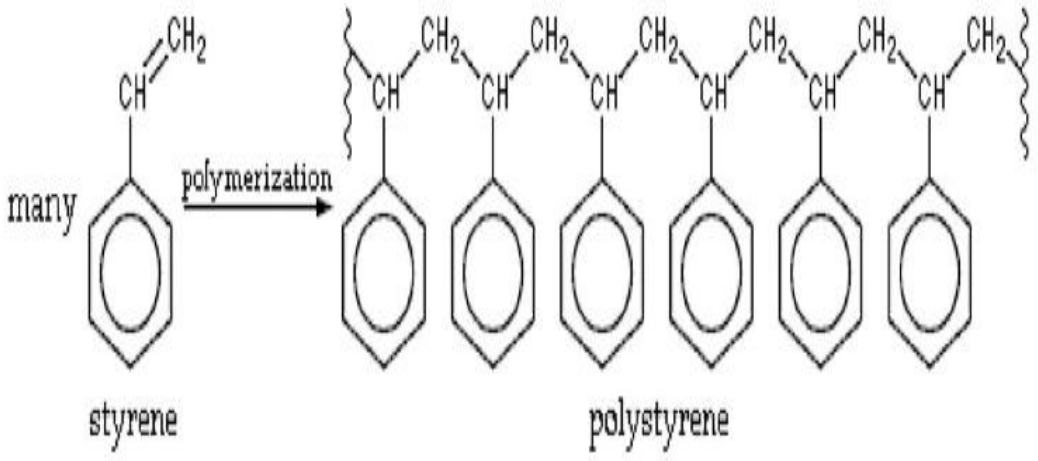

Figure (2.11) Microstructure of polystyrene [52]

Polystyrene is available in three distinct forms [52]:

1- General purpose polystyrene (GPPS), which is transparent and brittle.
2- High impact polystyrene (IPS or HIPS), which really is white, non-shiny, and relatively flexible.
3- Expandable or foam polystyrene (EPS) is the third group.

Table (2.3) shows common insulation materials with indicated to polystyrene that has poorer thermal conductivity[2] .

Table (2.3) Properties of common insulation materials[2]

Insulating material	Density kg/m³	Thermal conductivity w/m.k at 10 ℃	Compressive strength (Kpa)	Relative moisture absorption
Expanded polystyrene 15	15	0.04	35	Medium
Expanded polystyrene 30	30	0.037	110	Medium
Extruded polystyrene	32	0.27	300	Medium
Polyurethane foam	36	0.018	200	Low
Phenolic foam	32	0.027	170	Low
Cellular foam	125	0.41	700	Low
Mineral wool	24	0.045	Negligible	Very high

2.7 Substrate Material Used as Absorber Plate

Choosing the substrate material for manufacturing absorber plate crucial factor is to increase efficiency of the flat plate solar collector because the absorptivity the sun radiation and conversion the radiation to heat energy depend on absorber plate properties[13]. Additionally, the other properties must be considered through design FPSCs such as corrosion resistance, wear resistance, low density, and low cost. The degree the fragmentation the coating solution depends on the substrate materials hardness when increasing the hardness increases the fragmentation the coating such as graphite deposition[14].

There are many materials used as absorber plates in the FPSC and among these materials are aluminum and stainless steel[13].

Aluminum is a low-cost metal and has good thermal property when compared to stainless steel as shown in table (2.4). The temperature of aluminum rapidly rises from (0 to 10) minutes to (46) ◦C. Aluminum's excellent thermal conductivity of (200) w/m.k that allowed thermal energy to be spread throughout the material, increasing performance transformation of sun radiation to heat. Stainless steel metal is few thermal conductivity of (16.2) w/m.k, a less specific heat of (500) J/kg.k and a few thermal diffusivity of (4.2×10^{6}) m²/s, in comparison to aluminum. Thermal diffusivity is critical in defining the characteristics of a solar thermal absorber and determining whether it may be utilized as an absorber or a thermal energy storage device. Stainless steel absorbs a great range of heat but has a slow rate of energy propagation, whereas aluminum, which is a high thermal diffusivity and can absorb a great range of heat [13]. The surface texture of metal

results a change in the heat transfer when aluminum surface roughness increases the heat transfer increases[54].

Table (2.4) Thermophysical properties of solar thermal absorber plate materials[13].

Materials	Density kg/m³	Thermal conductivity w/m.k	Specific heat capacity J/kg.k	Thermal diffusivityx10⁶ m²/s
Aluminum (6063-T5)	2700	200	900	64
Stainless steel	8000	16.2	500	4.2

2.8 Coating Methods

2.8.1 The Coating Description

The coating is a word that refers to the process of covering the surface of an object (substrate) with a fresh layer that imparts new properties to the surface. Economic success is achieved by coating in the case substrate has poor properties. The coating is used for ornamental, functional, or a combination of the two objectives, relying on the substrate design. The coatings are applied from over entire substrate or only a fraction of it [55][56].

The coating layer can impart properties and specifications to the substrate material as a result of the enhancements inherent in the coating layer, such as increased adhesion, corrosion resistance, and enhancement of thermal, mechanical, and electrical capabilities [55][56].

Surface coatings have become more significant in industries as a result of their increased energy efficiency and extended service life for a variety of plants and structures [55][57]. There are a number of spray coating methods that work under normal temperatures such as: **i**) Warm spraying method, **ii**) Cold spraying method and **iii**) Spray (Airbrush Gun) method. **Warm Spray** is an atmospheric coating process through continuous impact and deposition of solid particles heated and accelerated by a supersonic jet controlled between 800~1900 k and 900~1600 m s^{-1} [58]. The significance of **Cold Spray** lies in the low process temperature, which usually ensures compressive residual stresses and allows for the formation of coatings on a thermally sensitive substrate [59]. The **spray air brush** process is classified into three stages, namely, 1) atomization process, 2) droplet flight and 3) film deposition[4].

2.8.2 Spray Coating Method (Airbrush Gun)

Spray airbrush is pneumatic techniques that separate up the liquid into droplets at nozzle using a flow of fluid pressured air or gas (e.g. N2 or argon Ar). The spray head's nozzle atomizes the workable fluid or solution, resulting in a constant flow of droplets [60].The surface tension property, viscosity property, fluid or (solution) density, gas flow characteristics, as well as nozzle design are the primary parameters affecting the atomization process [61]. Successful bonding occurs only when the critical particle velocity is exceeded, which is determined by the temperature and thermomechanical characteristics of the sprayed material[61][62].

This method introduces a dense graphite and multiwall carbon nanotube (MWCNTs) layer of approximately (1μm and 1.43μm) respectively into the surface by spraying graphite powder and MWCNTs with pressurized nitrogen gas[17][4]. The wetting behavior, substrate properties, working space, coating velocity, droplet size, and number of sprayed layers deposits all contribute to the coating layer's quality. Apart from the fluid-surface contact, the kinetic impact of the droplets has an effect on their spreading. Surface temperature also plays a significant influence. The most straightforward application of a pneumatic-based technology is an airbrush gun [62].

The setup spray airbrush system consists of the following items: (1) Spray gun: the gun contains a nozzle. At the nozzle, an atomization of the coat solution occurs. (2) Container: a container that holds the coat solution. (3) An air compressor is used to compress air or gas into the spray gun.

The distance between the nozzle and the sample surface is about (15-40) cm. The nozzle pinhole is about 1.5 mm [4].

The data show that the impact angle has a substantial effect on the deposition properties. The efficiency of relative deposition varies according to the spray angle[63]. Ultrasonication with directed carrier gases or electro-spraying is two more advanced spray generating techniques that are frequently used [62]. Spray coating is a well-known (industrial) technique for coloring car bodies. Figure (2.12) shows sprays air brush coating method.

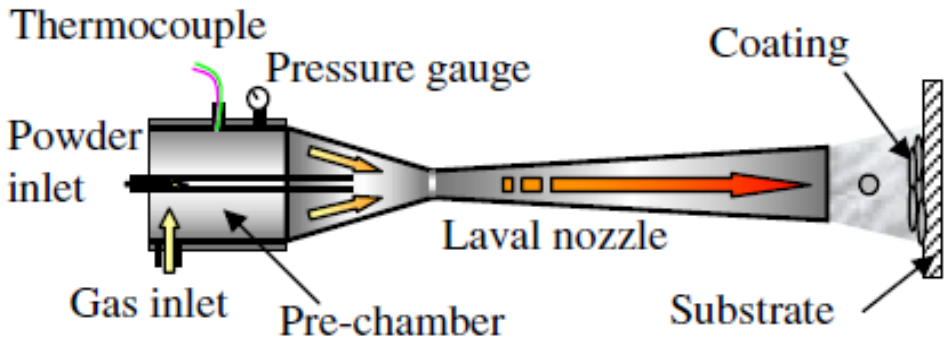

Figure (2.12) Schematic Diagram for Air Brush Spray Gun Process [63].

2.9 Numerical Analysis Introduction

2.9.1 Overview

There are three important steps in the computational modeling of any physical process: (i) problem definition, (ii) mathematical model, and (iii) computer simulation. The three choices for the numerical solution of Partial Differential Equations (PDEs) are the finite difference method (FDM), the finite element method (FEM), and the finite volume method (FVM)[64].

Each method illustrates a systematic numerical approach for solving PDEs, which makes them quite equivalent. The simplicity of implementation is a significant distinction. The most challenging methods are finite element and finite volume. For multi-physics analysis, the finite-element method is particularly useful because it allows user to combine various functions that approximately represent the solution in every element. Non-equispaced meshes are more generally approached using FEM and FVM (although this can also be done in the FDM). Since must solve conservation laws-based partial differential equations for CFD, the finite-volume method is a logical option for CFD issues. However, CFD may use finite elements as well as finite differences. Techniques for CFD with the finite-difference as well as finite-volume methods have been used and known about for a lot longer [65].Both the finite-element method and also the finite-volume method have the advantage of handling curved and random CAD geometries naturally. The advantage of the finite-volume method is that only the cell boundaries need to be evaluated for flux. This applies to nonlinear problems as well, making it even more potent for handling (nonlinear) conservation laws that appear in transportation-related problems [20].

Comparable to that same finite-element method, the finite-volume method's local accuracy is improved near to a corner of interest by fine-tuning the mesh surrounding that area. Moreover, it is difficult to easily create higher - level versions of the functions which the finite-volume method uses to approximate the solution. Comparatively to the finite-element as well as finite-difference methods, the finite-volume method has this drawback [65]. Therefore, ANSYS fluent program used the finite volume method.

2.9.2 Basics of Heat Transfer in Modeling ANSYS Software

The heat transfer in three modes [3] are :

1- Conduction: heat transfer through direct contact (molecular vibration) in medium.
2- Convection: heat transfer by movement of fluid.
3- Radiation: emission of energy by electromagnetic waves.

The steady state thermal analysis is to calculate the effect of steady thermal loads on system or component and for the purpose of determining temperature gradients, heat flow rates, and heat flux in objects that are caused by thermal loads that do not vary over time. This study employed steady state thermal analysis[66].

2.9.3 Calculate the Amount of the Energy Useful

Improving the efficiency of flat plate solar collector performance by increasing the energy useful from solar radiation and reducing heat loss, figure (2.13) shows solar collector system.

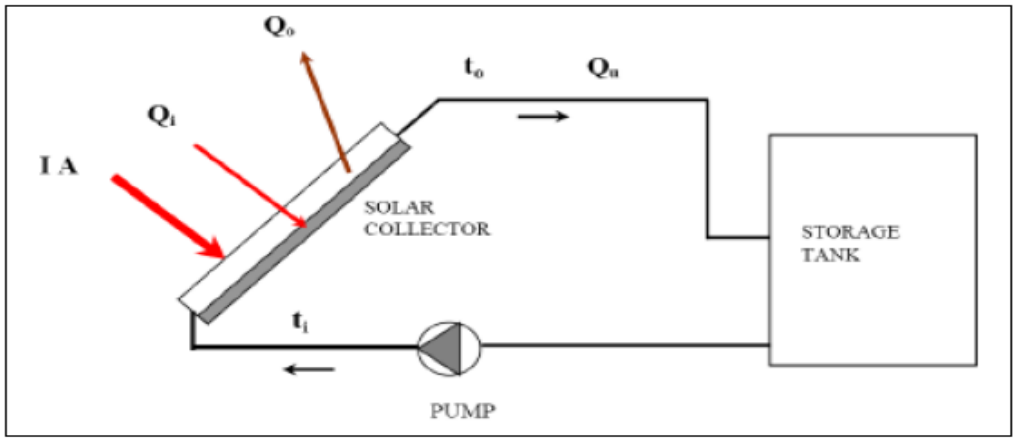

Figure (2.13) illustrate solar energy collection system[67].

The amount of solar radiation received by the solar collector is [67]:

$Qi = I.(\tau\alpha).A$ ..... (2.1).

Qi: the amount of solar radiation received (w).

I: intensity of solar radiation (w/m²).

$\tau\alpha$:transmittance considering only absorption. *A*:area of absorber plate (m²).

When enough heat is absorbed and the absorber plate becomes at a higher temperature than the surrounding atmosphere, there is a loss of heat energy by convection and radiation.

$Qo = UL.A.(Tc - Ta)$ ... . (2.2).

Qo: rate of heat loss (w). *UL*: overall heat transfer coefficient

Tc: collector temperature. *Ta*: ambient temperature.

The amount of heat energy used is calculated through the equation below:

$Qu = (Qi - Qo) = I\,\tau\alpha.A - UL.A(Tc-Ta)$ ..... (2.3).

Qu: the amount of heat energy useful (w).

The actual useful energy gain (*Qu*) is calculated by multiplying the collector heat removal factor (*FR*) by maximum useful energy gain. The equation (2.3) can be rewritten: $Qu = FR.A\,[I\,\tau\alpha - UL\,(Tc-Ta)]$ .... (2.4).

FR: collector heat removal factor. The figure (2.14) reveals incident, transmitted and reflected waves.

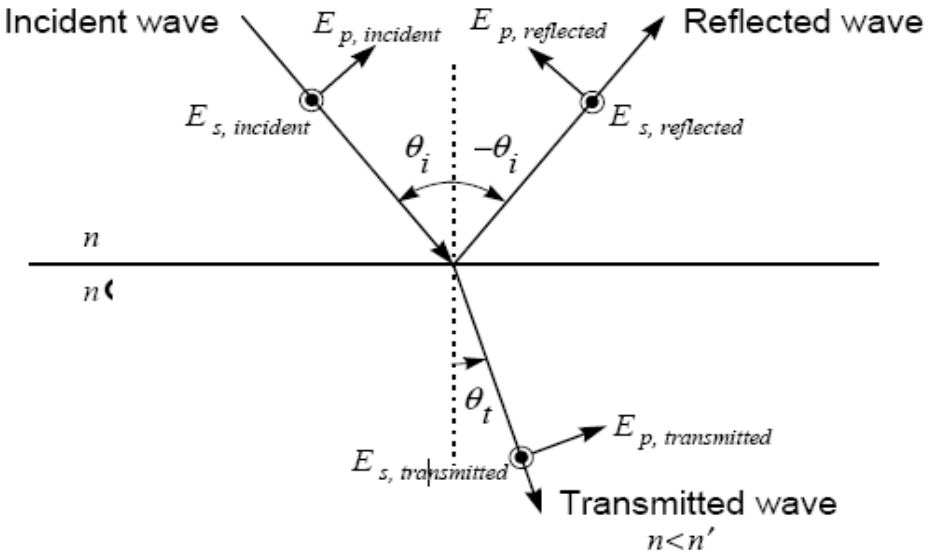

Figure (2.14) shows incident, transmitted and reflected waves[67].

2.9.4 Tetrahedral Element

A tetrahedral element resembles a triangle in two dimensions because it is a volume with four faces. For the volume element, weight functions are derived similarly to how triangles are derived. The volume's creating planes are comparable to the triangle's forming lines. Figure (2.15) shows tetrahedron elements types [21].

Creating the mesh takes time according to the complexity of the model. The more curves and cavities the model contains, the more time it takes to complete the mesh because the mesh is to determine the path of the calculation for the program [21].

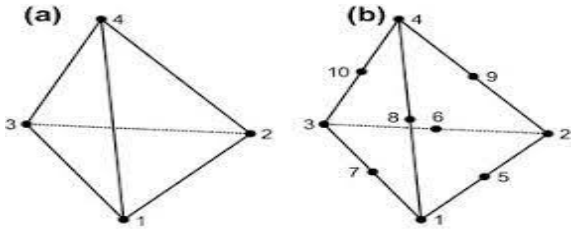

Figure (2.15) shows node order for (a) linear tetrahedron elements, (b) quadratic tetrahedron elements [21].

2.10 Literature Review

In this chapter a literature review was discussed in order to compare the present work with other researchers' works. The literature review contain the methods and mixture information and process techniques the materials used as coating materials to increase in thermal conductivity, increasing the thermal insulation in other side of the solar collector and for coating method , preparing substrate surface and numerical analyzes.

2.10.1 Literature Review for Thermal Conductivity and Insulation

Teixeira, et al., 2001: researched the using of cermet that demonstrates Cr-Cr2O3 or Mo-Al2O3 coatings produced by magnetron sputtering in a reacting environment for efficiency increase thermal solar collector. The resulting multilayered cermet has a thickness of around 300 nm but is composed of metallic chromium or (molybdenum) in a matrix of chromium oxide or (aluminum oxide) with a gradient in oxygen composition. The selective cermet graded films were generated by reactive DC magnetron sputtering of pure chromium, aluminum, and molybdenum as targets in an argon-oxygen plasma at varying sputtering pressures

varying from (5 *10⁻ ³ to 1.2* 10 ⁻ ²) mbar and substrate temperatures (150 and 250) C. According on the coating materials plus sputtering parameters, the coatings have such a good spectrum selectivity, having solar absorption extending from 0.88 to 0.94 as well as thermal emissivity spanning from (0.15 to 0.04) [6].

•**M.A.Alghoul et al., 2005:** studied the three primary kinds of solar collectors (flat plate, evacuated tubes, and heat pipe tubes), and gives details about different solar thermal collectors, describing what could be added utilizing heat pipe collectors in place of evacuated tubes and what could be added utilizing flat plate collectors in place of evacuated tubes as well as the assessment and comparison of the three types of solar collectors moreover additional information about thermal conductivity for material and technique applications. Selective coating materials must be relatively cheap and higher manufacture energy. The use of low-iron glass as a cover for the solar collector is considered the lowest cost. When using a vacuum insulator, there is an increase in insulation and a savings in the cost of the raw materials used. The manufacturing techniques must improve to decrease the manufacture cost. Phase change materials (PCMs) are particularly well suited for the storage of solar energy because they can increase solar efficiencies, which can result in a 30% reduction in solar collector area [2].

- **Cao, et al., 2004:** summarized the fundamental characteristics of ceramic materials used in thermal insulating coatings. In comparison to metals, ceramics are frequently superior oxidation, corrosion, and wear resistance, as well as thermal insulators. Apart from (Yttriua stabilized Zirconia), different materials using for thermal barrier coatings include (Lanthianum Zirconate) and; rare earth oxides. Mullite is a significant ceramic material due to its low density, good thermal durability, resistance to harsh chemical conditions, low thermal conductivity, and advantageous strength as well as creep characteristics. Engine testing conducted with both materials reveal that the Mullite coating has a much longer lifespan than the Zirconia coating. Mullite is a suitable alternative to Zirconia as a TBC material for purposes such as diesel engines wherein surface temperatures are lesser than those experienced in gas turbines and where temperature changes across the coating are significant [12].
- **Gong, et al., 2014:** investigated in the porous mullite ceramic in lower thermal conductivity (0.05 w⁄m.k). The porosity of porous Mullite is controlled by the amount of solid in suspension and the sintering temperature. Porous Mullite has

a greater porosity due to its high spherical pores and small porous on the interior walls. Mullite samples exhibit low thermal conductivity and an adequate mechanical strength. Sintered Mullite ceramics exhibited a multi-modal crystal structure characterized by large spherical pore spaces and small pores on interior surfaces. Their porosity is typically between (86) and (73) vol % and their own compressive strength is between (1to 22) MPa. At room temperature, measured values of thermal conductivity that use the transient plane source method yielded values as low as (0.09) w/m.k [10].

• **Li, et al., 2014:** studied adding thermal conductive fillers such as boron nitride (BN) and aluminum nitrite (AIN) using to increase thermal conductivity to silicon polyester resin and using a hot disk in thermal conductivity test. The research has been conducted on the various types of thermal conductive fillers and impact of their inclusions in large-thermal conductive coatings. The results indicate that as the quality fraction and coefficient of thermal conductivity of the thermal conductive fillers increase the thermal conductivity of the coating increases. By enhancing the coating's resistance to heat, corrosion, as well as adhesive strength, the coefficient of friction can rise as high as 3 $w.m^{-1}.k^{-1}$. So when thermal conductivity property of the coating is much less than 2 $w.m^{-1}.k^{-1}$, the overall coefficient of heat transfer is significantly influenced by the thermal conductivity of the coating [9].

•**Filli, et al., 2018:** developed the using antireflection coatings for solar thermal collectors which were compared with the performance of normal commercial black paint used in solar water heaters and solar stoves. Aluminum and iron absorber plates were created using blackboard paint, industrial black paint, and black (ABRO) spray (symbol for a commercial black spray coat product). When solar water heaters were tested using (ABRO) black spray, a temperature increases of (14.9) °C which was gained at the absorber plate outlet and (7.5) °C at the storage tanker's surface. Maximum stagnation temperatures of (99.2) °C and (107.5)°C are achieved when (973.5)w/m^2 clear sky radiation is used on black (ABRO) spray painted aluminum and iron sheet metal, respectively. That's because (ABRO) black paint absorbs the greatest amount of light with wavelengths less than (2.5) nm and emits the least amount of light with higher wavelength[5].

• **Sohn, et al., 2019**: studied the effects of shape and alignment of reinforcing phases on thermal conductivity (TC) and coefficient thermal expansion (CTE) in the composites materials such as graphite is reinforcing phase and copper matrix

that be fabricated by using the mechanical mixing . The effects of the size the reinforcing graphite on value thermal conductivity were more extensive than alignment but the alignment was more extensive on coefficient thermal expansion from size so must controlled on the shape, size, and alignment of reinforcing phase (graphite)[15].

Valipour1, Seyed, et al., 2019: investigated the application of selective coating to enhance performance, and increases thermal efficiency, and reduces heating loss through the increased absorptivity and decreased emissivity, using three different types of coated absorber plates such as: black-coated, black chrome-plated, and carbon-coated. The flow rate of (0.5 – 1.5) L ⁄min is used. When a flat plate collector is coated with carbon or black chrome, the thermal efficiency increases by 13% and 11.3 % respectively when compared to a black painted absorber plate. In the case of a flow rate (1.5) L ⁄min the solar collector's highest thermal efficiency is up to 64 % in case the plate is carbon-coated. The amount of energy removed decreases to 28.4 % and 35.4 % respectively for absorber plates coated with carbon and black chrome compared with coated black paint[68].

- **Zhang, et al., 2019:** studied the heat conduction mechanism throughout bulk polymers, crystalline particles, as well as carbon-based polymer matrix composites, and discuss recent research on interfacial thermal materials based on carbon nanotubes or graphene. The thermal conductivity of the composite containing was 1.75 w⁄m.k at a graphene: CNT percentage of 3:1, indicating a greater synergistic activity at this percentage. At 302k, the thermal conductivity of the prepared erythritol/ultrathin graphite foams (UGF)-carbon nano tube (CNT) composites has been (4.09 w⁄m.k), up to 1.8 fold those of the UGF/erythriol composites (2.26 w⁄m.k). The relative outcomes and progress are summarized, and several thermal conductive variables, including filler structure, filler orientation, filler dispersion, and interfacial thermal resistance are comprehensively reviewed. This article presents researchers working in the field of thermal conduction with highly accessible and exhaustive thermal conductive understanding[7].
- **Long, et al., 2019:** studied, in an acetic acid-ethanol solution, Anatase TiO2-modified Hollow Glass Microspheres (HGMs) were prepared by a sol–gel technique. Scanning electron, X-ray diffraction, zeta-potential measurement techniques, nitrogen-sorption measurement methods, and Fourier-transform infrared as well as ultraviolet-visible-near-infrared diffuse reflectance spectroscopies all revealed also that alkali adaptation of the HGMs had a

significant impact on the TiO2 film loading and crystal structure. The effects of various TiO2 loading rates also on reflective and heat resistance properties of the material were investigated. The internal surface temperature of the composite colorant coated on aluminum panel was lowered by 22.4˚C, and the near-infrared reflectance of 15.9% TiO2 coated on HGMs was 96.27 %. The TiO2/HGM composite pigments demonstrated superior solar reflective and heat barrier properties, indicating that they could be used to build exterior walls and ceilings[69].

- **Liu, et al., 2019:** studied producing (mullite)-based (nanofibrous aerogels) utilizing gel-casting and freeze-drying techniques. The electrospun nanofibers used for the matrix had varying Alumina/Silica mole ratios (3:2, 3:1, and 3:0), and the high temperature binders used were Silica sols. The arrangement of mullite-based fibrous aerogels was investigated, as well as the impact of aerogel structure on the samples' engineering properties. All (Mullite)-based (nanofibrous aerogels) have a comparable multilevel pore structure. The tiny pores were formed by the overlaps of nanofibers that formed the aerogel's porous foundation, whereas the larger pores were formed by ice crystal sublimation. (Mullite)-based (nanofibrous aerogels) are extremely dense (34.64–48.89 mg/cm^3) but also have a poor thermal conductivity due to their unique multilevel porous structure (0.03274–0.04317)w.m^{-1}k^{-1}[70].
- **Choi, et al., 2020:** developed the using of carbon nanotubes (CNTs) that have high surface area with Nickel metal to produce composite layer (film) with high density by use cold spray method on aluminum substrate. In the applications of thermal spraying, including cold spraying, it was not possible to deposit a composite layer of metal / CNTs containing more than 20% of a weight of CNTs, but by using a method low pressure cold spray system had a pressure 0.6 Mpa it became possible to depose a complex containing 65% of CNTs. Nickel particles connected to carbon nanotubes served as a deformable layer for deposition. As a result, a great-density (CNTs–nickel) composite film was gained, comprising of an upper film with a CNTs content bigger than around 65 wt % CNTs and a bottom film with a nickel content less than 35 wt % nickel The conclusion from this research is that adding metal powders to ceramic coatings gives flexibility to the coating layer and increases the percentage of ceramic materials used, especially by using the cold spray method[8].

- **Kishore Kumar, et al., 2021:** investigated the using of graphene and black paint as selective coatings on mild steel as absorber plate showing increasing in efficiency the collector by increase in absorptivity for solar reaction. Black paint and graphene are mixed in proportions of 1:1, 1:2, and 1:3. The ratio 1:3 (black paint to graphene) results in the highest stagnation temperature of 95.88 ℃ during 30 minutes of indoor testing with 800w/m². The absorption capacity of graphene and black paint coatings is on average 6% greater than that of standard black paint. The absorber surface with 1:3 ratio of black paint and graphene coating is observed to have an average thermal efficiency of 36.65% for the airflow rate of 0.2 kg/h, which is about 6.25% more than that of the standard black paint coating because of higher thermal conductivity of graphene particles. The Up to a wavelength of (200-1500) nm, the absorptivity is greater than 0.9 for graphene and black paint, the surface temperature of graphene and black paint coated surface is approximately 14.53% more than that of the absorber surface with black paint alone [71].
- **Alam, et al., 2021:** presented several strategies that have been employed to enhance the performance of flat plate solar collector (FPSC), and these techniques are described in this study. These strategies involve surface changes, its use of nanofluids, selective solar topcoat, and the use of a mini/macro channel, heat pipe, and vacuum surrounding the absorber. By enhancing the heat transfer rate, surface manipulation on the absorber/absorber tube is utilized to transfer the maximum amount of solar energy to working fluids. Wire mesh, coil, and twisted tapes inserted into the flow have the ability to boost the Nusselt number by 460 % at the expense of a significant pressure decrease. Significantly, a selective coating of Cu 0.44 Ti 0.44 Mn 0.84 can absorb up to 97.4 % of the energy from the sun. As heat transfer fluids, numerous nanofluids have been utilized since they not only improve performance but also reduce fluid stock. Consequently, these strategies play a vital role in the successful of FPSC [1].

2.10.2 Literature Review for Preparing Substrate Surface and Coating Methods.

- **Brand, et al., 2004:** investigated of two techniques for increasing the adhesion strength and durability of an epoxy coating material on an aluminum surface. The first way involves the application of a thin polymeric film of about (10) nm thickness on an aluminum surface material that is capable of chemisorption to the oxide surface. Poly (acrylic acide) (PAA), poly(ethylene alt

maleic anhydride) (PEMah), and poly(vinyl phosphonic acid) (PvPA) are used to create the polymeric layer. The second method involves immersing the substrate in hot water, which forms a porous pseudoboehmite oxyhyroxide layer by soaking the aluminum substrate in heated water for 60 seconds; a porous pseudoehmite oxyhydroxide layer with a pseudoboehmite structure is formed. The epoxy layer has been found to completely permeate the layer. The high hydroxyl density upon the oxide surface the large specific surface area, and the porosity all contribute to this system's excellent adhesion efficiency[72].

- **Hanada, et al., 2005:** described the process of pressure-spraying graphite on tool steel and the lubricating properties of the sprayed structural steel for metal-forming application fields. Compared to standard graphite coating, spraying tool steel offers superior lubricating capacity and lubrication life, as determined by friction testing. This technique deposits a high-density graphite layer of thickness (1µm) just on tool steel's exterior by spraying graphite powder with pressurized nitrogen gas. These findings indicate that this technique has the potential to significantly increase the life of a (metal-forming) mold and the precision of a work - piece[17].
- **Majid, et al., 2015:** investigated the aluminum and stainless steel hollow square rods in terms of their solar thermal absorber performance. The material type and shape have a direct effect on the solar air thermal collector's operating temperature and thermal energy storage capacity. Aluminum has a high thermal conductivity, whereas stainless steel has a high thermal storage capacity. Studies on aluminum (6063) as well as stainless steel needs to set with flat-black coated and uncoated surfaces, respectively, have been conducted. Both sets were exposed under 585 w/m² radiations and the temperature response was recorded. When a flat-black coating was applied to uncoated aluminum surface a considerable increase in temperature occurred. The aluminum surface coated and uncoated the increasing in temperatures of (67.2) ˚C and (48.3) ˚C, respectively. By increasing slope, heat transmission from the surface towards the interior airflow of the absorber likewise rises, resulting inside a quicker increase in air temperature[13].
- **Chun, et al., 2017:** studied the extent to which fragmentation and interlayer separation occur is determined via the substrate's hardness. The present work demonstrated the effect of the material upon that coating of graphite microparticles throughout thin film order to prepare at room temperature just using a nanoparticle

deposition system (NPDS). The evaluating of the accumulation graphite powder on a range of surfaces with varying degrees of hardness, such as polystyrene, copper, glass, and sapphire, as well as the surface deposition behaviors. Fragmentation and interlayer separation increase as the substrate hardness increases. With decreasing substrate hardness, the extent of fragmentation as well as interlayer separation reduces. Dry spray coating of micro - scale graphite powder resulted in dense films of disparate graphite on soft surfaces and thin films of segmented graphene constructions on hard substrate[14].

- **Muñoz, et al., 2019:** investigated the surface treatments which increase the efficiency of interaction between aluminum surfaces and coating layers. In this paper aluminum alloy AA2024 used. Treatments are including mechanical polishing, chemical etching and AR-plasma pre-treatment after that deposition of poly (methyl methacrylate). The tests work for the samples are morphology by SEM, surface chemical analysis by X-ray and wettability by contact angle. SEM images showed that using Ar-plasma as a pretreatment resulted in a relatively homogenous and fully incorporated poly-(methyl methacrylate) coating. The wettability of both the surface of the metal improved, which has been proven by contact and hysteresis angles. XPS spectra revealed that the Ar-plasma pretreated samples' Al-O/Al-OH intensity ratio does not clearly rely on angle measurement, which shows that the distribution of Al(OH) and Al_2O_3 on the sample surfaces is not uniform. There are some areas of the aluminum surface that are not entirely covered by Al_2O_3.This could describe the improvement in wettability, as well as the better interaction among methoxy groups of both the polymer (PMMA) and the hydroxylate aluminum surface, that led in more binding sites and greater adhesion, thereby enhancing barrier protection[16].
- **Meikandan, et al., 2020:** verified, in this paper, using the spray air brush for produce thin layer on a large flat substrate by using multiwall carbon nanotubes (MWCNTs) on copper substrate. The tests that used are surface roughness, microstructures, and wettability of the coated substrates and compared with pure copper substrate. The mechanical properties and surface roughness improved for (MWCNTs) coated copper substrates. Thickness of the coating is (1.43) µm at (0.4) wt% of (MWCNTs). The (MWCNTs) coated on copper substrate showing higher thermal conductivity than pure copper due to densified microstructure. The experimental results demonstrated that spray coating copper and MWCNTs nanocoatings is a suitable method for coating large surface area [4].

- **Mayer, et al., 2021:** investigated in pull-off strength test results of epoxy- and polyurethane-based coatings with three different powder fillers (carbonyl iron, ferrites, and graphite flakes). The fillers effect content on resin coated on the aluminum alloy surface (6061) that was investigated by pull-off strength. The (polyurethane) and (epoxy) coating were used in this paper and, the comparison was made between the two coatings. The (epoxy) coating showed greater adhesion on aluminum alloy (6061) substrate. The roughness of the substrate surface (aluminum alloy) increases the pull-off strength due to the increased mechanical overlapping among the resin and the surface of a metal. Pull-off strength reaches a maximum of (3.88) MPa; for (epoxy) coatings and (3.12) MPa; for (polyurethane) coatings[73].

2.10.3 Literature Review for Numerical Analysis.

Yang, Xun, et al., 2017: investigated under the simultaneous charging and discharging operation mode. Based on the solar heating system, a numerical calculation method of the tank temperature distribution under the simultaneous charging and discharging operation mode was proposed and validated by experiments. This numerical method offers a correlation between the output water temperatures of the tank and the input water temperatures of the tank, which can be used to optimize the thermal performance of the solar heating system in future studies. The calculated results showed that the system COP reached an average number of 3.0, which was nearly equal to that of gas-boiler heating system and much higher than that of electrical heating systems. A north-facing room and a south-facing room were both selected to test whether the room temperatures met the heating requirements. The test results showed that the north-facing room had an average temperature over 17 °C while the south-facing room was over20 °C, which illustrated that a good heating effect was achieved[74].

A.A. Hawwash, et al., 2018: presented experimental and numerical investigation of (FPSC) using different types of nanofluid are double distilled water (DDW) and alumina nanofluid with different weight concentrations of (1-3%) according to a specification ASHRAE Standard 86-93. The experiments were done in a hot climate in Egypt. Experiments showed that alumina nanofluid improved the thermal performance of (FPSC) compared with (DDW) by about (3% - 18%) at the lowest and highest temperature difference. Numerical analysis for evaluate the performance of (FPSC) for any nanofluid or (DDW) by using the ANSYS 17

software for any mass flow rate. When the alumina nanofluid concentration increased the thermal efficiency is increased to (0.5%) of the volume fraction. The pressure drop increases with the increase in the volume fraction of the nanofluid[75].

M. E. Nakhchi , et al., 2020: studied using of turbulent specifications and thermal improvements when using (CuO/water) in heat exchangers containing double v-cut of twisted tape. The Reynolds number in the range (5000-15000), the twisted ratio for the twisted tape is (5.25) and the cut-off ratio (b/c) ranges from (0 to 1.8). The volume fraction of nanoparticles is the range (0-1.5%). Using of model (k- ϵ) turbulent in numerical analysis. Thermal conductivity improved at volumetric fracture (1.5%) and Nusselt number improved about (138%) compared with normal twisted tape without cutting. The maximum thermal performance achieved is (η = 1.99) at a volumetric concentration of nanofluid (1.5%), cut-off ratio (1.8) and Reynolds number (5000) [76].

Verma, et al., 2020: presented study in the use of heat exchanger tube design by comparing the manifold flat plate solar collector (FPSC) manufactured in the form of single spiral and a number of riser tubes connected with headers in conventional type for (FPSC) while maintaining the same parameters for both designs through the results. Increasing the thermal efficiency of the single spiral collector about (21.94%) and the efficiency of exergy is improved about (6.73%) compared with the conventional design of (FPSC). The use of single spiral design results in savings in materials used up to (30%), savings in maintenance costs and performance equivalent to the conventional design of flat plate solar collector (FPSC) [18].

2.11 Table (2.5) Summary of Group from Researchers Above

Researchers	Work	Results
Teixeira, et al., 2001	Using the cermet that demonstrates Cr-Cr2O3 or Mo-Al2O3 coatings produced by magnetron sputtering in a reacting environment for efficiency increase thermal solar collector.	Multilayered cermet has a thickness of around 300 nm but is composed of metallic chromium or (molybdenum) in a matrix of chromium oxide or (aluminum oxide) with a gradient in oxygen

		composition.
Li, et al., 2014	studied adding thermal conductive fillers such as boron nitride (BN) and aluminum nitrite (AIN) using to increase thermal conductivity to silicon polyester resin	Quality fraction and coefficient of thermal conductivity of the thermal conductive fillers increase the thermal conductivity of the coating increases. By enhancing the coating's resistance to heat, corrosion,
Filli, et al., 2018	Using antireflection coatings for solar thermal collectors which were compared with the performance of normal commercial black paint used in solar water heaters and solar stoves using (ABRO) black spray.	Temperature increases of (14.9) °C which was gained at the absorber plate outlet and (7.5) °C at the storage tanker's surface. Maximum stagnation temperatures of (99.2) °C and (107.5)°C are achieved.
• Valipour1, Seyed, et al., 2019	Using three different types of coated absorber plates such as: black-coated, black chrome-plated, and carbon-coated. The flow rate of (0.5 – 1.5) L⁄min is used.	Flat plate collector is coated with carbon or black chrome, the thermal efficiency increases by 13% and 11.3 % respectively when compared to a black painted absorber plate.
• Kishore Kumar, et al., 2021	Investigated using the graphene and black paint as selective coatings on mild steel as absorber plate. Black paint and graphene are mixed in proportions of 1:1, 1:2, and 1:3.	The ratio 1:3 (black paint to graphene) results in the highest stagnation temperature of 95.88 ℃ during 30 minutes with 800w/m². The absorption capacity of graphene and black paint coatings is on average 6% greater than that of standard black paint.
• Gong, et al., 2014	Investigated in the porous Mullite ceramic in lower thermal conductivity (0.05w⁄m.k).	Mullite samples exhibit low thermal conductivity and an adequate mechanical strength. Their porosity is typically between (86) and (73) vol % and their own compressive strength is between (1to 22) MPa.
• Liu, et al., 2019	Studied producing (Mullite)-based (nanofibrous aerogels) utilizing gel-casting and freeze-drying techniques. The electrospun nanofibers used	(Mullite)-based (nanofibrous aerogels) are extremely dense (34.64–48.89 mg/cm³) but also have a poor thermal conductivity due to their

	for the matrix had varying Alumina/Silica mole ratios (3:2, 3:1, and 3:0).	unique multilevel porous structure (0.03274–0.04317) $w.m^{-1}k^{-1}$.
• Majid, et al., 2015	Investigated of aluminum and stainless steel hollow square rods in terms of their solar thermal absorber performance.	Aluminum has a high thermal conductivity, whereas stainless steel has a high thermal storage capacity.
• Sohn, et al., 2019	Studied the effects of shape and alignment of reinforcing phases on thermal conductivity (TC) and coefficient thermal expansion (CTE) in the composites materials such as graphite is reinforcing phase and copper matrix.	The effects of the size the reinforcing graphite on value thermal conductivity were more extensive than alignment but the alignment was more extensive on coefficient thermal expansion.
Yang, Xun, et al., 2017	Investigated under the simultaneous charging and discharging operation mode. Based on the solar heating system, a numerical calculation method of the tank temperature distribution	The test results showed that the north-facing room had an average temperature over 17 °C while the south-facing room was over 20 °C.
A.A. Hawwash, et al., 2018	Presented experimental and numerical investigation of (FPSC) using different types of nanofluid are double distilled water (DDW) and alumina nanofluid with different weight concentrations of (1-3%).	Alumina nanofluid improved the thermal performance of (FPSC) compared with (DDW) by about (3% - 18%) at the lowest and highest temperature difference. Numerical analysis for evaluate the performance of (FPSC) for any nanofluid or (DDW) by using the ANSYS 17 software.

CHAPTER THREE

EXPERIMENTAL PART AND NUMERICAL ANALYSIS

Chapter Three

Experimental Part and Numerical Analysis

3.1 Introduction

In this chapter experimental part focused on used materials and its composition for increase the thermal conductivity and increase thermal insulation , preparation methods and coating process , finally explain how the devices work that used in the measurements for this study, while numerical analysis for the results obtained from experimental work are investigated. The experimental work and numerical analysis distributed to seven parts:

1- Preparation the substrate surface for coating process for both samples the conductivity and insulation.
2- Tests are conducted on the powders that making the coating mixture before mixing.
3- Preparation coating mixture for increase thermal conductivity and the materials that used in this the mixture.
4- Preparation the coating mixture for increase thermal insulation and the materials that used in this the mixture.
5- Coating process using spray air brush method.
6- The measurements that used to assess the happened development in the coated samples.
7- Numerical analysis works using the results obtained by simulation with (ANSYS 16.1) software.

The figure (3.1) illustrates the stages of the experimental process that was utilized in this research. Spray air brush method was used for both conductive and insulating coatings and by mixing magnetic stirrer bar. Tests were performed on coating mixtures as well as on samples after coating for both conductive and insulating coatings.

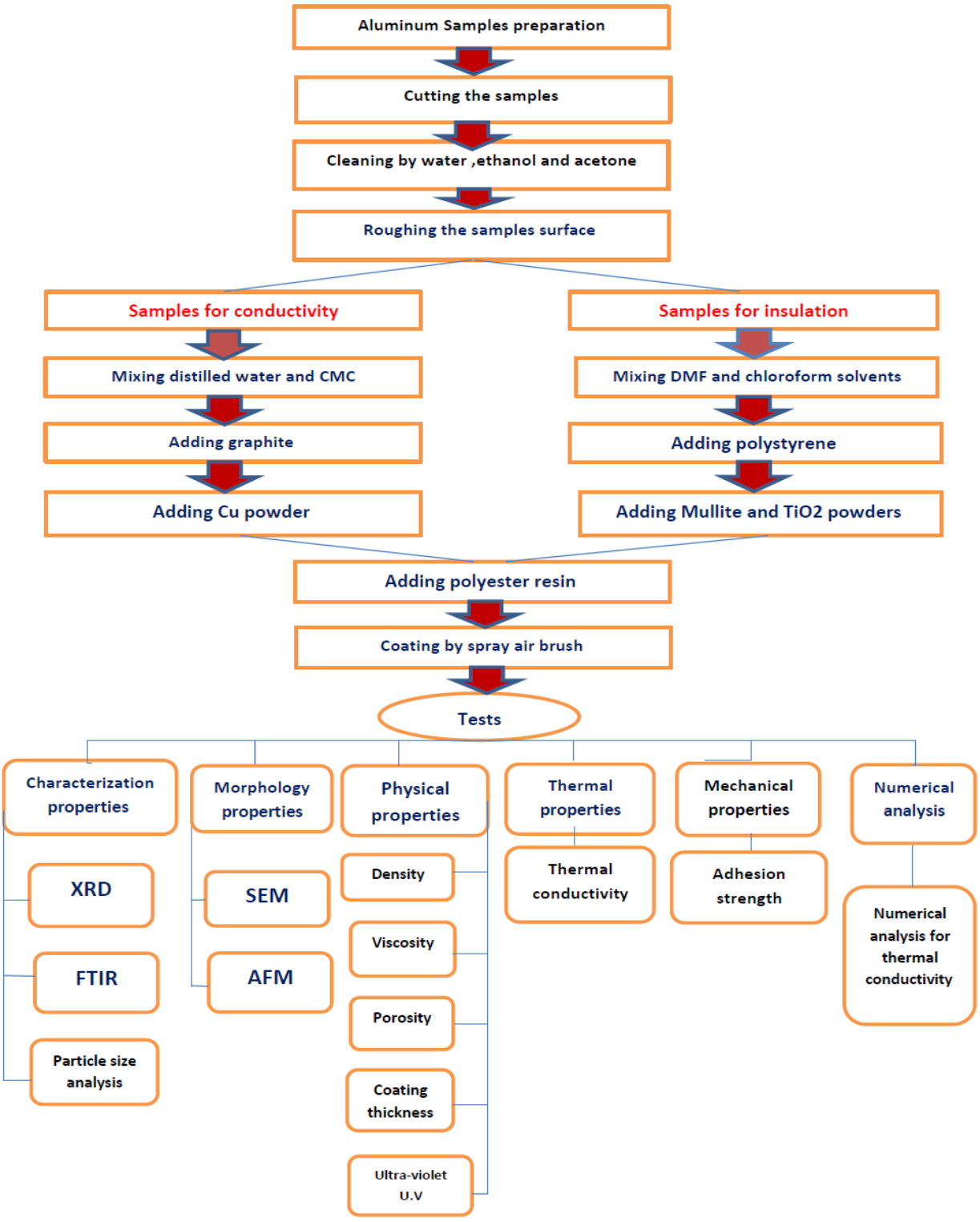

Figure (3.1) schematic showing the experimental work

3.2 The Used Materials

3.2.1The Used Materials for Increase Thermal Conductivity

The materials used in this study to coating the flat plate solar collector which caused the increase thermal conductivity and absorptivity as shown in the table (3.1).

All coating materials used to increase thermal conductivity were purchased from the Iraqi local markets.

Table (3.1) illustrates the materials and chemicals that used for increase conductivity.

Materials	Chemical formula	Purity %	Appearance	Fabrication place
Graphite	C	99.95	glossy black powder	EG INDUSTRY Co.,LTDGUILIN FACTORY
Carboxymethyl cellulose(CMC)	$(CH_2\text{-}COOH)x$	99.5	White to cream fine powder	QINGDAO SINOCMC CHEMICAL CO.,LTD/CHINA
Copper	Cu	99.5	Red to blackish red powder	Chem-Lam NV Idustriezone “De Arend”2 B-8210Zedelgem /Belgium
Polyester resin	$(C_{10}H_8O_4)x$	-	Clear, Yellowish liquid	Saudi Industrial Resins Limited

3.2.2 The Used Materials for Decrease Thermal Conductivity

Materials used in this article's flat-plate solar collector coating from the back side to decrease Thermal Conductivity are listed in the table (3.2).

All coating materials used to increase thermal insulation were purchased from the Iraqi local markets.

Table (3.2) displays the materials and chemicals that used for increase thermal insulation.

Materials	Chemical formula	Purity %	Appearance	Fabrication place
Mullite	$3Al_2O_3.2SiO_2$	99.9	yellowish white	Henan Xinmi Changxing Refractory material Co.,Ltd.(China)
Titanium dioxide	TiO_2	99.8	White powder	Hongwu Inter National Group Ltd.-Chaina
Polystyrene	$(C_8H_8)X$	-	transparent granules	APS American Polymers Services Inc.
Dimethyle floramide (DMF)	$H.CO.N(CH_3)_2$ or (C_3H_7NO)	99	Liquid	THOMAS BAKER(CHEMICALS)PVT.LTD.B3&B4,MIDC,CHEMICAL ZONE,AMBERNATH421 501.INDIA
Chloroform	$CHCl_3$	99	Liquid	THOMAS BAKER(CHEMICALS)PVT.LTD.B3&B4,MIDC,CHEMICAL ZONE,AMBERNATH421 501.INDIA

3.3 Preparation Samples

The substrate used is made of aluminum plate with a measure of about (0.5mm) for the samples to be coated for the purpose of increasing thermal conductivity and the samples to be coated for the purpose of decreasing the thermal conductivity in this research. The aluminum metal has thermophysical properties shown in table (3.3).

Table (3.3) illustrates thermophysical properties for aluminum metal[13].

Material	Density. kg/m^3	Thermal conductivity w/m.k	Specific heat capacity. J/kg.k	Thermal diffusivity.$*10^6$,m/s^2
Aluminum	2700	200	900	64

The aluminum metal sheet cutting to different dimensions to appropriate the requirements for all the tests that achieved as shown in table (3.4).

Table (3.4) illustrates samples dimensions used.

Sample dimensions	Sample form	Test
40x30x0.5 mm	Rectangular	XRD
10x10x0.5mm	Square	SEM and AFM
Diameter 40 mm, thickness 0.5mm	Circular	Thermal conductivity
50x50x 0.5mm	Square	Adhesion strength

After cutting process, the samples cleaning by acetone solution, methanol solution and distilled water to removing the dust and grease from samples surface.

In order to increase the adhesion strength and the surface area between the coating layer and the substrate surface, the substrate surface must be roughed which leads to an increase in mechanical bonding. The roughness working by used sandpaper (600) with conformity at constant deep as much as possible.

The samples again cleaning by (acetone, methanol) solutions and distilled water to removal the particles and dust from roughness process and to ensure sample surface remains cleanly with high level, according to the specifications ISO8502-6 and ISO8503[77].

3.4 Preparation Coating Mixture

3.4.1 The Mixture for Increase Thermal Conductivity

The used materials in the coating for increase thermal conductivity obtained from local markets.

The coating mixture for increased thermal conductivity is prepared as follows:

Step one: The Carboxymethyl cellulose (CMC) powder mixing with warm distilled water around (35 ˚C) with present the magnetic stirred bar for one hour until it turns into gel solution and removes all the bubbles and the amount (CMC) that solved in water between (4.7 % to 5%) wt. according the used samples [30][31].

Step two: the graphite powder was then added to the gel mixture (6.8% to 7%) wt.[78]. The graphite powder was gradually added to the mixture with a continuous magnetic stirred bar for (40) minutes. After producing a homogeneous gel mixture, the graphite powder became regularly diffusive in everywhere around in mixture.

Step three: the polyester resin was added to the mixture and then subjected to continuous magnetic stirred for (20) minutes. The amount of polyester resin to be added to the mixture is (4.7% to 5%) wt.

Step four: adding (1, 2, 3, 4) wt. % from copper powder. The coating materials mix with magnetic stirring bar for (30) minutes.

The materials and the mixing percentages are used in this research showing in the table (3.5). Figure (3.2) shows the samples coated to increase thermal conductivity.

Table (3.5) displays the ratios of used materials in all samples used to increase conductivity.

Sample NO.	Distilled water	Carboxymethyl cellulose (CMC)	Graphite	Polyester resin	Copper
G0	-	-	-	-	-
G1	83%	5%	7%	5%	-
G2	82%	5%	7%	5%	1%
G3	81.5%	4.8%	6.9%	4.8%	2%
G4	80.5%	4.8%	6.9%	4.8%	3%
G5	79.8%	4.7%	6.8%	4.7%	4%

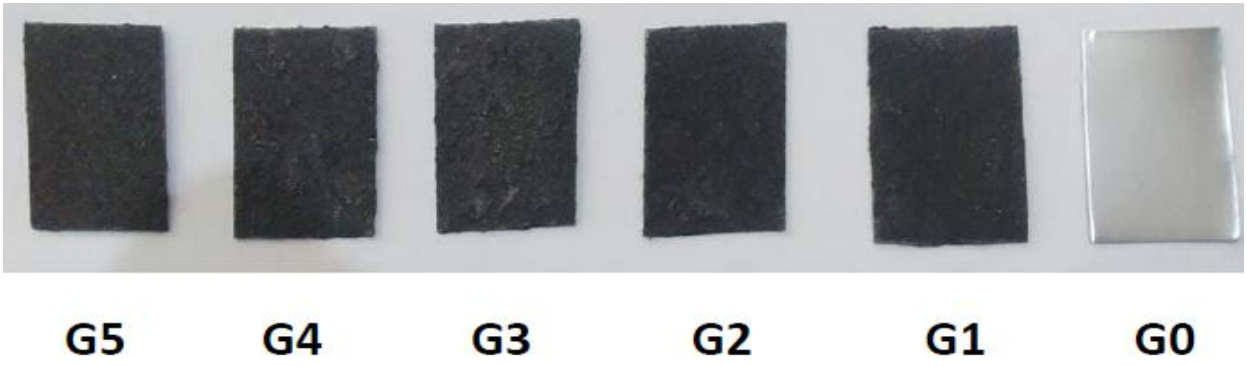

Figure (3.2) shown the samples coated for improving the thermal conductivity.

3.4.2The Mixture for Decrease Thermal Conductivity

The used materials in the coating for the purpose of decreasing the thermal conductivity purchased from local markets.

The coating mixture for increase thermal insulation is prepared by following steps:

Step one: The solvents mixing together by magnetic stirred bar. The solvents are Chloroform and Dimethylefloramide (DMF) and mixed in equal proportions for a period (10) min.

Step two: The polystyrene adds to solvent solution mixture gradually and used closed vessel to avoid evaporation and volatility the solvents because the toxicity solvents and the polystyrene need long period to solve. The required time for the polystyrene to solve about (2) hour with continuous magnetic stirred bar in order to remove all bubbles in the solution mixture.

Step three: adding the polyester resin from (8% to 9%) wt. with continuous magnetic stirred for period (10) min.

Step four: adding the percentages (0.75%, 2.25% and 3.75%) wt. from Mullite powder.

Step five: adding the percentages (0.25%, 0.75% and 1.25%) wt. from Titanium dioxide. The coating materials mix with magnetic stirring bar for (40) minutes.

The coating layers sorts are displayed in following table (3.6).

The sum of coating percentages for ceramic materials (Mullite and Titanium dioxide) in the sample (S2) is (1%), the sample (S2) is (3%), and the sample (S4) is (5%). Figure (3.3) shows the samples coated to decreasing thermal conductivity.

Table (3.6) displays the ratios of used materials in all samples used to increase insulation.

Sample NO.	DMF	Chloroform	polystyrene	Polyester resin	Mullite	TiO2
S0	-	-	-	-	-	-
S1	38%	38%	15%	9%	-	-
S2	38%	38%	15%	8%	0.75%	0.25%
S3	37.5%	37.5%	14%	8%	2.25%	0.75%
S4	37%	37%	13%	8%	3.75%	1.25%

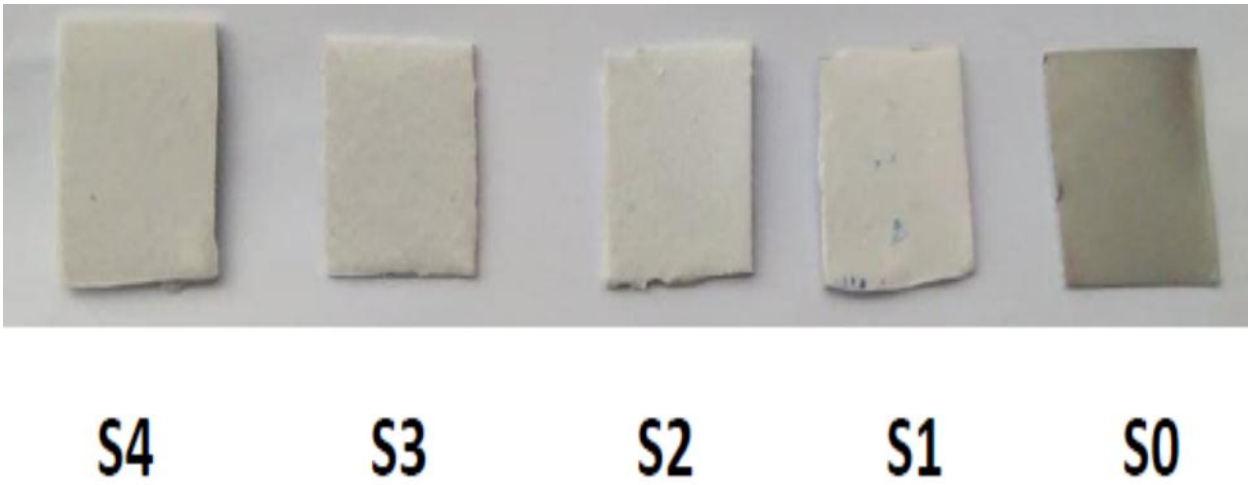

Figure (3.3) shown the samples coated for improving the thermal insulation.

3.5 The Coating Method (Spray Air Brush).

The simplest form of pneumatic –based system is spray gun air brush. The spray gun air brush method comprised of:

1- Spray gun: This part of the device leads to atomization of the coating suspension and conversion to droplets. Spray container: contains on the coating suspension usually fixed on the spray gun. Container capacity about 800ml.
2- Air compressor: which working on air compress into spray gun by means of elastomeric ducts.

The gun contains a lever that controls the vertical or horizontal spraying method. It contains also a valve that can control the size of droplets generated by the atomization of the coating solution. The distance between the nozzle and the sample surface is about 15 cm [4]. The nozzle pinhole is about 1 mm. After completing the preparation of the surface of the samples, they are placed on a flat horizontal surface, and the coating site must be as far as possible isolated and clean during coating. The coating is done by spraying either vertically or horizontally, and one layer of coating for both types of coatings to increase or decrease the thermal conductivity. After completing the coat spraying, the samples are placed in an isolated place until the complete drying of the paint layer.

Table (3.7) displaying the parameters for spray gun air brush. Figure (3.4) illustrate the spray air brush system.

Table (3.7) the coating parameter for spray air brush equipment.

Operation gas	Model number	Max. viscosity	Input power	Gas temperature	Gas pressure	Coating distance
Air	TT5006	50 DIN-s	500 W	(20-30) □C	0.1 – 0.2 bar	15 cm

(a) (b)

Figure (3.4) illustrates the spray air brush system. (a) spray gun air brush device (b) electric air compressor.

3.6 The Measurements

After the coating process and coating layer dried the group of measurements done to determine the developments in the coating layer properties such as thermal conductivity and insulation, absorptivity and porosity ratios. The measurements classified according to the following:

3.6.1 Characterization Properties

3.6.1.1 X-Ray Diffraction (XRD) Test

X-ray diffraction test a non-destructive technique that gives information about the crystal structure, chemical composition and physical properties of materials. Using the XPert Hing ScorePlus software, the X-ray test report was analyzed by matching the result peaks with standard peaks for each material using JCPDS (Working Group on Powder Diffraction Standards) cards. The X-ray diffraction test was performed in Laboratories of the Department of Ceramics and Building Materials, College of Materials Engineering, University of Babylon. The (XRD)

test is primarily used to describe the crystallographic structure of the materials which is based on Bragg's law[79][80]: $n\lambda=2d\sin\theta$ ….. (3.1)
Where (λ) is the wavelength of incident wave, (n) is positive integer, (θ) is the angle of thudding, (d) is interplanar distance as showing in figure (3.5).

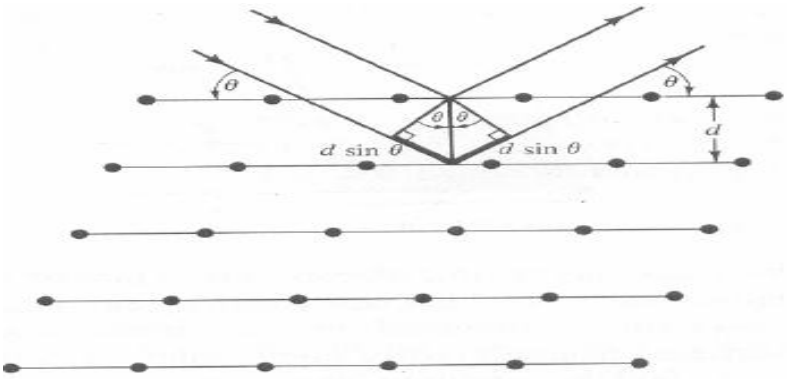

Figure (3.5) show Bragg's law diffraction[79].

Because of the movement of the sample stage, diffracted from its source is incident on the surface of the material, and it is reversed from sample with different angles. The beam will then be converted by the detector (indicating) on the other side. Lastly, as shown in figure (3.6), the detector will convert as well as transfer data[79] .

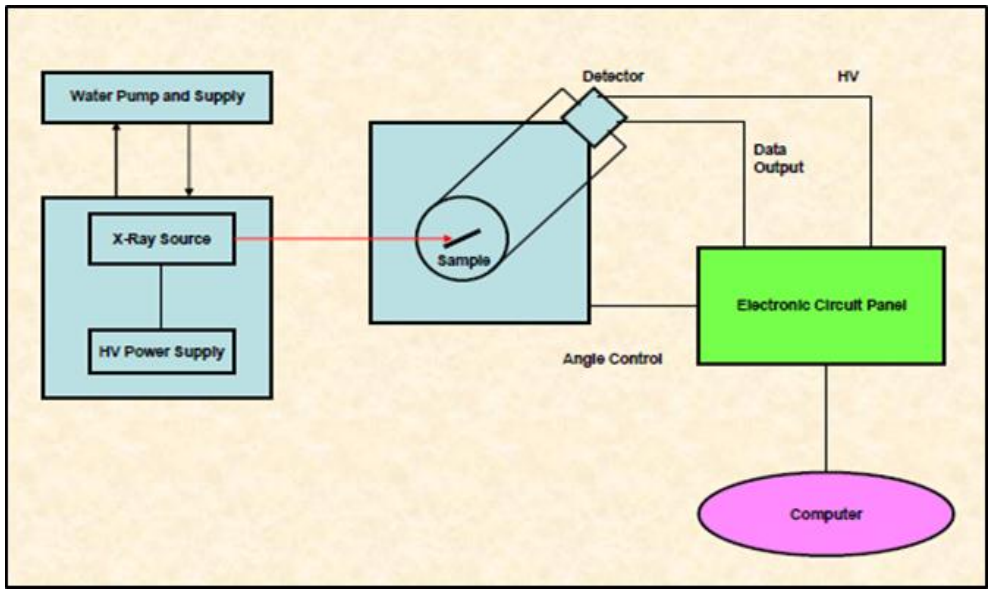

Figure (3.6) show analysis principle XRD device[79].

3.6.1.2 Fourier Transmittance Infrared Spectrophotometer (FTIR) Test

Examination of the (FTIR) in Laboratories of the Department of Polymers, University of Babylon, College of Materials Engineering.The device (IRA Affinity SHIMADZU) displays the highest sensitivity (30000:1) with maximum analysis ($0.5cm^{-1}$) for several reasons high energy ceramic light source, temperature controlled, and high-sensitivity detector. Test (FTIR) is used to find out the quality of the organic and inorganic chemical bonds and their constituent elements after mixing and coating processes and determine the extent of absorbance and transmittance, which is an indicator of thermal conductivity property. The device works by absorbing the sample infrared radiation of certain wavelengths and converting it into molecular vibrations that cause the polar moments of the coating molecules to change. The (FTIR) test draw the relation between the transmittance and the inverse of the wavelength (frequency).

3.6.1.3 Particle Size Analysis Test

(Battersize 2000 Laser) the particle size analyzer used for particle size analysis. The measuring range of the device for particle sizes ranges (0.02µm-2000 µm). The test was conducted at the University of Babylon \ College of Materials engineering \ Laboratories of the Department of Ceramics and Building Materials, according to ASTM E112-12 [81].

A light from a laser beam is directed at the suspension containing the particles of the sample material, which leads to a scattering of the laser beam. The scattering angles depend on the particle size and particle shape of the sample material. The intensity of the scattering gives information about the distribution, quantities and size of particle. The device (Battersize 2000 Laser) is associated with a computer equipped by a program that contains the laser reflection patterns for comparison and calculating the size and particle distribution of the samples materials.

3.6.2 Morphology Properties

3.6.2.1Scanning Electron Microscopy (SEM) Test

The scaning electron microscopy (SEM) works to enlarge a specific area in a high-resolution image using high-energy electrons. The samples is placed under vacuum to ensure that the electrons beam remains focused and does not interact with airborne particles. (SEM) has a huge magnification ability that enables the

analysis of coated and uncoated samples. The examination was carried out in Laboratories of the Department of Ceramics and Building Materials, College of Materials Engineering, University of Babylon. The (SEM) device is (VEGA3) that contain on electron gun tungsten heated filament. The magnification of (VEGA3) device from (3x-1000000x).

3.6.2.2 Atomic Force Microscope (AFM) Test

Atomic force microscope (AFM) a device used in nanotechnology to determine and draw surface topography in nano and micro dimensions. It has a high analytical capability, allowing it to analyze the surface structure and smoothness of materials. The AFM test was conducted in the Polymeric materials Engineering & Petrochemical Industries Section laboratories at Babylon University's College of Materials Engineering. Using an atomic force microscope device (Enhanced Inc., AA 3000, United States, Category Angstrom, Scanning Probe Microscope).

3.6.3 Physical Properties Tests

3.6.3.1 Density Test

Density is a physical property of the material and it is called volumetric mass. The law of density states that it is the quantity resulting from dividing mass by volume according to the law in equation (3.4): $\rho=m/v$ ..... *(3.4).*

ρ: density, *m:* mass, *v:* volume. According ASTM D792-20 [82].

The units of density are (kg/m³ or g/cm³). Measure the density of the conductive coating and insulation after drying, by calculating the volume of the coating (the dimensions of the coating with thickness), the weight of the sample before coating and after coating, and extracting the coating mass from the difference between the two weights and calculate the density of the coating from the law (mass / volume).

Use a (MatsuHaku) density tester device to measure the density of the coating mixture in the liquid state of both the conductive and insulating coatings. The device has a digital screen that gives a reading directly after placing the liquid coat mixture on the device. The liquid density test was carried in Laboratories of the Department of Polymers, University of Babylon, College of Materials Engineering , according to ASTM D1475-13[83].

3.6.3.2Viscosity Test

Viscosity is the resistance of a liquid material to flow. The value of this resistance can be determined by using a device rotational viscometer from

BROOKFILD company. It can also be used to measure specifications related to viscosity. The factors that affect the viscosity measurement in this device are the specific rotational speed, the spindle type used, and the temperature of the sample to be examined, because all these parameters have a significant impact on determining the value of the viscosity must be used the same conditions when measuring the viscosity of a certain group of samples. Types of spindles are used to measure viscosity according to the range of viscosity values to be measured . The viscosity test was carried out in Laboratories of the Department of Polymers, University of Babylon, College of Materials Engineering according to ASTM D2197-16 [84].

3.6.3.3 Calculating of the Porosity

The porosity percentages were calculated for both samples conductive and insulation by means of test images Scanning Electron Microscopy (SEM) using the (Image J) software by determining the light areas, which are the coat material and the dark areas that are the pores and calculating the percentage of those areas. The (image J) sofware has been used in many fields, especially the medical field, in analyzing images to facilitate giving accurate results [85][86].

3.6.3.4 Coating Thickness Measuring

Using coating thickness guage meter of model TT260 from (Time company) in Laboratories of the Department of Polymers, University of Babylon, College of Materials Engineering according to ASTM D7091-22 [87].

A portable device that can measure quickly, is non-destructive and accurately measures the thickness of the coating. The device is adapted for measuring thickness in two ways (magnetic method) and (eddy current method) [87].

Magnetic method: work principle magnetic method consist of the probe which with magnetic metals formed a closed magnetic circuit during contact of the probe with the coating. Since the non-magnetic coating alters the magnetic resistance, the depth of the coating can be estimated using the magnetic resistance[87].

Eddy current method: principle of operation the probe coil produces an electromagnetic field when a high-frequency alternating current is present. Eddy current which will develop on the metal substrate so when probe and coating come into contact. The feedback on the coil in the probe is impacted by the alternating current. Measurement of the feedback's impact can be used to determine the coating's thickness. The second method (eddy current method) was used to test the

coating thickness of the conductive and insulation samples in this work, since the substrate used is non-magnetic (aluminum).

3.6.3.5 Ultra-Violet Visible (U.V) Test

The Ultra-Violet visible test. It is used in two spectrums, visible and ultraviolet, some time even a portion of the infrared spectrum. The occurrence of absorption and reflection is affected by the color of the chemical material and its transparency. Test U.V visible test within the spectroscopic limits of ultraviolet and visible rays, particles are exposed to electromagnetic rays in the visible and ultraviolet fields, resulting in the irritation of electrons and their transfer to higher energy levels [88]. The energy difference between the levels to which the electrons are transferred is due to the absorption of the energy of the photon, as in the equation below[89]:

$E=h.v=h.c/\lambda$ ... (3.5) at E=energy, h = Blanck constant, v = frequency, c= ligth velocity, λ =wavelength.

The Ultra-Violet visible test was carried out in Laboratories of the Department of Polymers, University of Babylon, in College of Materials Engineering.

The device that used in this test is UV- 1800 SHIMATZU Spectrophotometer. The device gives wavelengths ranges from (190 to 1100) nm [89]. The samples are in the liquid state (coating mixture) and the present solvent is used as a reference for measuring the coating mixture in the apparatus.

3.6.4 Thermal Properties Tests

3.6.4.1 Thermal Conductivity Test

To calculate the value of thermal conductivity used Lee Desk device .It consists of four metal discs (A, B, C, H) figure (3.7 a). The first (A) is a disc of copper, after it the place of the sample(S), and then another (B) disc of copper, and then a disc that is a heater (H), and finally disc of copper as well (C).

The principle of the device's work is to convert electrical energy into heat through the heated disk, and then heat is transmitted from the disk to the next disk until it reaches the last disk after a certain period of time. The temperatures are recorded on each disc (T_A,T_B ,T_C) by thermometers attached to the three discs.

And through special equations, the value of thermal conductivity (K) is calculated. The potential difference applied to the heater is (6) v and the current passing through it is (0.25) amp. The thermal conductivity test was performed by

Laboratories of the Department of Physics\ University of Technology, according ASTM C408-88 [90].

Thermal conductivity calculations using a Lee disk device [91]:

1- From the equation (٣.2) calculating the value of (*e*) which is the amount of heat passing through the unit area of the disk material per second of its units (w/m².˚C).

$$I.v = \pi r^2 e(TA+TB) + 2\pi re[ds\,TA + ds.1/2(TA+TB) + dB\,TB + dC\,TC] \quad \ldots\ldots (3.2)$$

I: passing current with unit (Amp), *v*: equipped voltages with unit (volt)

2- From equation (٣.3) we find the value of thermal conductivity (K) in units (w/m.˚C) after entering the value (*e*) obtained from equation (3.2).

$$K\,(TB-TA/ds) = e\,[TA+2/r(dA+1/4ds)TA+1/2r.ds.TB] \quad \ldots\ldots (3.3)$$

(TA, TB, TC) discs temperature (A, B, C) respectively in (˚C).

(dA, dB, dC) discs thickness (A, B, C) respectively about (12 mm) for each disc.

(ds) Sample thickness in (mm).

(r) Disc radius (20 mm) for each disc [91]. The table (3.8) below show the temperature values measured by the thermometer on each disk and the thickness measurement of each sample. Figure (3.7) b, illustrate the Lee disc device for thermal conductivity test.

Table (3.8) illustrates the temperatures (*TA, TB, TC*) on each disc and the thickness of each sample.

Samples NO.	*TA* (˚C)	*TB*(˚C)	*TC*(˚C)	*ds* (mm)
G0,S0	31	31.5	31.5	0.50
G1	27.5	28	28	0.80
G2	32	32.5	32.5	0.89
G3	33	33.5	33.5	0.93
G4	34	34.5	34.5	0.9
G5	36.5	37	37	0.9
S1	32	33.5	33.5	1.2
S2	25	27	27	1.06
S3	27.5	30	30	1.25
S4	32	35	35	1.33

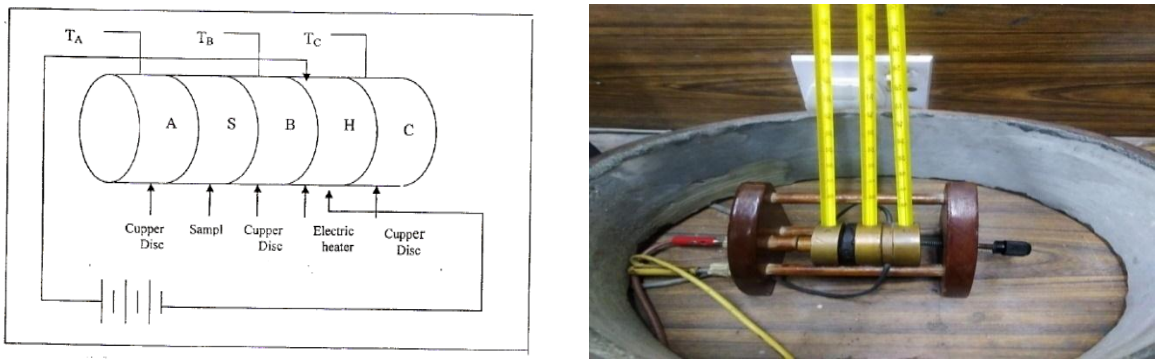

(a) (b)

Figure (3.7) Device of thermal conductivity test (a) Schematic showing discs Lee arrangement. (b) Disc Lee device.

3.6.5 Mechanical Properties Tests

3.6.5.1 Adhesion Strength Test

The adhesion test instrument is (PosiTest AT) , which measure coating adhesion to metal, wood, concrete, as well as other rigid substrates. The adhesion strength test was carried out in Laboratories of the Department of Polymers, University of Babylon, and College of Materials Engineering, according to the specification ASTM D4541[92]. The samples dimensions that can use in this device are (20, 50) mm diameter and (50*50) mm square. The (PosiTest AT) device used dollies by putting adhesive on the surface of the dolly and then sticking the dolly on the coat to check the adhesion strength. The test method is inexpensive because after cleaning the dolly surface; it can be used again. Before applying the adhesive, the surfaces of the coating and dolly must be cleaned well. Figure (3.8) the (PosiTest AT) device that used to measure the adhesion strength.

Figure (3.8) illustrate the (PosiTest AT) device for measure the adhesion strength.

3.7 Numerical Analysis

Numerical analysis is carried out by simulating using the ANSYS 16.1 software in analysis system which is fluid flow (fluent) on the surface of the absorber plate and heat exchanger tube before coating and after coating. The program installs ANSYS 16.1 from ANSYS Software Company and starts with a geometry building of flat plate solar collector (FPSC) that consists of four solid (which are heat exchanger pipe walls, absorber plate, coating layer and fluid) consider the fluid among the solid, according to the representations of the program, then makes mesh. From set up switch enters energy sources models, materials and the boundary conditions. The results are reviewed and the steps are detailed below.

3.7.1 Geometry Building

The model of (FPSC) is drawn using the capabilities of the ANSYS16.1 software and with the specified dimensions. Various shapes of heat exchanger cross-sections were tested and a semi-circle was selected for ease of work. The semicircle tube section is initially drawn with its specified dimensions, and then the absorber plate. After that the coating layer for the sample G5 is drawn have thickness (0.4mm). The geometry dimensions for (FPSC) are shown in table (3.9). Figure (3.9) shows geometry building by ANSYS 16.1 software.

Table (3.9) shows the dimensions of the geometry (FPSC).

Plate dimensions (mm)	External semicircle tube dimensions(mm)	Inner semicircle tube dimensions (mm)	Coating thickness (mm)	Distance between the arcs(mm)	total tube length (mm)
1500x1000x0.5	Diameter =25.4	Diameter =22.8	0.4	140	10400

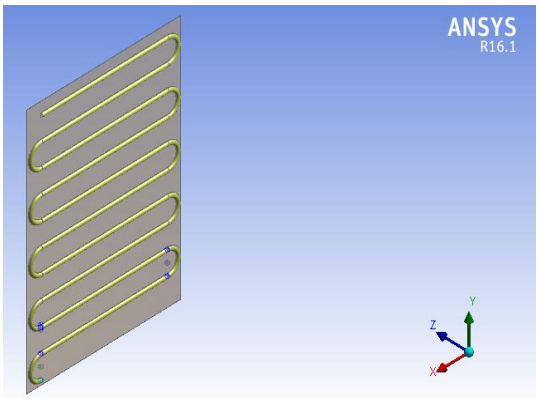

(a) Flat plate solar collector

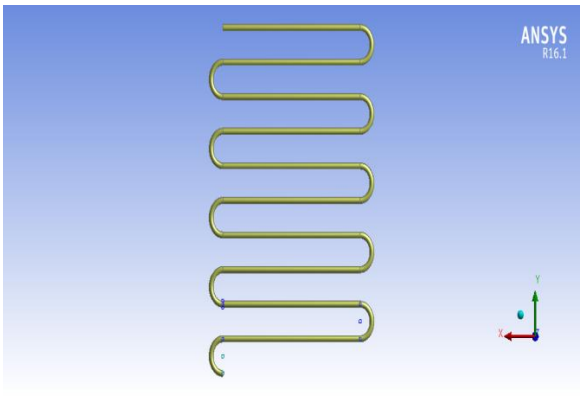

(b) heat exchanger tube

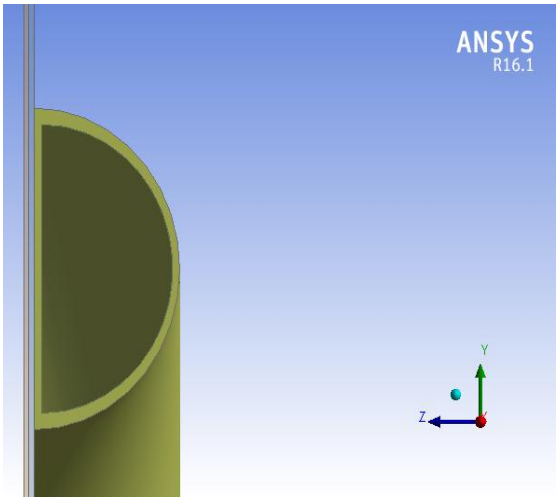

(c) coating layer, absorber plate and tube

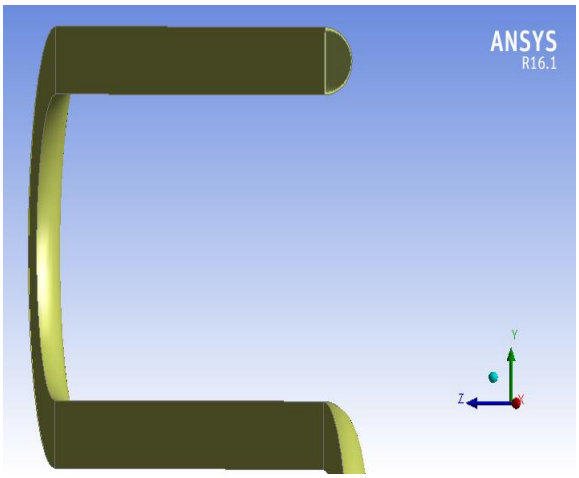

(d) cross section for tube

Figure (3.9) (a, b, c, d) Shown is the geometry construction of a flat plate solar collector by ANSYS 16.1 software features.

3.7.2 Meshing

In order to obtain a high accuracy in the simulation of the effect on the model, it must be divided into very small parts called elements and they are surrounded by nodes. The nodes are generated by the intersections of the dividing lines of the elements, which perform calculations using special equations for the program. The above partition process is called mesh. Make mesh with high accuracy to get good and perfect results.

Surfaces label: the surfaces of the geometry which are important in the work of the collector must be named as follows:

1- Coating: absorber plate coating layer.
2- Surface: absorber plate metal surface.
3- Out: fluid outlet flow.
4- In: fluid inlet flow. As showing in figure (3.10).

The distinction between solid and liquid was made from the Geometry window, then from the details of Body window, and from the option Fluid /Solid chose the Fluid in the case the body is fluid.

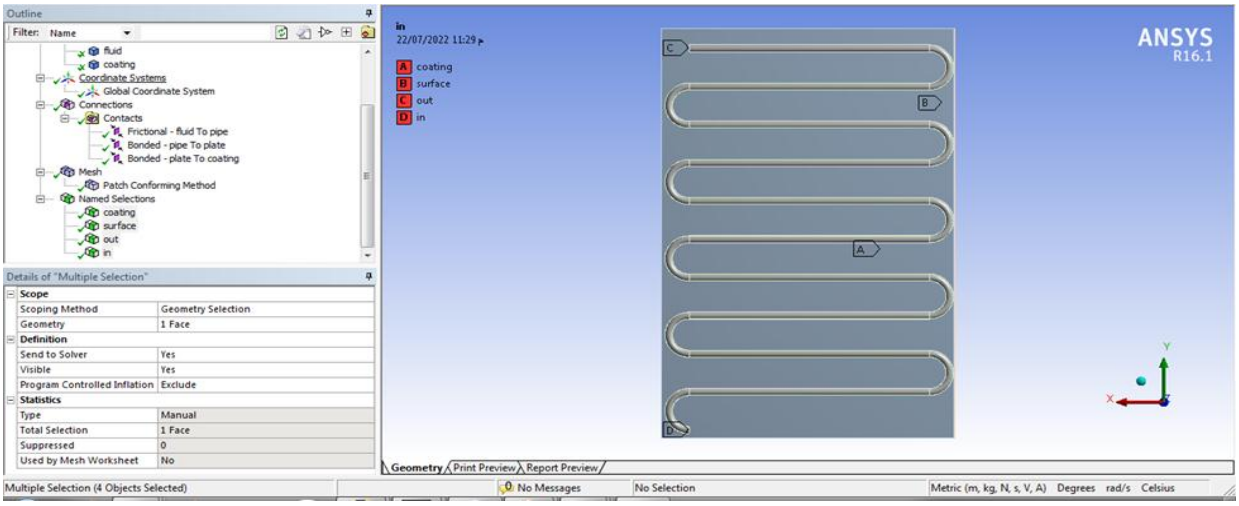

Figure (3.10) shows surface names for geometry.

Before doing meshing, the regions of contact between the existing solids must be determined. In this thesis, there are four solids that have been identified in the program, which are (heat exchanger pipe walls), (absorber plate), (coating layer) and (fluid), and there are three types of contact between them, which are as follows:

1- Contact frictionless between fluid and heat exchanger pipe internal walls.
2- Contact bonded between heat exchanger pipe external walls and absorber plate.
3- Contact bonded between absorber plate and coating layer.

The figure (3.11) (a, b, c) illustrates the contact regions between four solids.

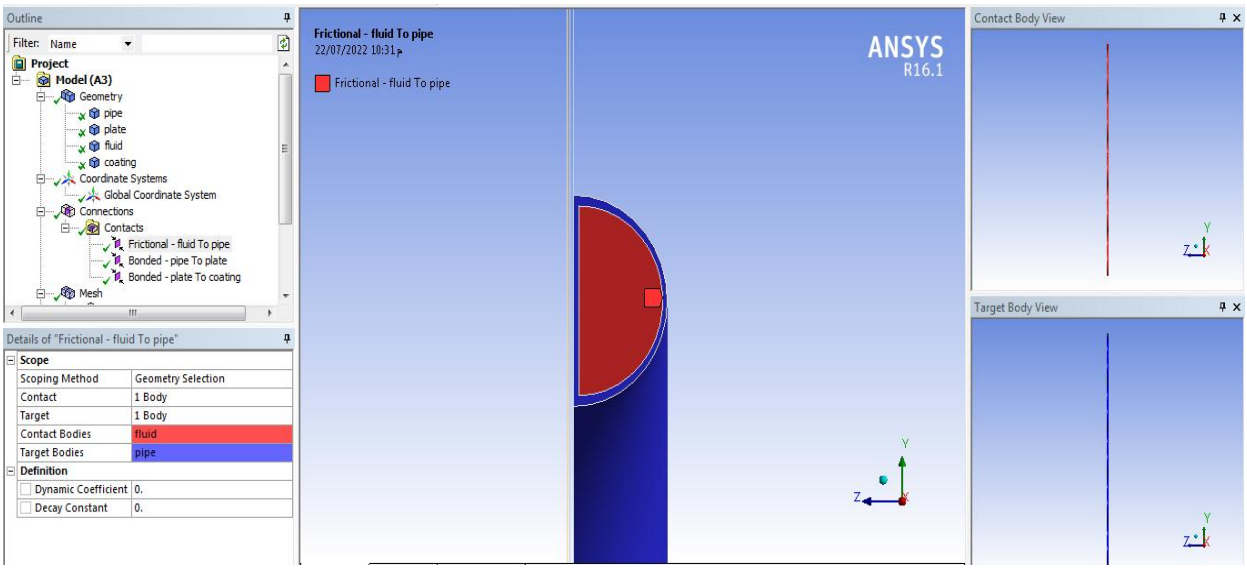

(a) the contact area between the inner walls of the tube and fluid.

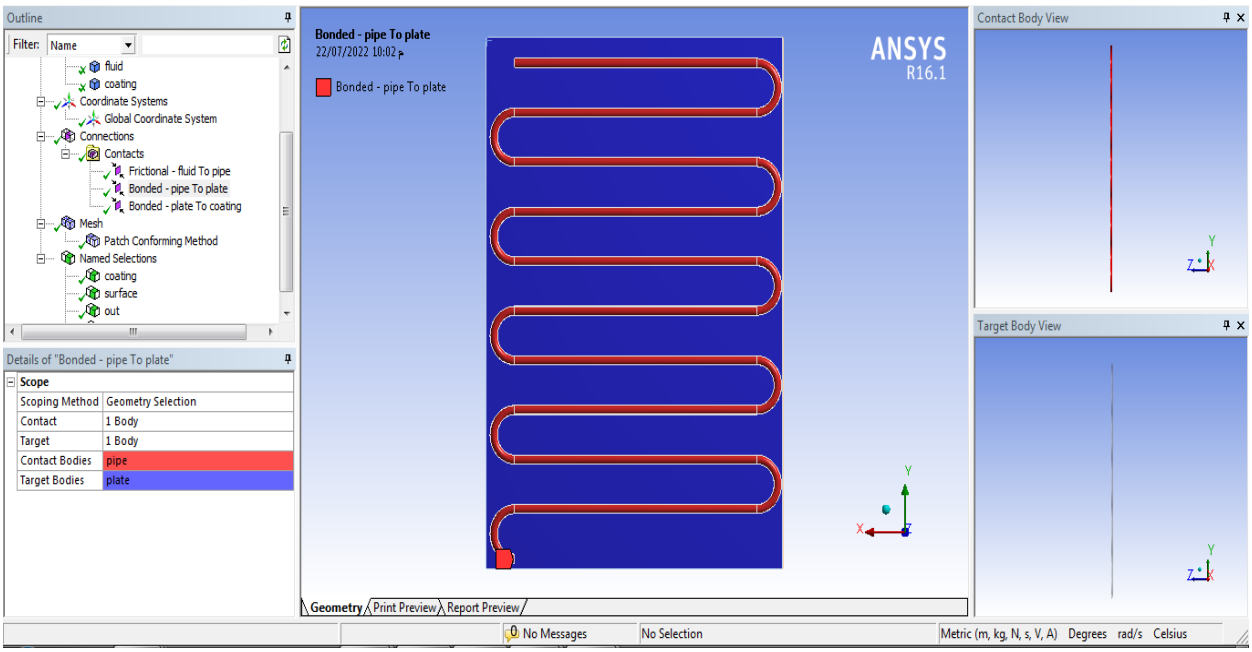

(b)the contact area between the tube and absorber plate.

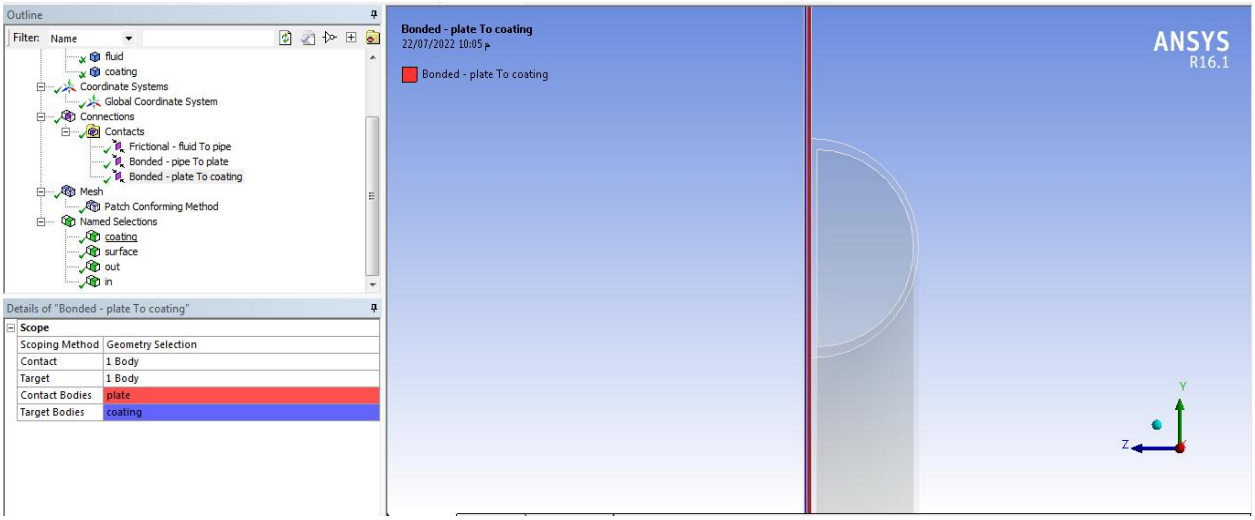

(c) the contact area between the coating layer and absorber plate.

Figure (3.11) (a, b, c) shows the regions of contact between the existing solids.

After completing the work of the shape of the contact regions and surfaces named of the solids, the mesh is applies and adjusts the program options as follows:

1- Mesh is done by insert, method and Tetrahedrons method.
2- The use of advanced size function (curvature: on).
3- The Relevance center : Fine
4- The Smoothing: High.

5- The Transition: Slow.
6- The Span angle center: Fine.
7- Total number of the mesh elements (634367) and the total number of nodes (186575). Figure (3.12 a, b, c, d) shows the mesh method.

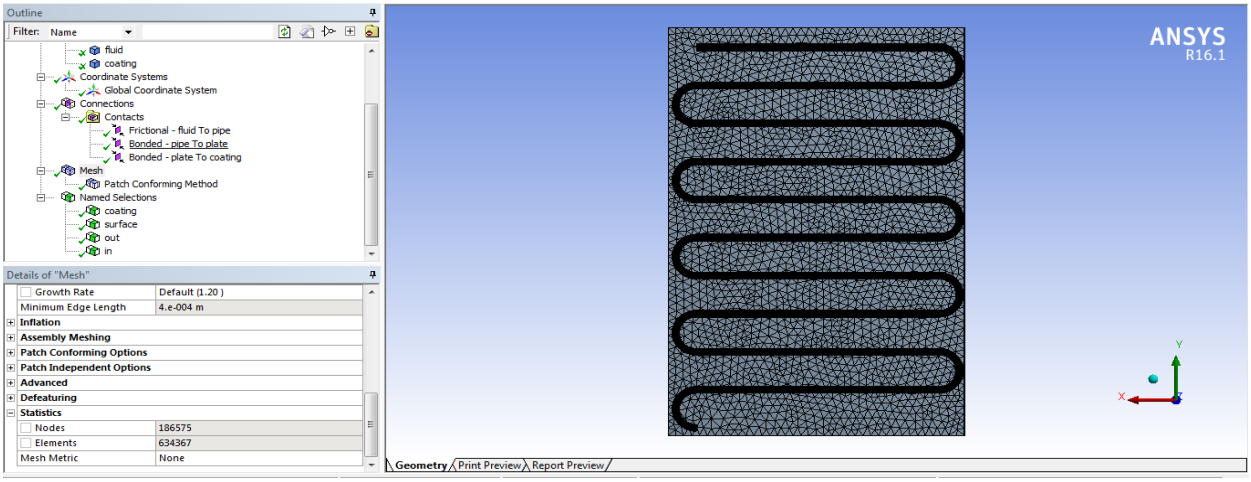

(a)The meshing for absorber plate and heat exchanger tube.

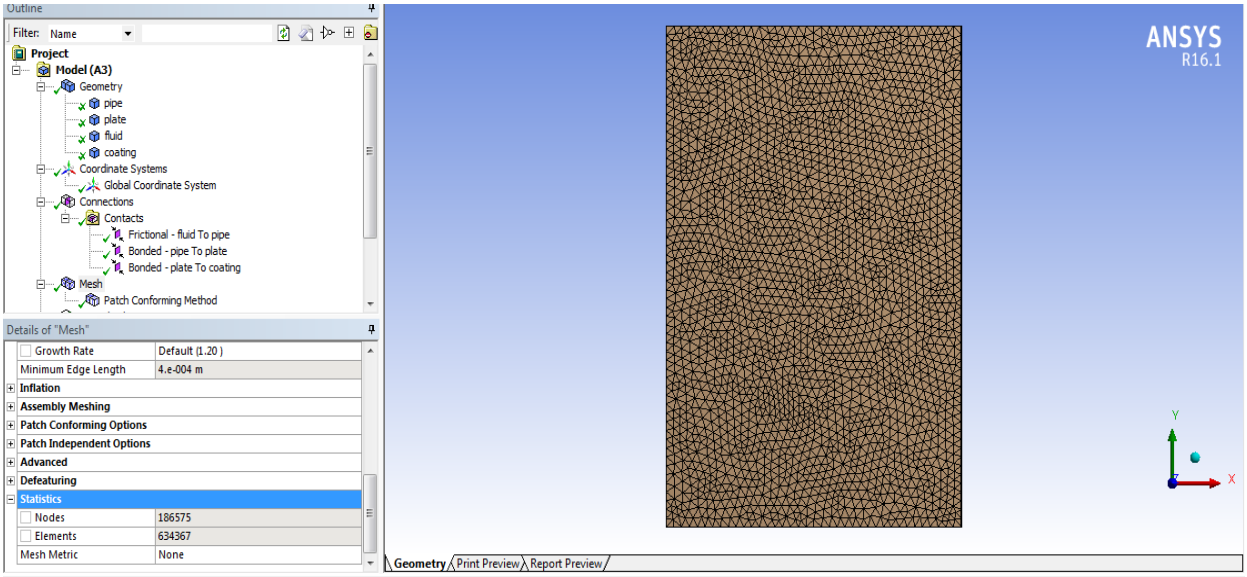

(b) The meshing for absorber plate and showing elements and nodes numbers.

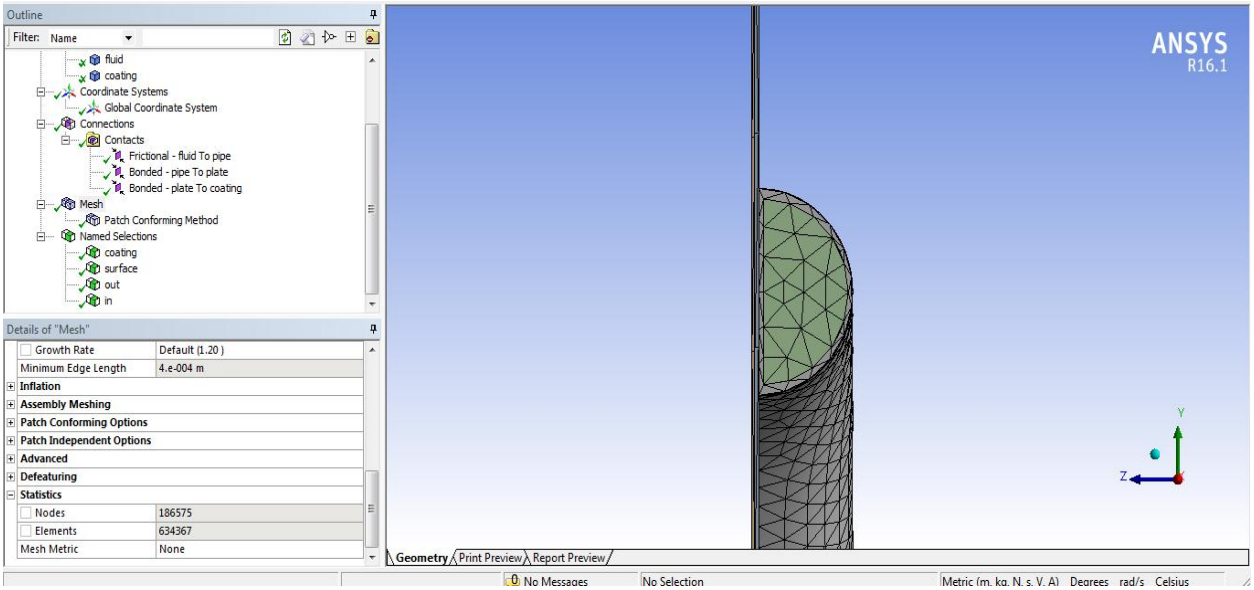

(c) The meshing shows cross section for heat exchanger tube.

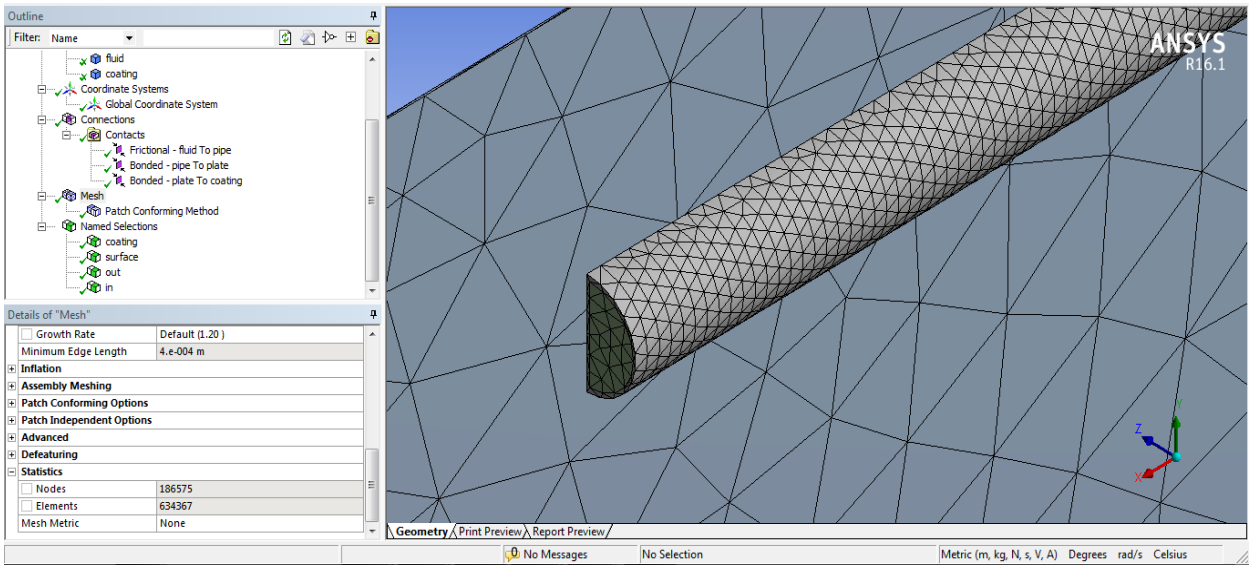

(d) The meshing for bonding place between absorber plate and heat exchanger tube.

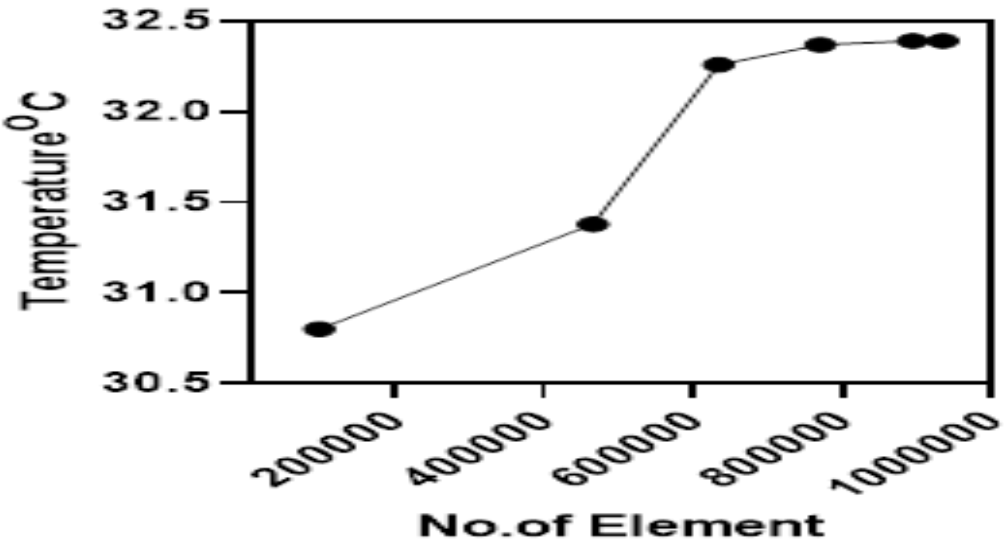

(e) shows the effect of the number of elements on the change in temperature.

Figure (3.12) (a, b, c, d) shows the construction of a mesh for the model of the flat plate solar collector,(e) shows relationship between number of elements and temperature

The optimization mesh generation can predict by numerically solution of random point until reach to excepted accuracy by increases the number of elements and decreases element size. The figure (3.12 e) above shows the relation between the number of elements and temperature of water inside pipe in ˚C for random point.

3.7.3 Entering Data and Calculating Results

Enter all the important data used in the software ENSYS 16.1 through the setup window and from the model as follows:

Energy

The energy switch: is on the opening (on).

Viscosity

From the viscosity option choose (k-epsilon), (standard) then (standard wall functions) and (curvature correction).

Radiation

Radiation model choose (Rosseland) and then from the option (solar ray tracing) enter the values of (Longitude) (Latitude) and (Time zone), and then choose from (mesh orientation) north and east according to the city in which the measurement is located. The data for longitude and latitude were entered for the city of Babylon, where the longitude is (44.4) and the latitude is (32.5)[93].

Materials

Enter the properties of the materials used in the experimental work, which are density, specific heat, thermal conductivity, and viscosity. The table (3.10) shows the materials properties that used in ANSYS16.1 software.

Table (3.10) illustrates the materials properties for aluminum and coating layer.

Materials	Density (ρ) kg/m³	Specific heat (Cp) J/kg.k	Thermal conductivity (K) w/m.k
Aluminum	2719	871	202
Coating	0.729	623	364.89

Boundary Conditions

Enter boundary conditions according to the data used in the experimental work, which are as follows:

The inlet: from the option thermal has the water inlet temperature (293k) and mass flow rate (0.05 kg/s). The direction specification method is Normal to Boundary.

Absorber plate: the heat source is generated by thermal radiation and is fixed on the surface at absorbance values (Direct visible=0.9) and (Direct IR=0.9). The thickness of the used aluminum plate (0.5mm) and the thickness of the coating layer (0.4mm) were entered.

Outlet: is outflow.

After entering the entire important data make (solution initialization) and then (Run calculation).

Coupling

For the purpose of defining interfaces surfaces between solids that lead to the production of proper heat transfer between the solid and fluid surfaces, the coupling option is implemented

Work coupling in order to connect the solid with the liquid by opening a window (Fluid flow fluent) and a window (steady state thermal). The Geometry is attached in both windows, that consist of solid and fluid after that open (mesh) and work (suppress) for the solid, and install the outer walls separating the fluid and the solid (interfaces). Then enter the window (set up) and from the option (boundary

condition) specifying the type of walls to (interface). The data entered in window (mesh interfaces) which is the mesh interfaces name, interface zone side1 and interface zone side2 and selection the option (coupled wall) and finally (create).

The figure (3.13) illustrate the coupling system method for ANSYS 16 software.

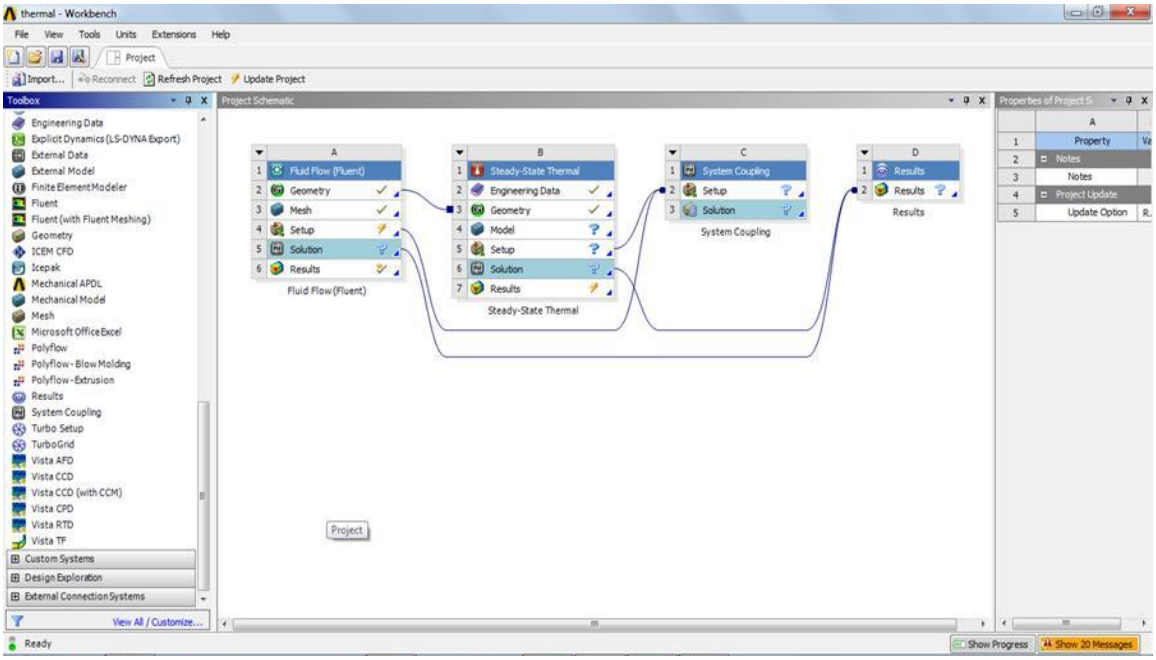

Figure (3.13) shows coupling system for ANSYS software.

CHAPTER FOUR

THE RESULTS AND THE DISCUSSION

Chapter Four

The Results and the Discussion

4.1 Introduction

The aim of this chapter is to assess the growth and development that take place on absorber plate after the coating process through a number of tests conducted on the coated samples and the coating mixture for both cases thermal conduction and insulation. The tests, conducted on coatings and powders, can be divided into six main groups: the first group characterization properties tests, the second group morphology properties tests, the third group is physical properties tests, the fourth group is thermal properties tests, the five is mechanical properties tests and finally, numerical analysis of the simulation for performed regions of heat concentration and fluid flow.

4.2 The Measurements

4.2.1 Characterization properties

4.2.1.1 X-Rays Diffraction (XRD) Test

Diffraction of X-rays for powders used in both thermal conductive and thermal insulating coatings to certain the purity and chemical composition of the compounds and elements.

(XRD) test for the powders used in coatings to increase thermal conductivity are graphite, Carboxymethyl cellulose (CMC), and copper powders in figures (4.1), (4.2) and (4.3) respectively. In the figure (4.1) graphite is according to the reference card (00-008-0415). The crystal system is hexagonal.

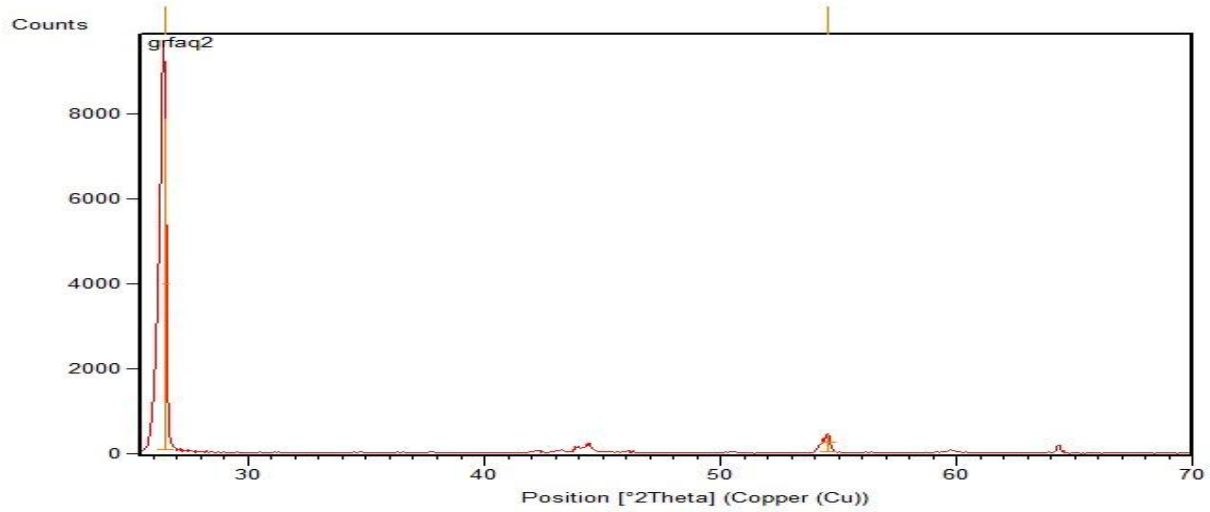

Figure (4.1) the (XRD) test analysis for graphite powder

In the figure (4.2) carboxymethyl cellulose material is observed according to the reference card (96-222-2008) with a chemical formula ($O_{24}C_{24}H_{48}$) the crystal system in the form Orthorhombic.

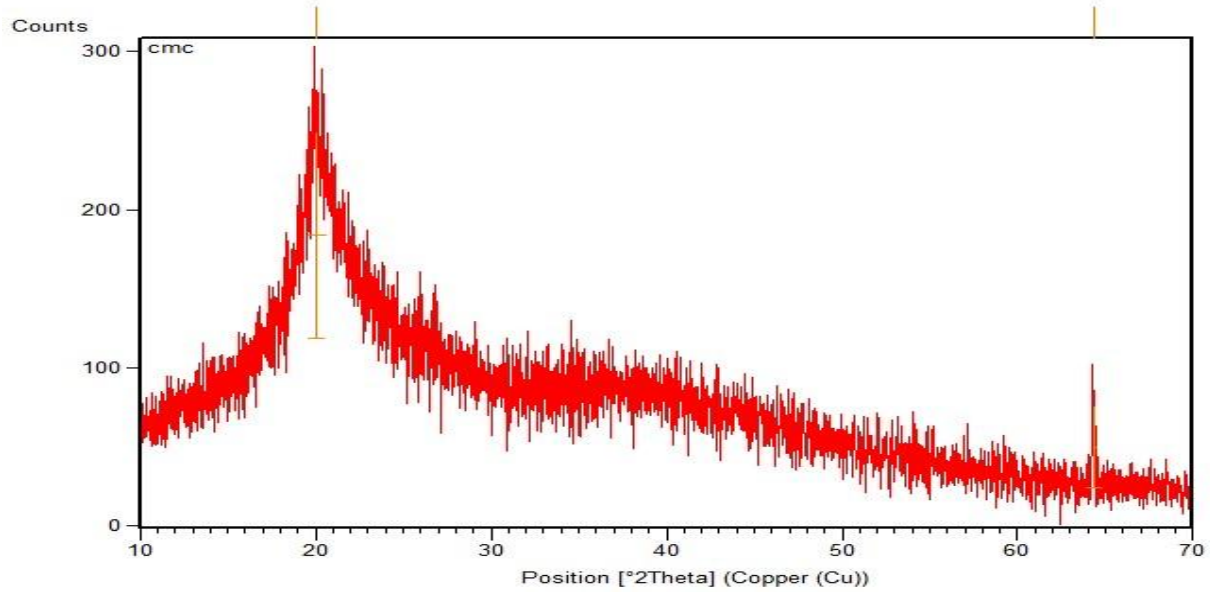

Figure (4.2) the (XRD) test analysis for Carboxymethyl cellulose (CMC).

In the figure (4.3) copper material is observed according to the reference card (00-003-1005) in a chemical formula (Cu) the crystal system in the form cubic.

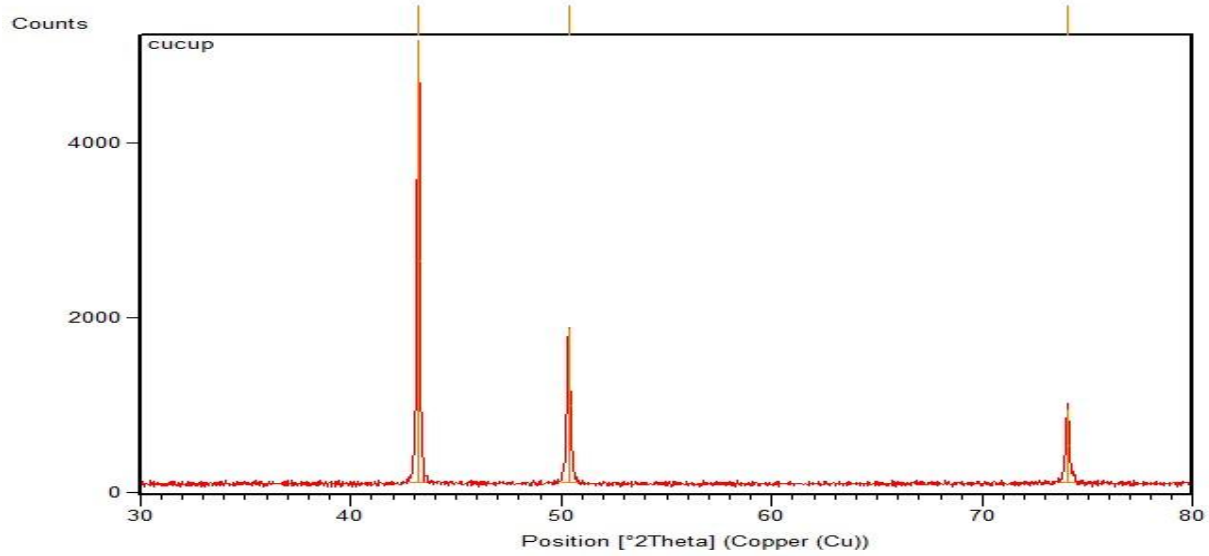

Figure (4.3) the (XRD) test analysis for copper powder.

The (XRD) test the powders used in coatings to increase the insulation are Mullite and Titanium dioxide in the figures (4.4) (4.5) respectively. In the figure (٤.٤) the material of Mullite (aluminum silicate) is observed according to the reference card (00-044-0003) in the crystal system in the form of Orthorhombic.

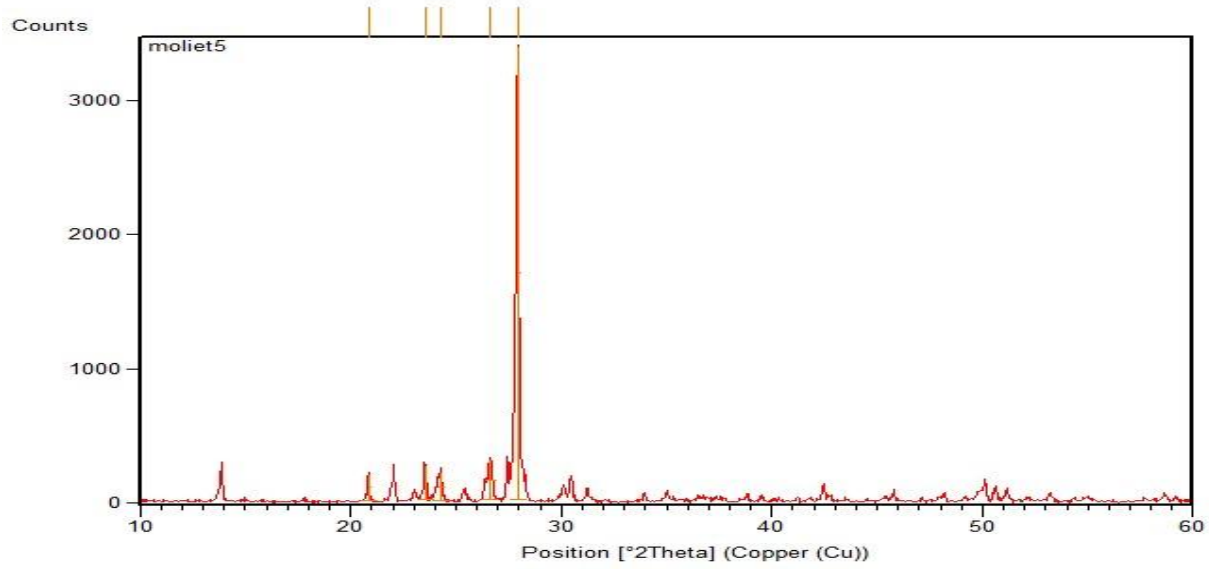

Figure (4.4) the (XRD) test analysis for Mullite powder.

In the figure (4.5) Titanium dioxide material is observed according to the reference card (01-089-4921) in a chemical formula (TiO2) ,Anatase phase the crystal system in the form tetragonal.

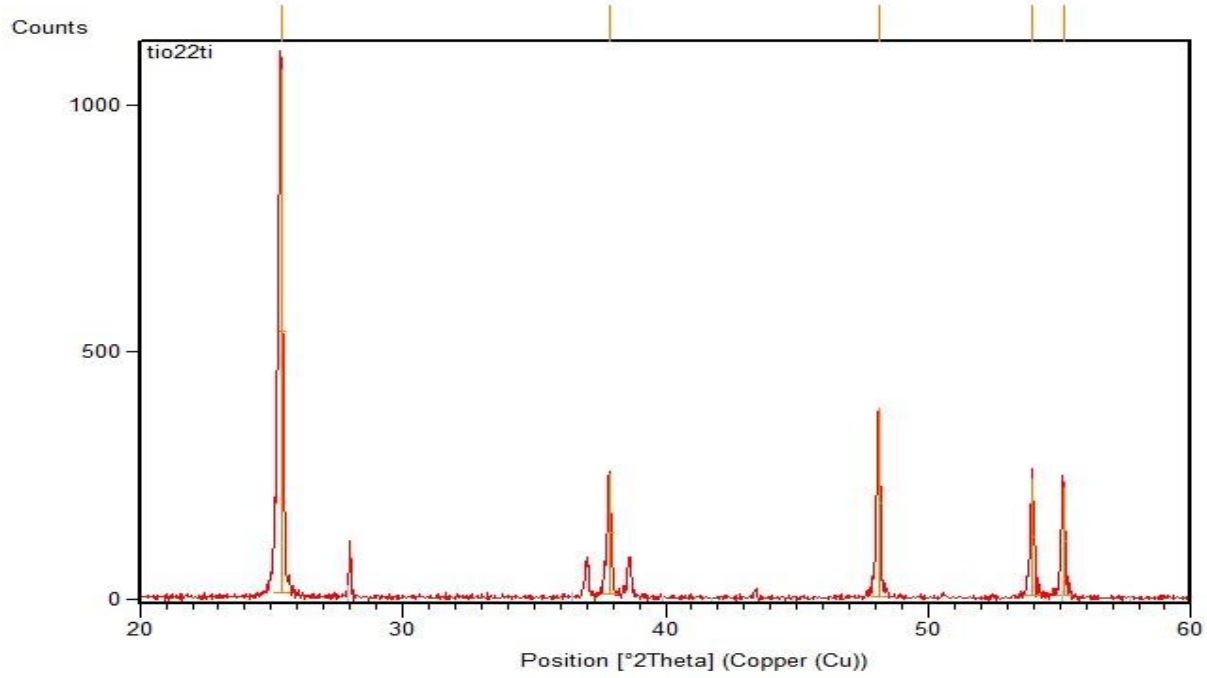

Figure (4.5) the (XRD) test analysis for TiO2 powder.

Examination X-Ray Diffraction (XRD) was conducted on three samples, two of the samples coated to increase thermal conductivity, namely (G1, G5) and one coated to increase thermal insulation (S4).

For samples that are coated to increase the conductivity, the analysis of (XRD) test noting the appearance of compounds consisting of carbon, oxygen and hydrogen resulting from carboxymethyl cellulose and graphite materials, which are ($O_8H_{12}C_8$) , the reference card (96-411-6151) and crystal system is monoclinic , the second compound is (O12C36H32) the reference card (96-223-6163) and crystal system is monoclinic as shown in the figure (4.6).

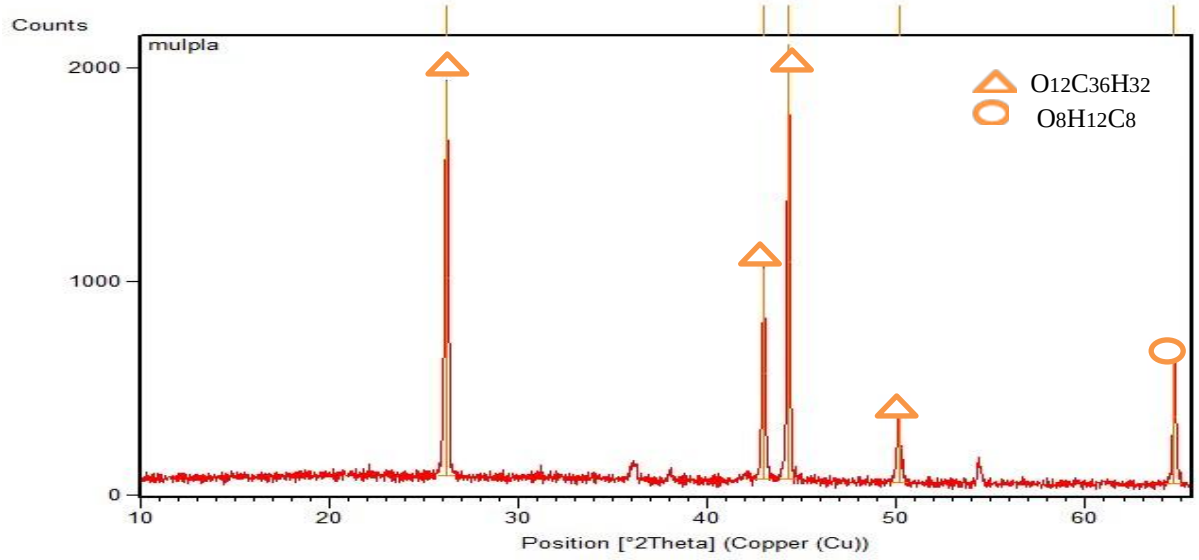

Figure (4.6) the (XRD) test analysis for sample G1.

While from the analysis of the XRD test noting the appearance of compounds consisting of carbon, oxygen, hydrogen and copper, resulting from carboxymethyl cellulose and graphite, and from the addition of percentages of copper, which are ($Cu_4O_{24}C_{72}H_{88}$), the reference card (96-722-0197), crystal system monoclinic the second compound ($CHCuO_2$) the reference card (00-014-0804), as shown in the figure (4.7).

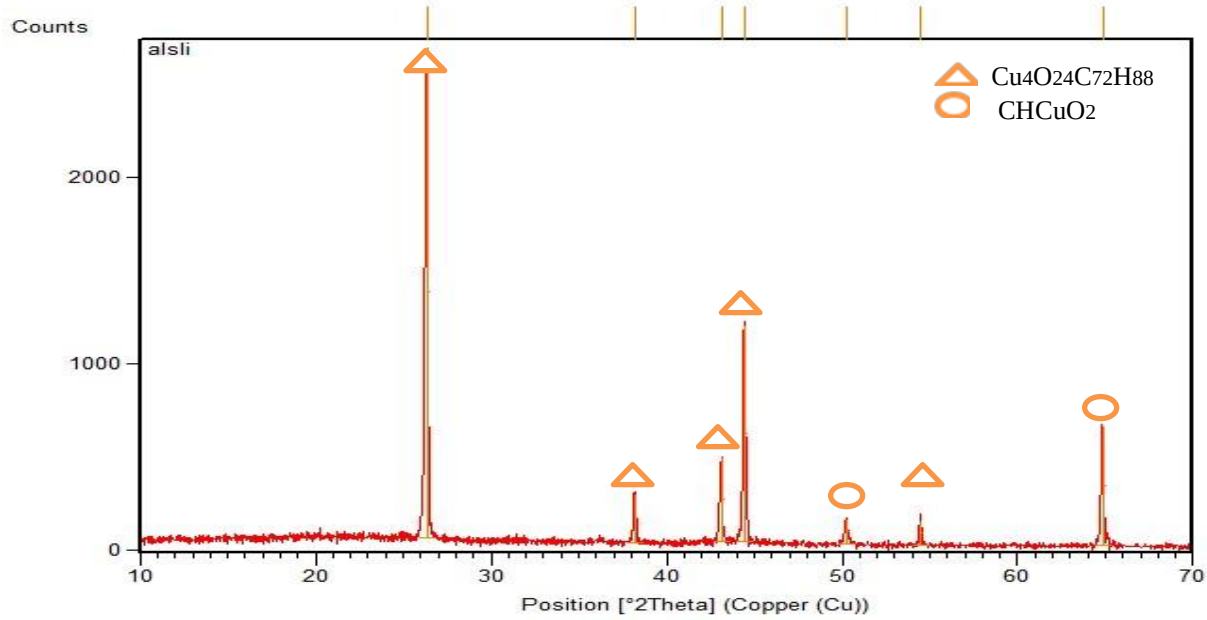

Figure (4.7) the (XRD) test analysis for sample G5 with name and formula for match cards.

The sample coated to increase the insulation the analysis of the XRD test of noting the appearance of compounds consisting of Aluminum Silicate, resulting from Mullite, and Titanium dioxide from adding proportions of it which are ($Al_{1.31}Al_{1.87}Si_{9.61}O_{24}$)$_{.93}$, the reference card (01-088-2286), crystal system cubic the second compound (TiO_2) the reference card (01-083-2242) crystal system tetragonal, as shown in the figure (4.7).

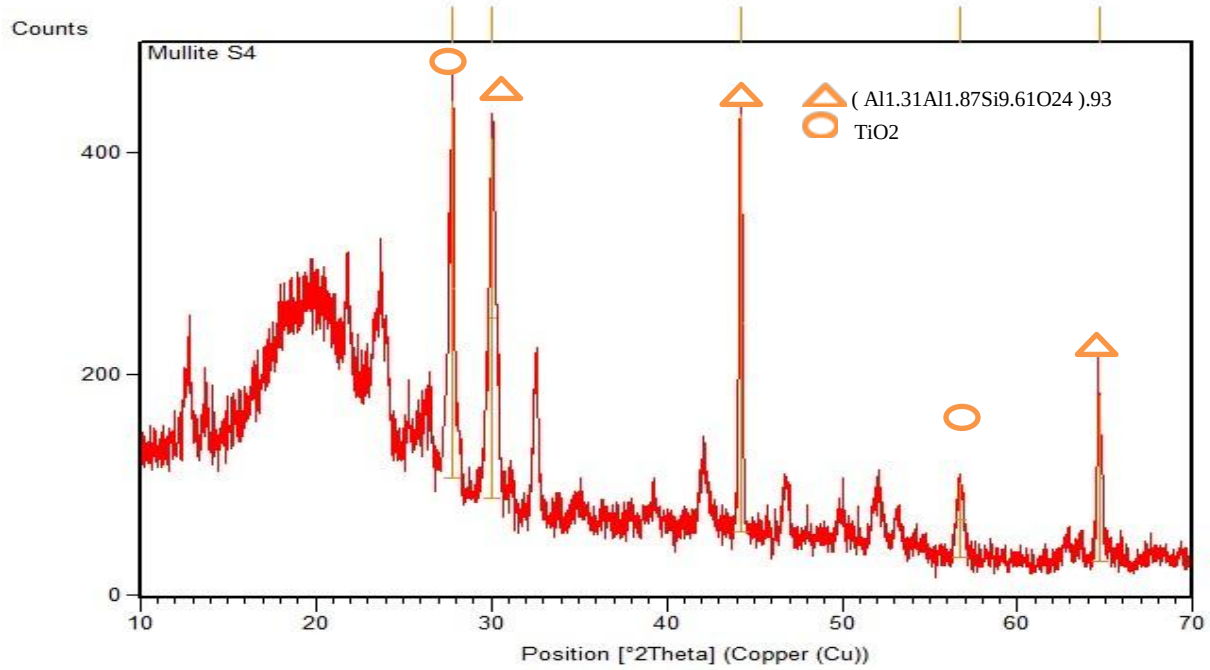

Figure (4.8) the (XRD) test analysis for S4 sample.

4.2.1.2 Fourier Transforms Infrared Spectrophotometer (FTIR)

From (FTIR) test, it is possible to obtain the absorption and transmission efficiency by the type of bond present for both conductive and insulating samples.

The conduction and insulation samples (G5), (S4) shows the number of peaks more than five peaks, and this indicates that the chemical analysis of a materials whose composition is complex. The extent of test (FTIR) used is mid IR spectrum and ranges from (600-4000) cm^{-1} is divided into four regions according to[94]:

First region have frequency reign between (2500-4000) cm^{-1} peaks appeared within three frequencies, which are (2592.33, 2885.51, 3425.58) cm^{-1} for the conduction sample (G5). The absorbance is inversely proportional to the transmittance and reflectivity and that is to note the expanding peak, which are (3425.58 cm^{-1}) with low transmittance values (1.85%). This indicates the

presence of high absorbance and a wide range. While a large number of peaks appeared in this range for insulation sample (S4) about eight peaks are (2522.89, 2683.62, 2854.65, 2924.09, 3024.38, 3155.54, 3448.72, 3873.06) cm^{-1} the presence of an expanding peak (3448.72 cm^{-1}) with a high transmittance value (3.15%) indicates a low absorbance compared to the conduction sample. The peaks appear in conduction and insulation samples in this range resulting from the (O-H) bonds [94].

The second region with frequencies (2000-2500) cm^{-1} of triple bonds, which is (C ≡ C) is produced by alkyne compounds. This region is characterized by high transmittance ranges, although the triple bond is weak, the conduction sample test shows six peaks of its frequencies are (2075.41, 2121.70, 2167.99, 2206.57, 2245.14, and 2468.88) cm^{-1}, while testing the insulation sample in this region, three peaks of their frequencies appear (2121.70, 2260.57, 2337.72) cm^{-1}. The triple bond is a diagnostic tool for the presence of absorption by organic compounds in this range of frequencies [94].

The third region (1500-2000) cm^{-1} doubles which are (C=C) (C=O) appear in the conduction sample (G4) three peaks of frequency are (1573.91, 1620.21, 1751.36) cm^{-1}. While the insulation sample (S4) five peaks of frequency (1597.06, 1658.78, 1720.5, 1874.81 and 1944.25) cm^{-1}. When the frequency of the peaks is above than (1775 cm^{-1}) to indicate active carbonyl group or ring carbonyl carbon, while the peaks frequency from (1700-1750 cm^{-1}) is simple carbonyl compounds, and between (1495-1615 cm^{-1}) aromatic rings. Double bonds are characterized by few vibrations compared to single bonds and lead to less absorbance [94]. The double bonds present in the insulation sample are more than the conduction sample (G4) and the result is less absorbance in the insulation sample (S4).

The fourth region is the fingerprint region (600-1500 cm^{-1}), in the conduction sample (G5) there is a strong signal at the frequency (1111.00) cm^{-1} resulted from Alkyl-substituted ether, C-O stretch, while the insulation sample shows strong signals at frequency (1280.73 cm^{-1}) resulting from C-O stretching aromatic ester. The transmission of the peak (1111.00 cm^{-1}) of the conduction sample is in the limits of (1.95%), while the transmission of the peak of the insulation sample (S4) (1280.73 cm^{-1}) is in the range of (3.10%), which means that the absorbance of the conduction sample is much higher than the absorbance of the insulation sample. The fingerprint region is specific to chemical show of a material utilized [94]. The

figure (4.9) represents the conduction sample (FTIR) test (G5) and the figure (4.10) shows (FTIR) test for the insulation sample (S4).

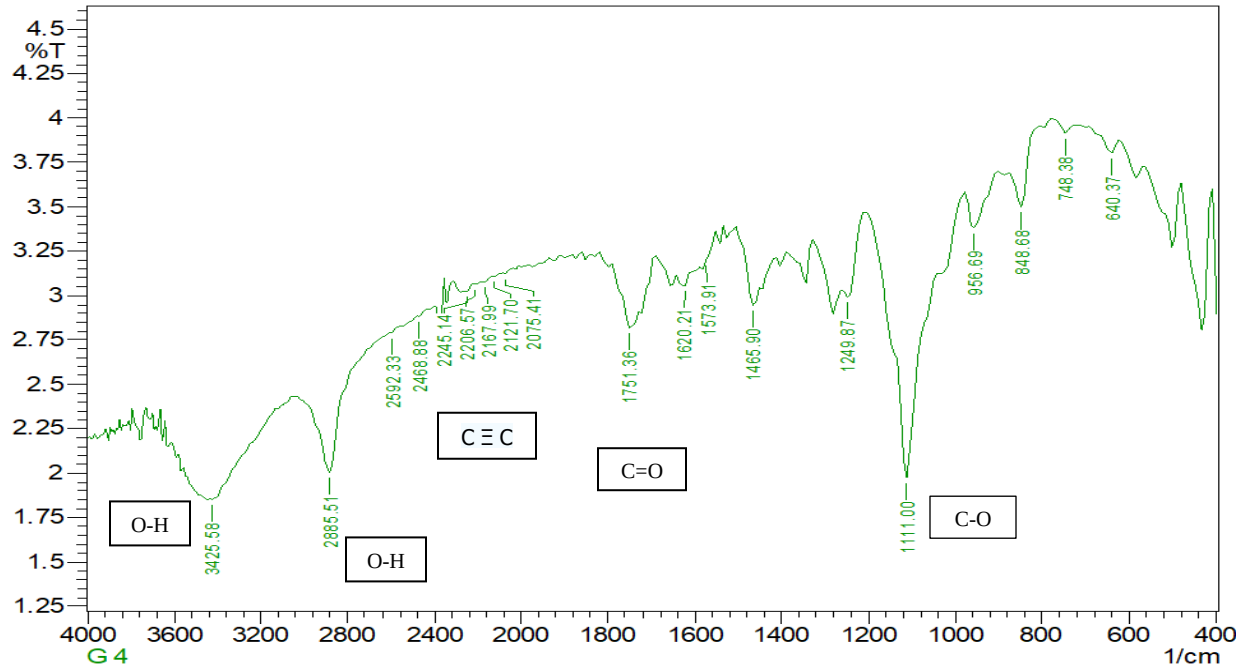

Figure (4.9) illustrate FTIR test for sample (G5)

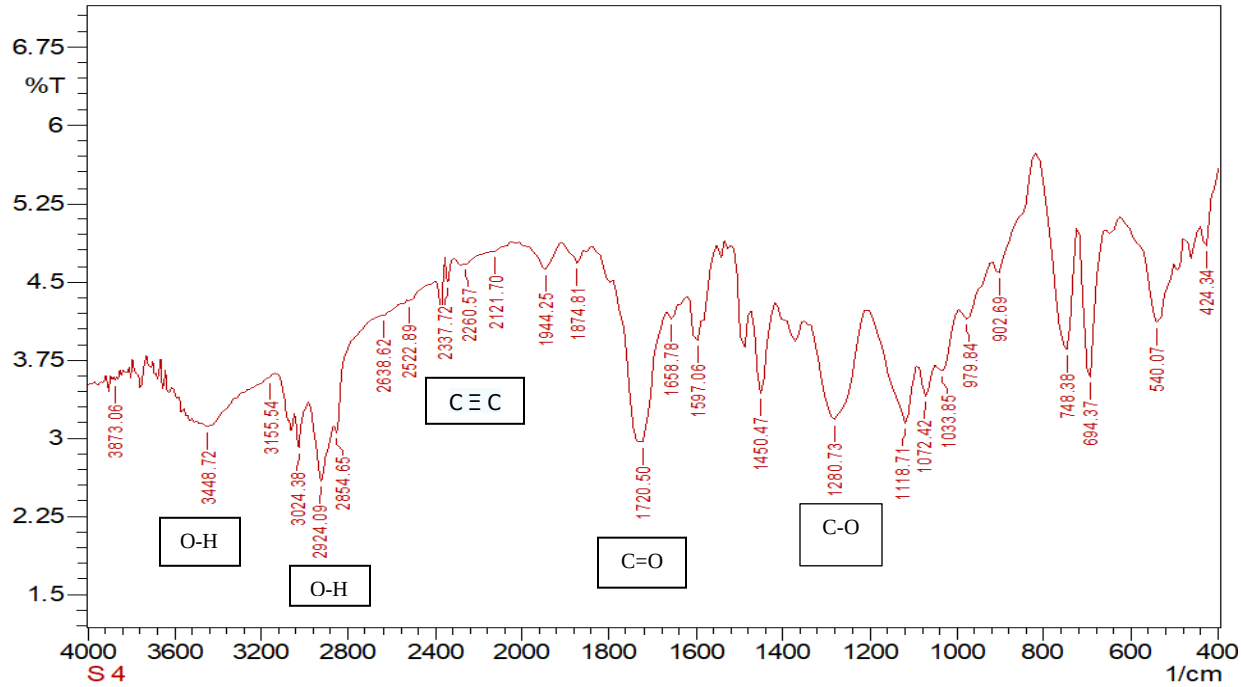

Figure (4.10) illustrate FTIR test for sample (S4).

4.2.1.3 Particle Size Analysis Test

The objective of the particle size analysis test is to know the sizes of the powders used, the gradation, distribution of their sizes and quantities.

The samples that were made for this test are in the form of powder, which are (Graphite, Copper, Mullite, Titanium dioxide).

The particle size analysis test for graphite powder material (C) showed that the average particle size is (D50= 25.74µm) and the surface area is (SSA=30.46 m²⁄kg), as shown in figure (4.11).

The particle size analysis test for copper powder material (Cu) showed that the average particle size is (D50= 12.04µm) and the surface area is (SSA=85 m²⁄kg) as shown in figure (4.12).

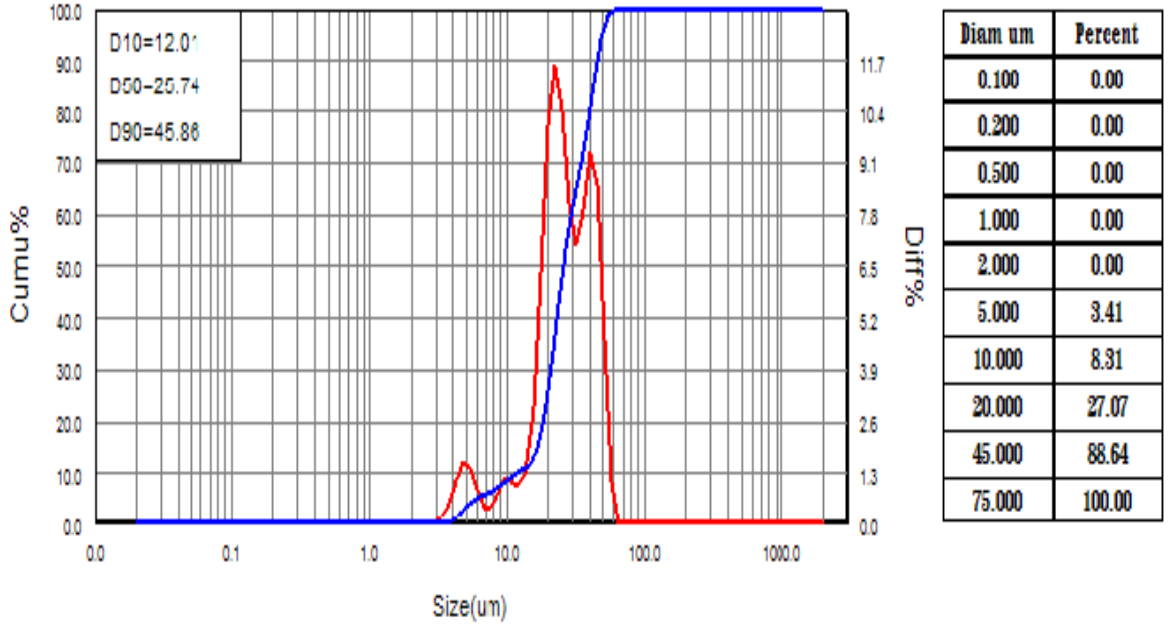

Diam um	Percent
0.100	0.00
0.200	0.00
0.500	0.00
1.000	0.00
2.000	0.00
5.000	3.41
10.000	8.31
20.000	27.07
45.000	88.64
75.000	100.00

Figure (4.11) show particle size analysis for graphite powder material.

The particle size of graphite powder is twice the particle size of copper powder, where the copper particles occupy the interspaces of the graphite particles, and this leads to an increase in the coating density and a reduction in the pores and gaps between the grains, the results of the density test and the SEM test confirm this.

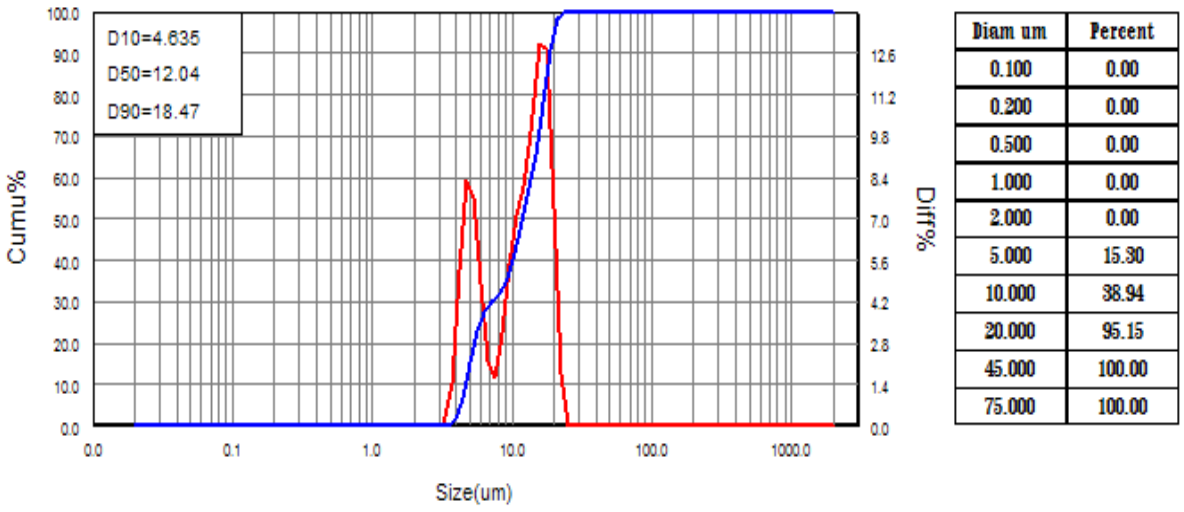

Diam um	Percent
0.100	0.00
0.200	0.00
0.500	0.00
1.000	0.00
2.000	0.00
5.000	15.30
10.000	38.94
20.000	95.15
45.000	100.00
75.000	100.00

Figure (4.12) show particle size analysis for copper powder material.

The particle size analysis test for Mullite powder material (3Al2O3.2SiO2) showed that the average particle size is (D50=9.488µm) and the surface area is (SSA=155.9 m²⁄kg) as shown in figure (4.13).

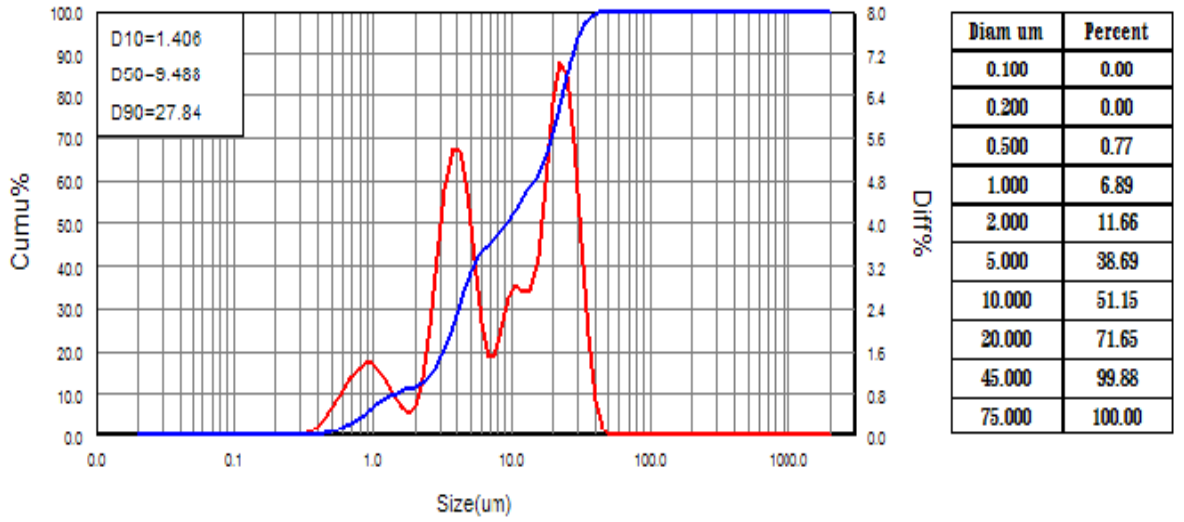

Diam um	Percent
0.100	0.00
0.200	0.00
0.500	0.77
1.000	6.89
2.000	11.66
5.000	38.69
10.000	51.15
20.000	71.65
45.000	99.88
75.000	100.00

Figure (4.13) show particle size analysis for mullite powder material.

The particle size analysis test for Titanium dioxide powder material (TiO2) showed that the average particle size is (D50= 0.302µm) and the surface area is (SSA=1922 m²⁄kg) as shown in figure (4.14).

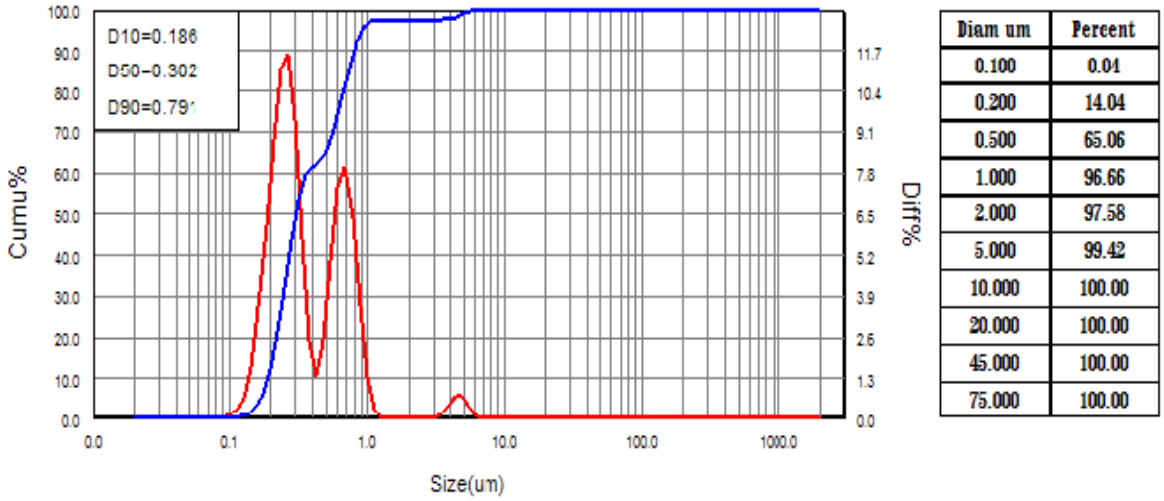

Diam um	Percent
0.100	0.01
0.200	14.04
0.500	65.06
1.000	96.66
2.000	97.58
5.000	99.42
10.000	100.00
20.000	100.00
45.000	100.00
75.000	100.00

Figure (4.14) show particle size analysis for TiO2 powder material.

The size of the Titanium dioxide particles is much less than the size of the Mullite particles and this is the reason for the aggregation of the titanium dioxide particles around the surface of the Mullite particles, resulting in the formation of large spaces and pores and a decrease in the density of the coating, the results of the density test and the SEM test confirm that.

4.2.2 Morphology Properties Tests

4.2.2.1 Scanning Electron Microscope (SEM) Test

Scanning Electron Microscope (SEM) test was conducted on samples coated to increase thermal conductivity and samples coated to increase thermal insulation.
The test images of the samples to increase the thermal conductivity showed the coating layer consisting mainly of graphite and grains of copper powder dispresed on the coating layer. The coating layer of the conduction samples is shown in the images and the cross-section image of a layer of coating with a high density and few pores. The test (SEM) is carried out on samples (G1) containing only graphite with Carboxymethyl cellulose (CMC) and samples (G4, G5) containing graphite, Carboxymethyl cellulose (CMC) and percentages of copper powder. The images show the presence of large ripples (high roughness) and large proportions of cavities increases the surface area and as a result increases the absorption of solar radiation falling on the coating. Figures (4.15), (4.16) and (4.17) showing SEM images for conductive samples. Figure (4.17) represents cross-section images of conduction sample.

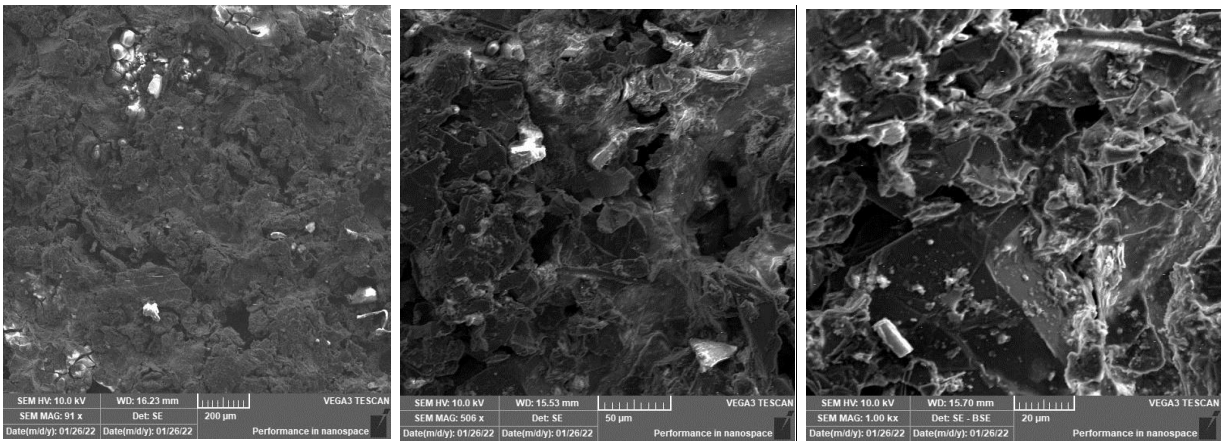

(a) (b) (c)

Figure (4.15) the SEM test for conductive sample G1 (a) MAG 91 X (b) MAG 506X (c) MAG 1000X.

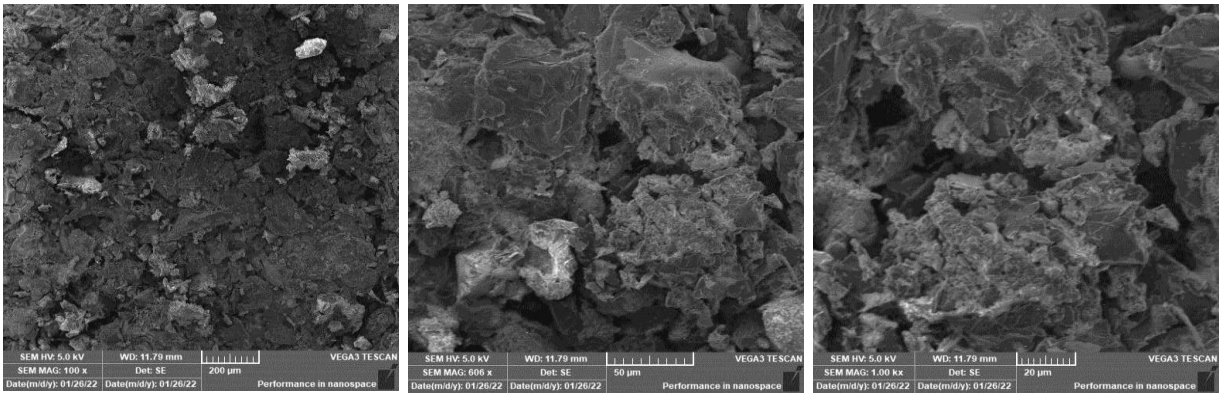

(a) (b) (c)

Figure (4.16) the SEM test for conductive sample G5 (a) MAG 100 X (b) MAG 606X (c) MAG 1000X.

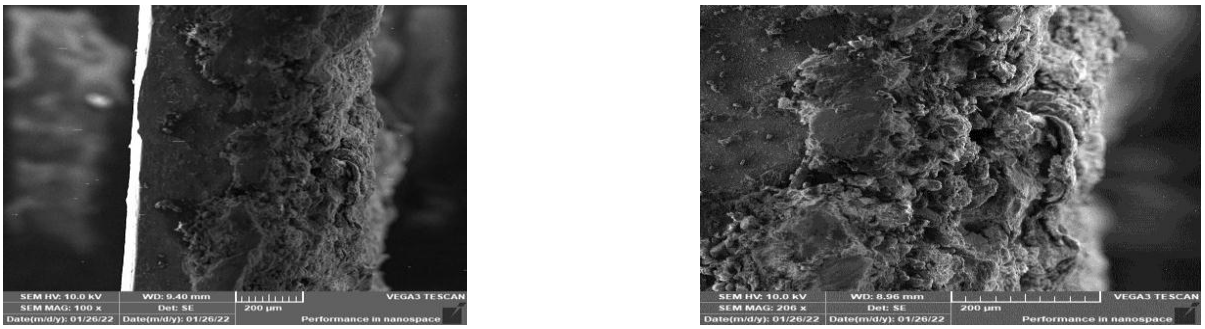

(a) (b)

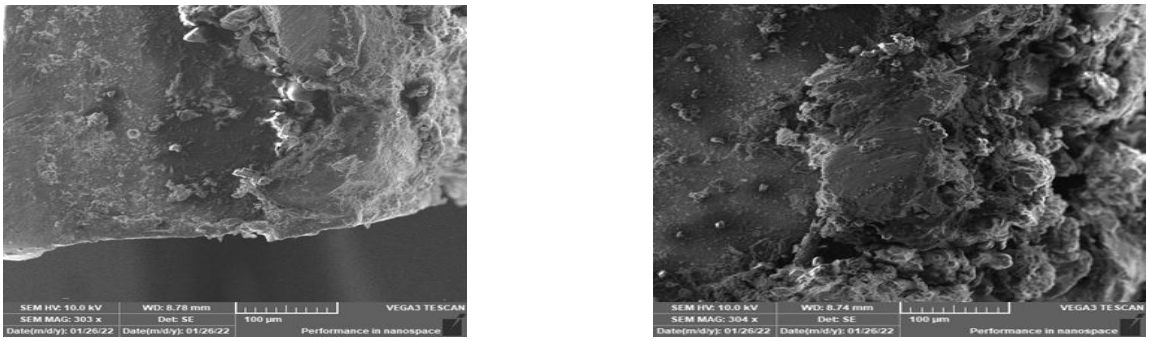

(c) (d)

Figure (4.17) the SEM test for cross section of conductive sample G4 (a) MAG 100X (b)MAG 206X (c)MAG 303X (d) MAG 304X.

While the coated samples to increase thermal insulation the SEM test images of the insulation samples (S2), (S3) and (S4) showed that the insulating coating layer contains a high percentage of pores. The SEM test showed white spots indicating Titanium dioxide and the matrix is a mixture of Mullite and Polystyrene. The formed pores contain air or hydrocarbon gases, whose thermal insulation is higher than most solid insulating materials. As a result, when there are high percentages of porosity, the insulation increases to high values. Cross-sectional images for test (SEM) of samples coated with insulating coating which show that they contain a large percentage of pores. Figures (4.18), (4.19) and (4.20) showing SEM images for insulation samples. Figure (4.20) represents cross-section images of insulation sample.

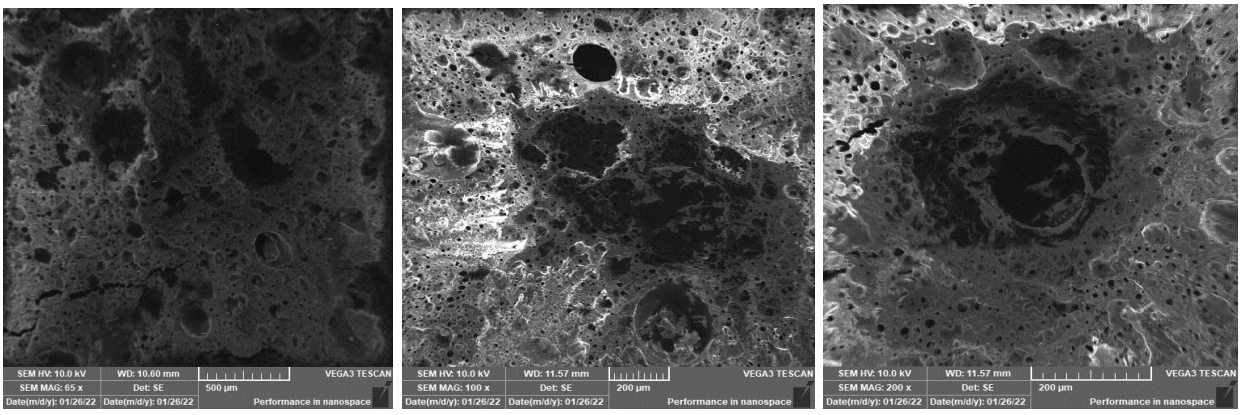

(a) (b) (c)

Figure (4.18) the SEM test for insulation sample S2 (a) MAG 65X (b)MAG 100X (c)MAG 200X.

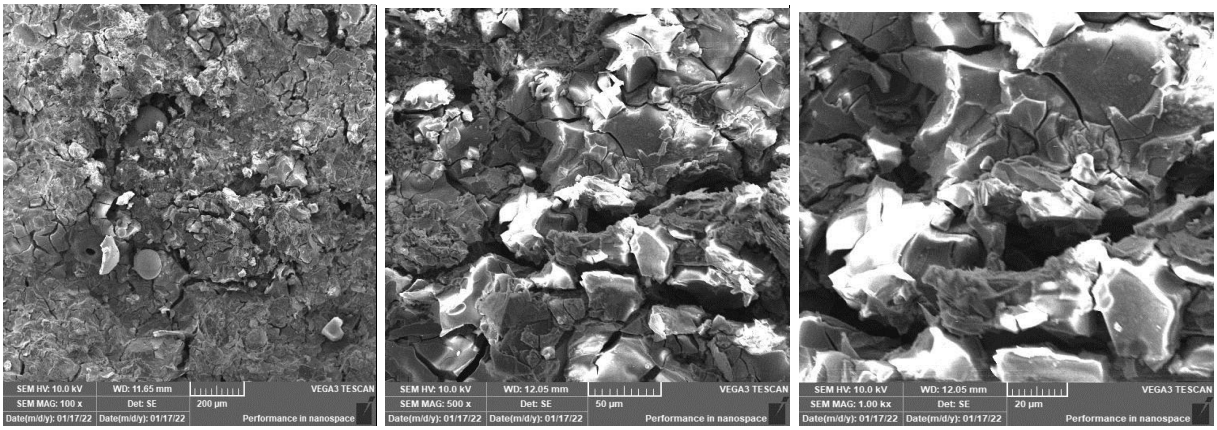

(a) (b) (c)

Figure (4.19) the SEM test for insulation sample S3 (a) MAG 100X (b) MAG 500X (c) MAG 1000X.

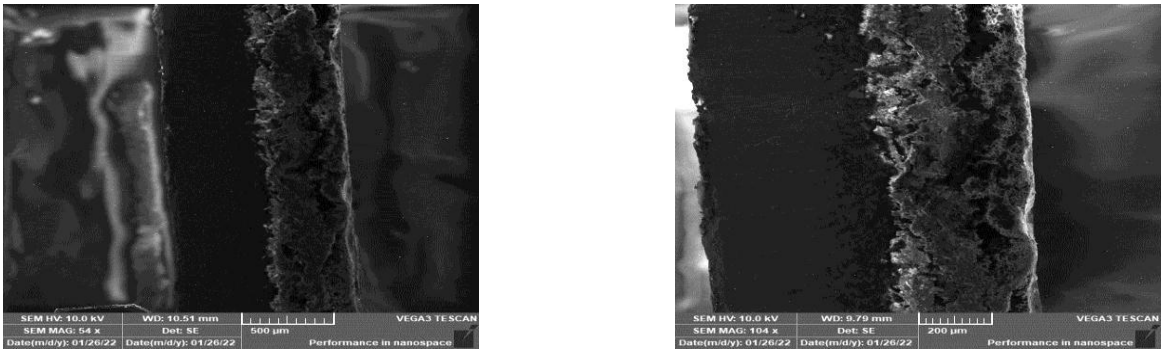

(a) (b)

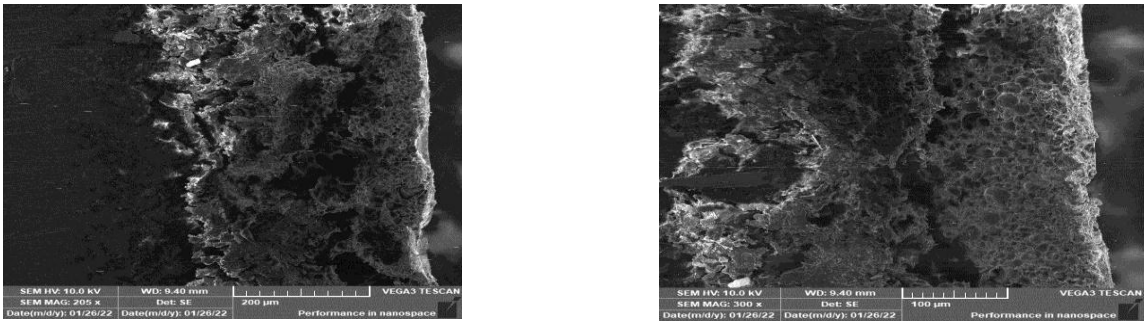

(c) (d)

Figure (4.20) the SEM test for cross section of insulation sample S4 (a) MAG 54X (b)MAG 104X (c)MAG 205X (d) MAG 300X.

4.2.2.2 Atomic Force Microscopy Test (AFM)

The purpose of this test is to give an indication of the surface morphology and surface roughness that have the large effects on the absorptivity and thermal conductivity. The AFM test is performed for samples coated to increase thermal conductivity, and samples coated to increase thermal insulation.

The roughness average for conductive sample (G5) that contain higher ratios of graphite and copper powder is (44.5 nm) larger from the insulation sample that contain higher ratios of Mullite and TiO2 powders (S4) and has roughness average (5.81nm). When the surface roughness is high the surface area is large [95].The different between the roughness averages indicates when high roughness the absorptivity increase as a result, it leads to an increase in thermal conductivity, while the low roughness (smooth) the reflection increase while the absorptivity and thermal conductivity decrease. Figure (4.21) illustrate (AFM) tests three dimension for both samples conductive and insulation.

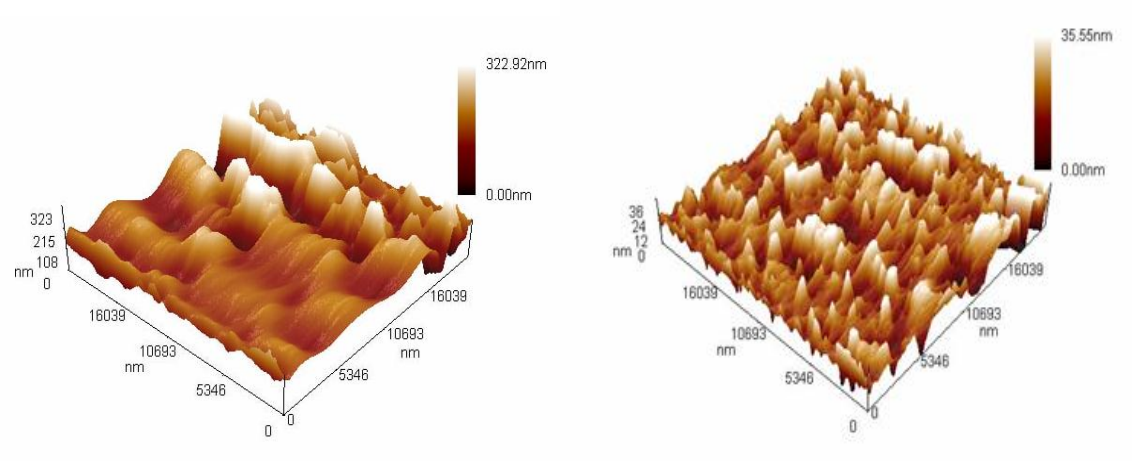

(a) (b)

Figure (4.21) Illustrate (AFM) tests (a) (AFM) test three dimension for (G5) conduction sample. (b) (AFM) test three dimension for (S4) insulation sample.

The high roughness of the samples coated to increase the thermal conductivity results from the components of the coating materials, which are mainly graphite grains, that leads to an increase in the surface area of the coating exposed to sunlight, thus increasing the absorptivity , thermal conductivity and reducing the reflectivity as in figure (4.21)(a) image three dimension. Figure (4.22) shows the (AFM) test in the two dimensions for conductive sample (G5).

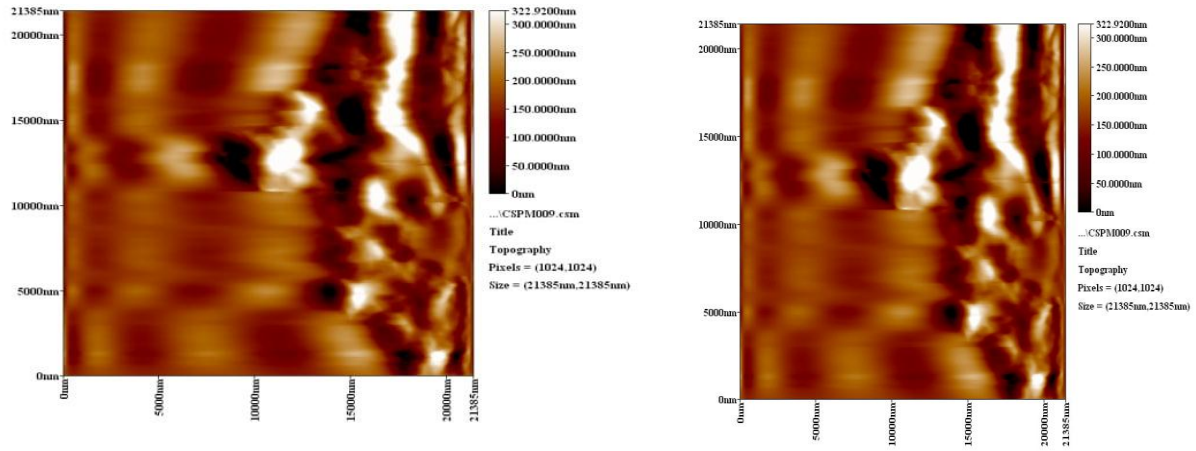

Figure (4.22) illustrate two dimension (AFM) test for (G5) sample.

While the sample that is coated to increase thermal insulation (S4) has a small surface roughness of the coating compared to the conductive sample (G5), as shown in figure (4.21)(b) image the three dimension, a small surface roughness of the coating means a small area exposed to sunlight. This is due to the components of the coating materials, which consists mainly of Mullite and Titanium dioxide. Mullite acts as a thermal barrier to the thermal solar radiation [12], while Titanium dioxide increases the reflectivity of the solar rays beam [69]. Figure (4.23) shows (AFM) test in the two dimensions for insulation sample.

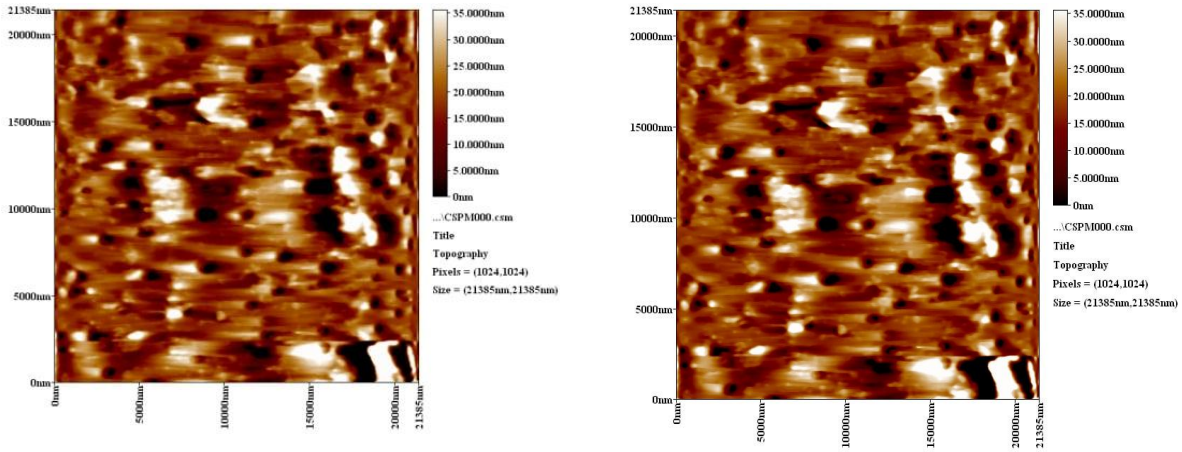

Figure (4.23) illustrate two dimension (AFM) test for (S4) sample.

4.2.3 Physical Properties Tests

4.2.3.1 Density Test

Measurement of the density of dry coating for conduction samples was the coating density of the sample (G1) is (0.687kg/m³) and the coating density of the sample (G5) is (0.729kg/m³). Measurement of coating density of insulation samples, coating density of the sample (S2) is (0.335 kg/m³) and coating density of the sample (S4) is (0.317 kg/m³).

The density of the conduction sample (G5) is higher than (G1) because it contains a small percentage of porosity. Figure (4.24) shows the relationship between density and thermal conductivity for conductive samples. Thermal conductivity was found to increase with density from (0.2 to 1 w/m. k) for densities from (1.1 to 2.3 g/cm³) due to increase surface contact between particles as found in the source [96]. The density of the insulation sample (S4) is less than (S2) because it contains a high percentage of porosity, so the thermal insulation of the sample (S4) is higher than the sample (S2). Figure (4.25) shows the relationship between density and thermal conductivity for insulation samples.

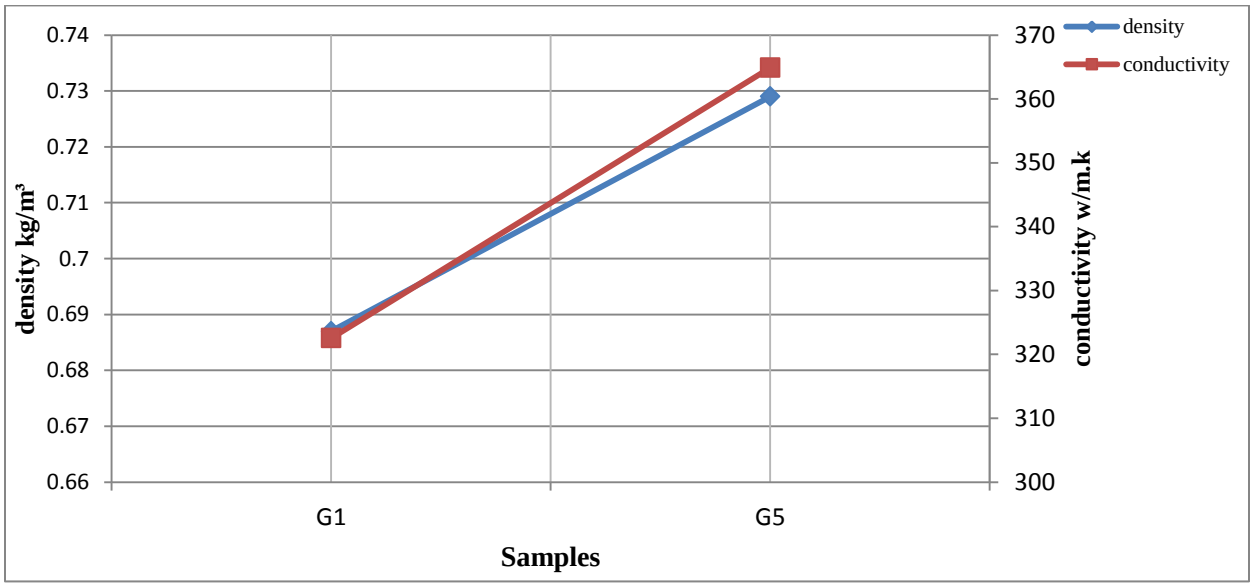

Figure (4.24) shows the effect of density on thermal conductivity for conductive samples.

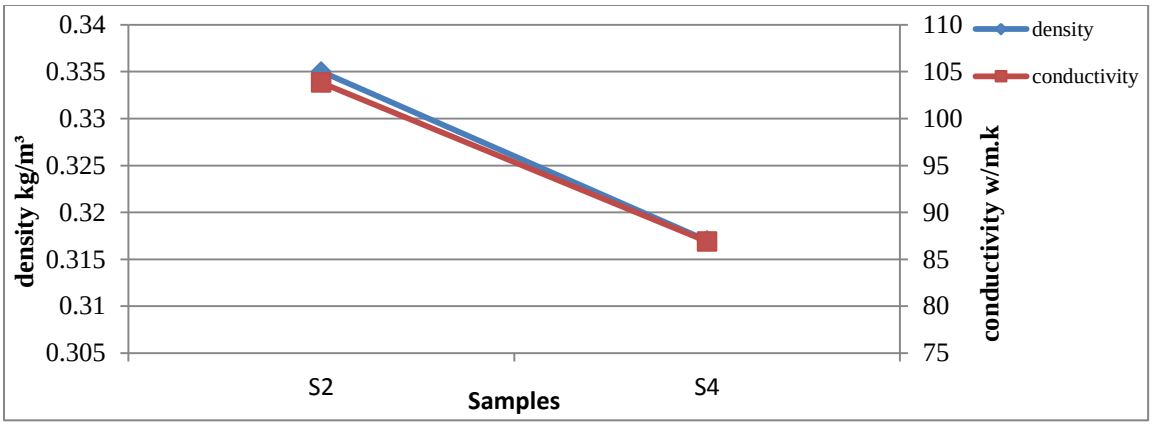

Figure (4.25) shows the effect of density on thermal conductivity for insulation samples.

The density of the coating mixture is measured in liquid state for samples coated to increase thermal conductivity (G1) and (G5) are (1.0387 kg/m³) and (1.0719 kg/m³) respectively. The increase in the sample density (G5) is due to the addition of percentages of copper powder. The density of the coating mixture is measured in liquid state for samples coated to increase the thermal insulation (S2) and (S4) are (1.1442 kg/m³) (1.2177 kg/m³) respectively. The increase in the density of the sample (S4) is due to the increase in the proportions of Mullite and Titanium dioxide from 1% to 5%. The difference of solvents for the mixture and materials used (ratios of polymeric materials) of samples coated to increase thermal conductivity and thermal insulation is an important factor in the installation of the final coating structure and the formation of pores after the coating mixture dries. Figure (4.26) appears effect the density on the conductivity for conductive and insulation samples.

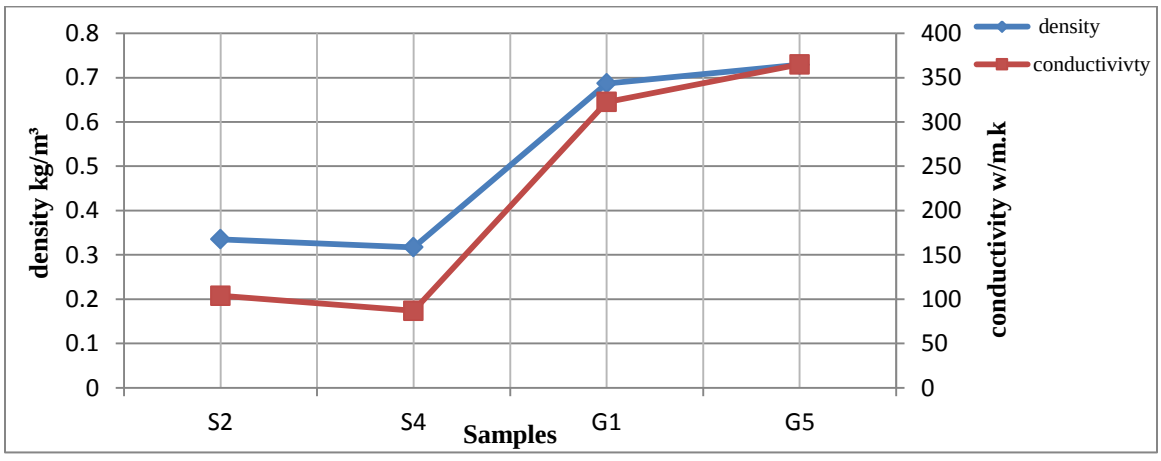

Figure (4.26) shows the effect of density on thermal conductivity for all conductive and insulation samples.

4.2.3.2 Viscosity Test

Viscosity test of (G1,G5) and (S2,S4). Viscosity values were taken at shear rate (20 s^{-1}) and temperature (25 ˚C). The viscosity of conduction samples (G1, G5) was (0.3447, 0.3591) poise (P) respectively. The viscosity of the insulation samples (S2, S4) was (0.7547, 0.7608) (P) respectively. The results of the viscosity examination of conduction samples are lower than that of the insulation samples, which corresponds to density test for samples at liquid case because the density of conduction samples is lower than that of the insulation samples. Viscosity is a measure of the intermolecular forces and the shapes of molecules as it gives an indication of the friction between the two layers of a liquid. Density and viscosity are two different properties that are not necessarily compatible [97]. Figure (4.27) illustrates the values of viscosity and liquid density of conduction and insulation samples. The density of the coating layer of the conduction samples after its complete drying is higher than that of the insulation samples due to the different nature of the solvents used and the components of the coating materials. The coating mixture to increase the thermal conductivity contains a lower percentage of polymeric materials (5%CMC and 5% Polyester resin), while the coating mixture to increase the insulation contains the percentage of polymeric materials (15%Polysterene and 9% Polyester resin) that is why the density of insulation samples is higher than the density of conductive samples in the liquid state, after the coating layer dries, the situation reverses due to the evaporation of polymeric materials.

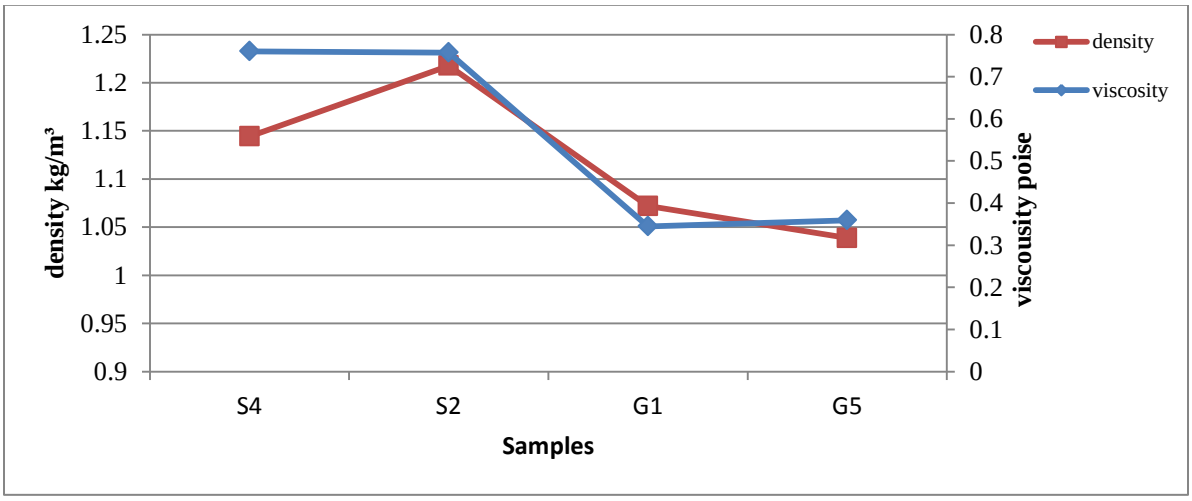

Figure (4.27) shows the relationship between the values of viscosity and liquid density of conduction and insulation samples.

4.2.3.3 Porosity Measurement

For the purpose of measuring the porosity and knowing its percentage, the images of (SEM) are analyzed by using the (image J) software, and the results are as follows:

Image analysis (SEM) of the sample (G5) is the porosity ratio (2.93%).

The image magnification is (100 x), the red color is the conductive coating material which is graphite with a percentage of copper powder, while the black color is pores as shown in figure (4.28a). Figure (4.28b) is the image (SEM) before conducting the analysis.

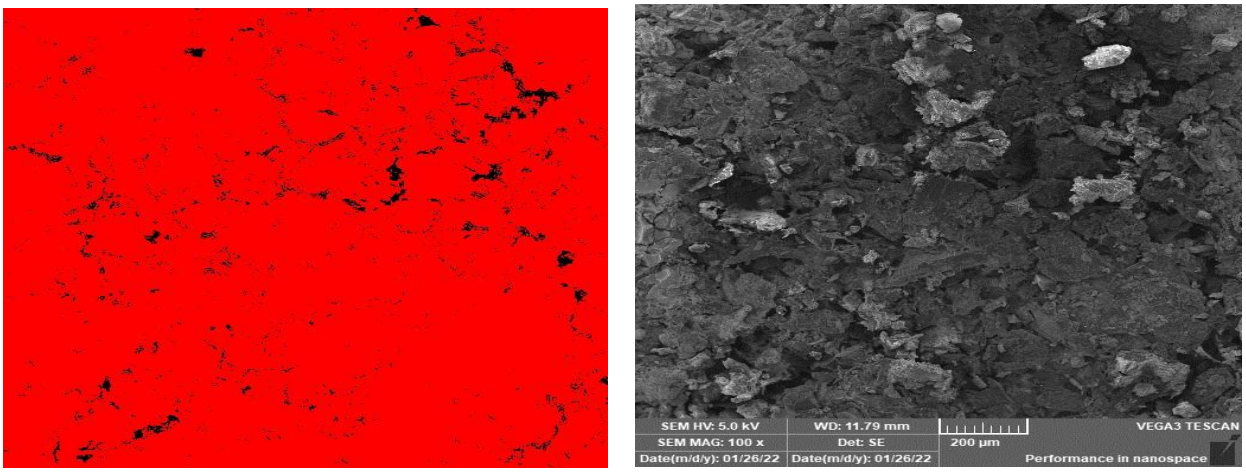

(a) (b)

Figure (4.28) (a) reveals the analysis of image (SEM) for the conduction sample (G5), (b) the same image as the previous sample(G5) before analysis.

Image analysis (SEM) of the sample (G1) the porosity ratio is (5.33%). The image magnification is (91x); the red color is the conductive coating material, which is graphite material only, while the black color acts the gaps and pores as shown in figure (4.29a), and figure (4.29b) contains the image (SEM) before conducting the analysis. The present digital image analysis method by used imageJ sowftware is able to capture all the pore of different sizes varying from micro to nano meter [96].

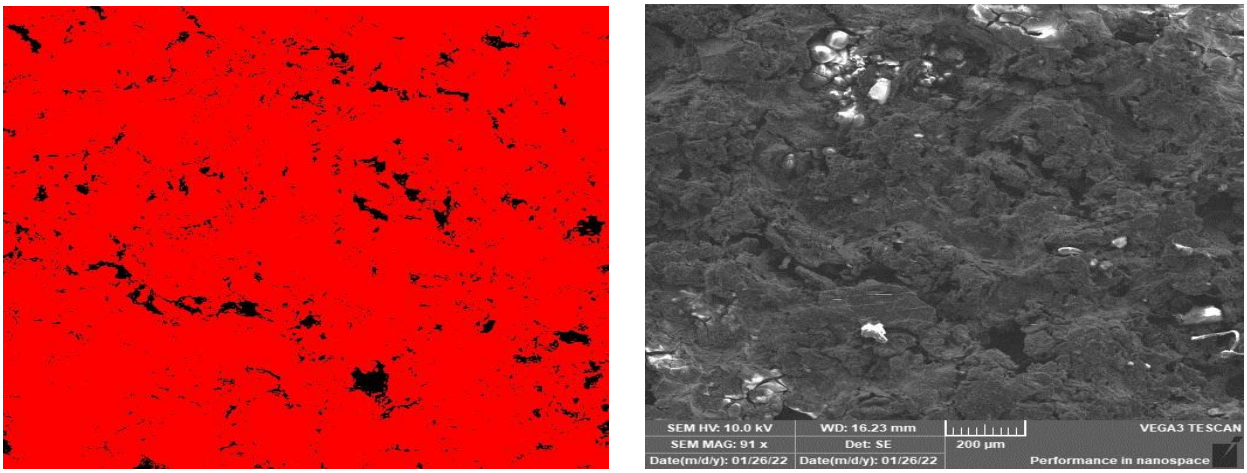

(a) (b)

Figure (4.29) (a) reveals the analysis of image (SEM) for the conduction sample (G1),(b) the same image as the previous sample(G1) before analysis.

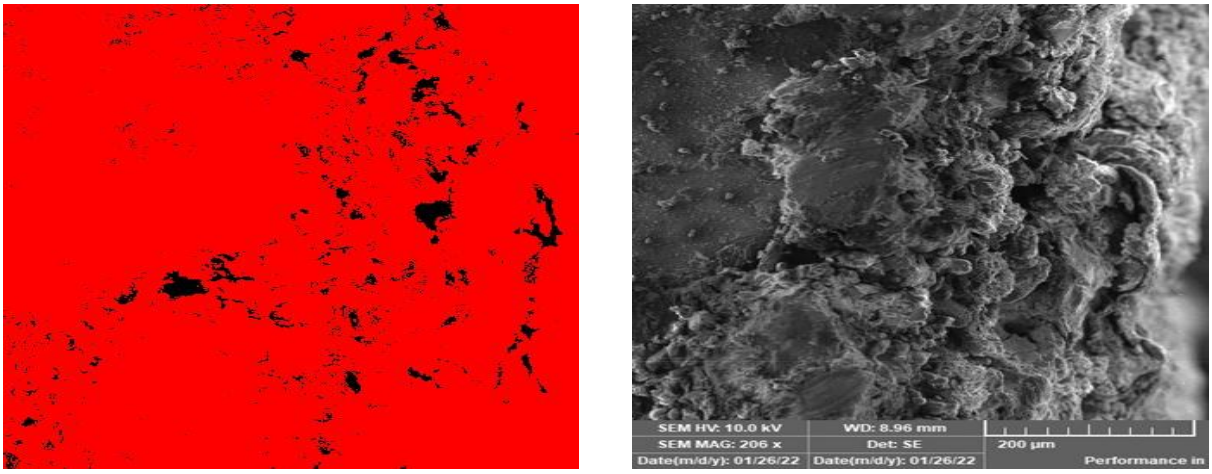

(a) (b)

Figure(4.30) (a) shows the analysis of the cross-sectional image (SEM) conduction sample (G4) ,(b) the same image as the previous sample(G4) before analysis.

Analysis of the cross-sectional image (SEM) of the sample coated with conductive coating (G4) finds the porosity ratio (4.62%). The image magnification is (206 x), the red color is the conductive coating material which is graphite with a percentage of copper powder, while the black color is pores as shown in figure (4.30a). Figure (4.30b) is the image (SEM) before conducting the analysis. Figure (4.31) shows the effect of porosity on thermal conductivity property for conduction samples.

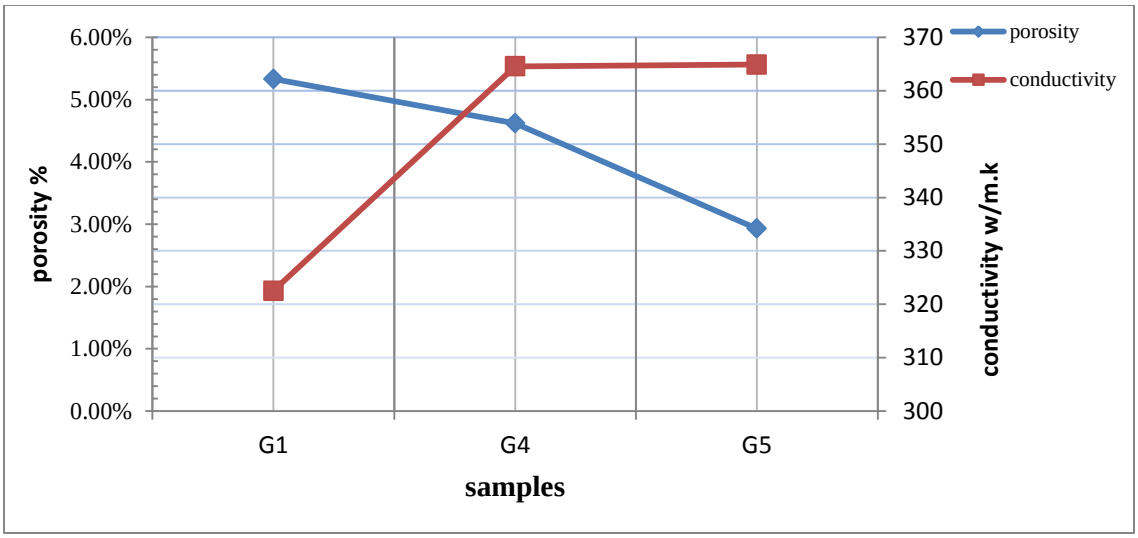

Figure (4.31) shows the relationship between porosity and thermal conductivity of conduction samples.

Analysis of samples coated with insulating coating (mullite with titanium dioxide) for the purpose of calculating the porosity, shows the following results: Image analysis (SEM) of the sample (S3) that contained on percentages of (Mullite and TiO2) is 3% the porosity ratio about (55.5%).The image magnification is (100 x); the red color is the insulation coating material, while the black color is pores, as shown in figure (4.32a). Figure (4.32b) is the image (SEM) before conducting the analysis.

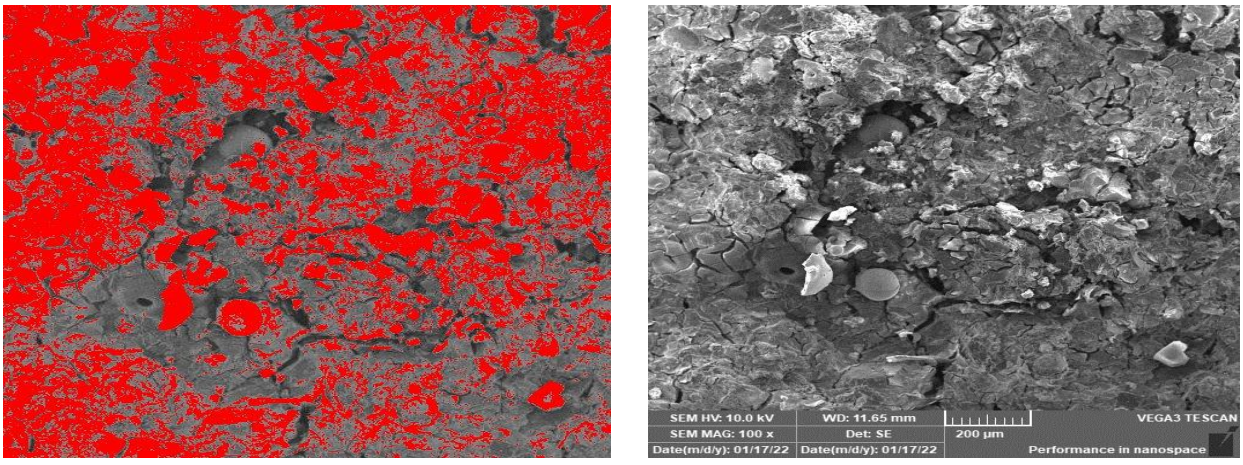

(a) (b)

Figure (4.32) (a) reveals the analysis of image (SEM) for the insulstion sample (S3),(b) the same image as the previous sample(S3) before analysis.

Image analysis (SEM) of the sample (S2) that contained on lower percentages of (mullite and TiO_2) is 1% the porosity ratio about (41.27%).
The image magnification is (100 x); the red color is the insulation coating material, while the black color is pores, as shown in figure (4.33a). Figure (4.33b) is the image (SEM) before conducting the analysis.

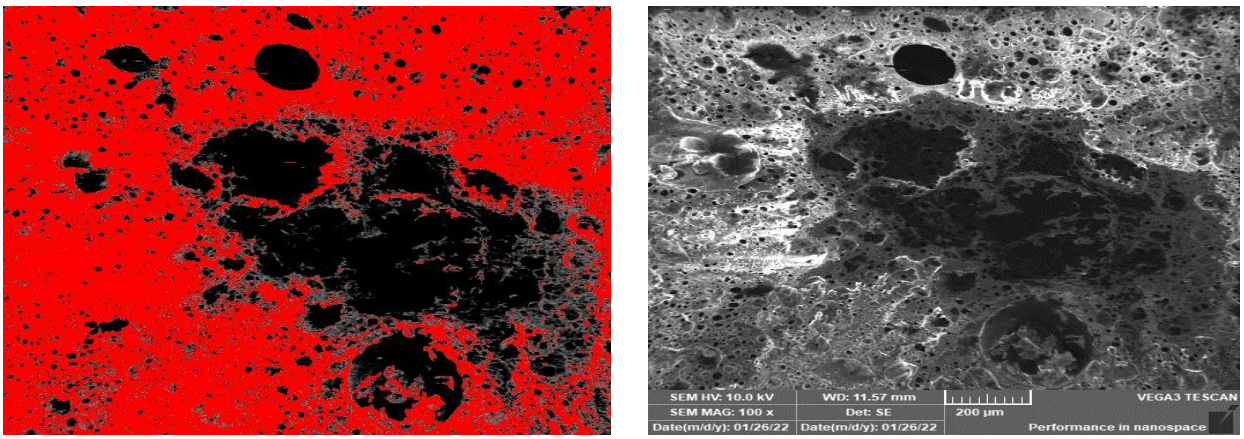

(a) (b)

Figure (4.33) (a) reveals the analysis of image (SEM) for the insulation sample (S2), (b) the same image as the previous sample(S2) before analysis.

Analysis of the cross-sectional image (SEM) of the sample coated with insulation coating (S4) that contains the highest percentage of insulating coating (5%), the porosity ratio about (68.28%). The image magnification is (205 x); the red color is the insulation coating material, while the black color is pores, as shown in figure (4.34a). Figure (4.34b) is the image (SEM) before conducting the analysis. The porosity of porous Mullite coatings can reach between (73-86%vol) to give insulation up to (0.09 w/m.k)[10].

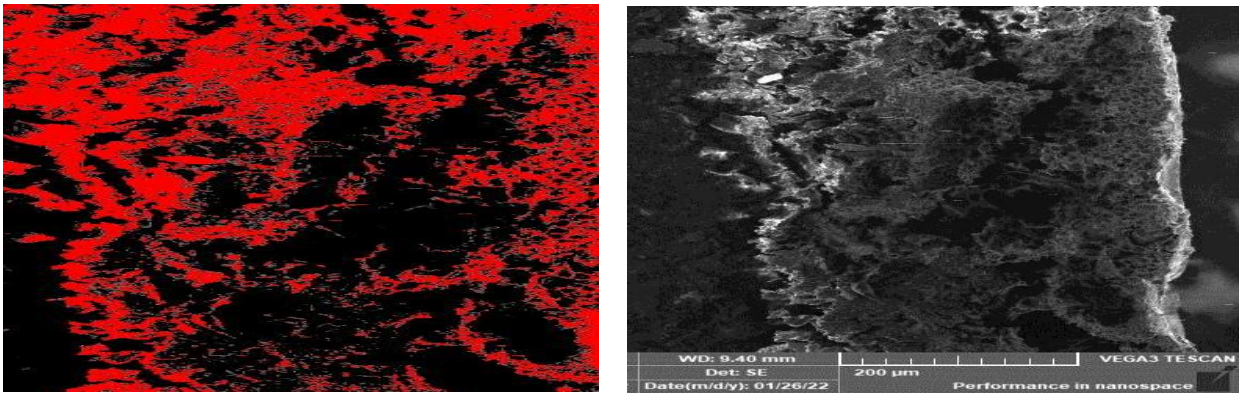

(a) (b)

Figure(4.34) (a) shows the analysis of the cross-sectional image (SEM) insulation sample (S4) ,(b) the same image as the previous sample(S4) before analysis.

The figure (4.35) shows the effect of porosity on thermal conductivity for insulation samples.

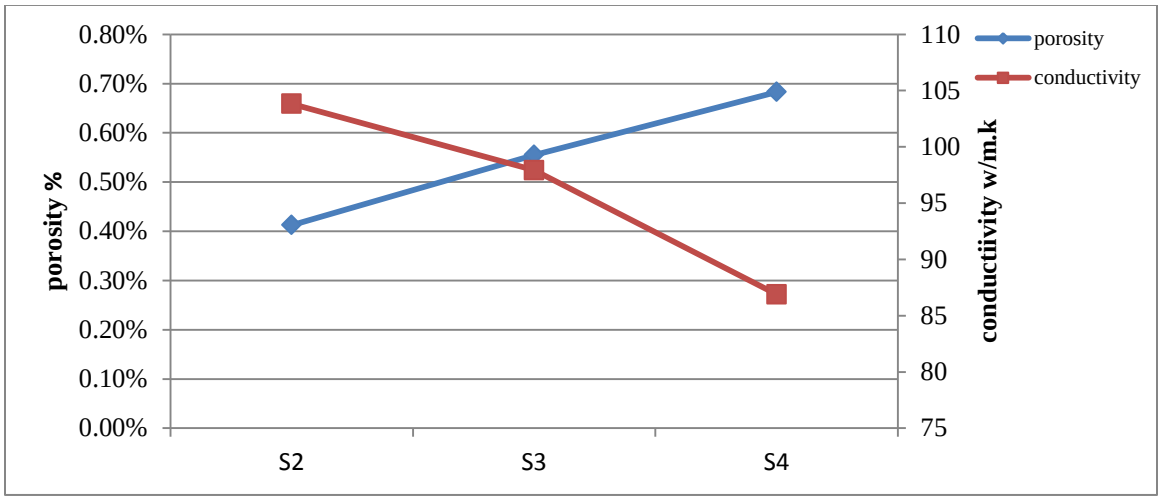

Figure(4.35) shows the relationship between porosity and thermal conductivity for insulation samples.

Figure (4.36) show the effect of porosity on the thermal conductivity and figure (4.37) illustrates the relationship between the density and porosity of both conduction and insulation samples.

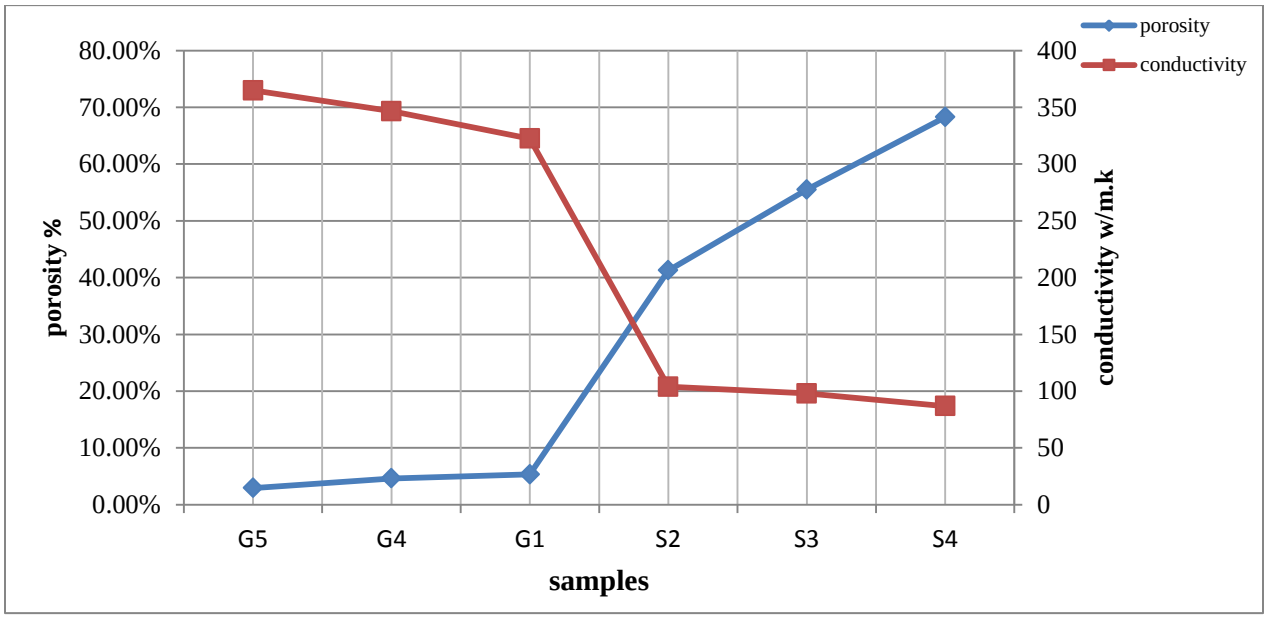

Figure(4.36) shows the relationship between the porosity and thermal conductivity of conductive and insulation samples.

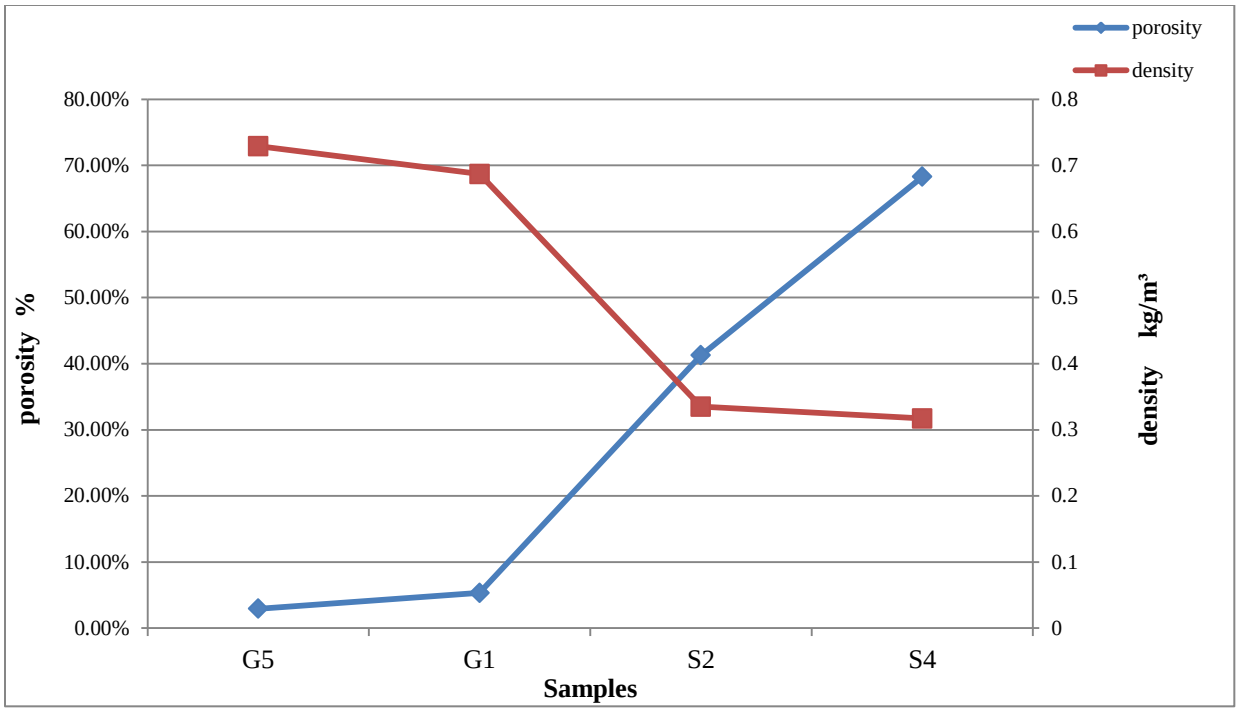

Figure(4.37) shows the relationship between the porosity and density of conductive and insulation samples.

4.2.3.4 Coating Thickness Measurements

The thickness of the insulating coating layer is higher than the thickness of the conductive coating layer, because the density of the coating mixture in the liquid state (before the coating layer dried) of the insulation coating mixture was higher than the coating density of the conductive mixture in the liquid state. The insulating coating layer contains a large percentage of pores that resulted low density which are the main reason for high thermal insulation. The mean coating thickness for conductivity layer is (405 µm) while the mean coating thickness for insulation layer is (715µm). The coating thickness insert in calculations measuring thermal conductivity test. The figure (4.38) shows the coating thickness values for samples coated for the purpose of increasing the thermal conductivity while figure (4.39) shows the coating thickness values for the samples coated for the purpose of increasing the thermal insulation. Temperature analyses are performed for various coating thicknesses from (0.2 to 1.6 mm) excluding the bond coat layer as found in the source [98].

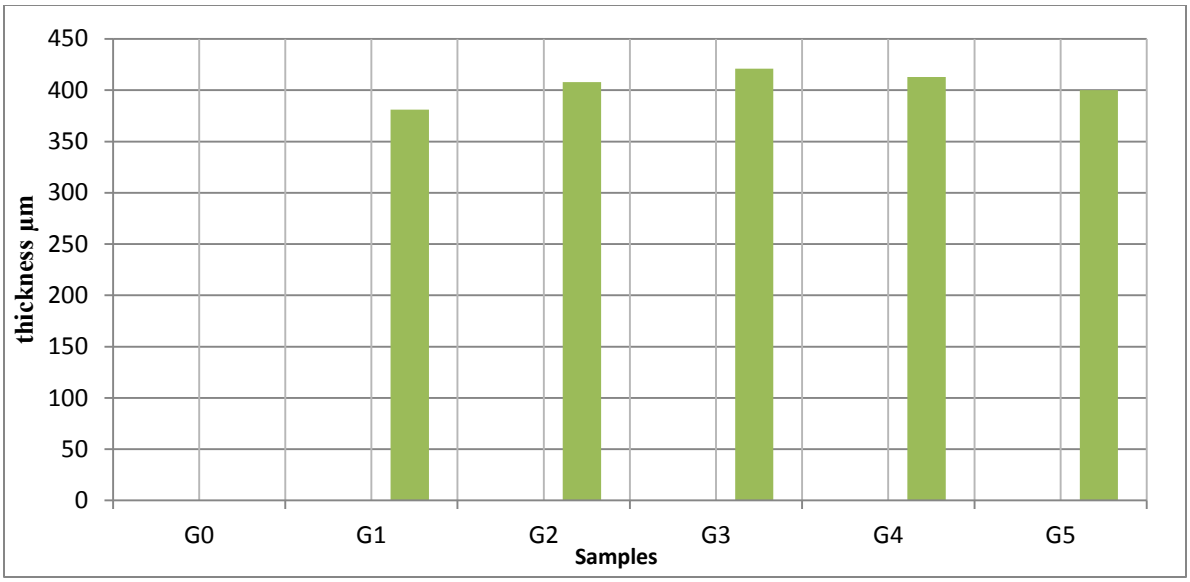

Figure (4.38) shows the coating thickness for conductivity samples.

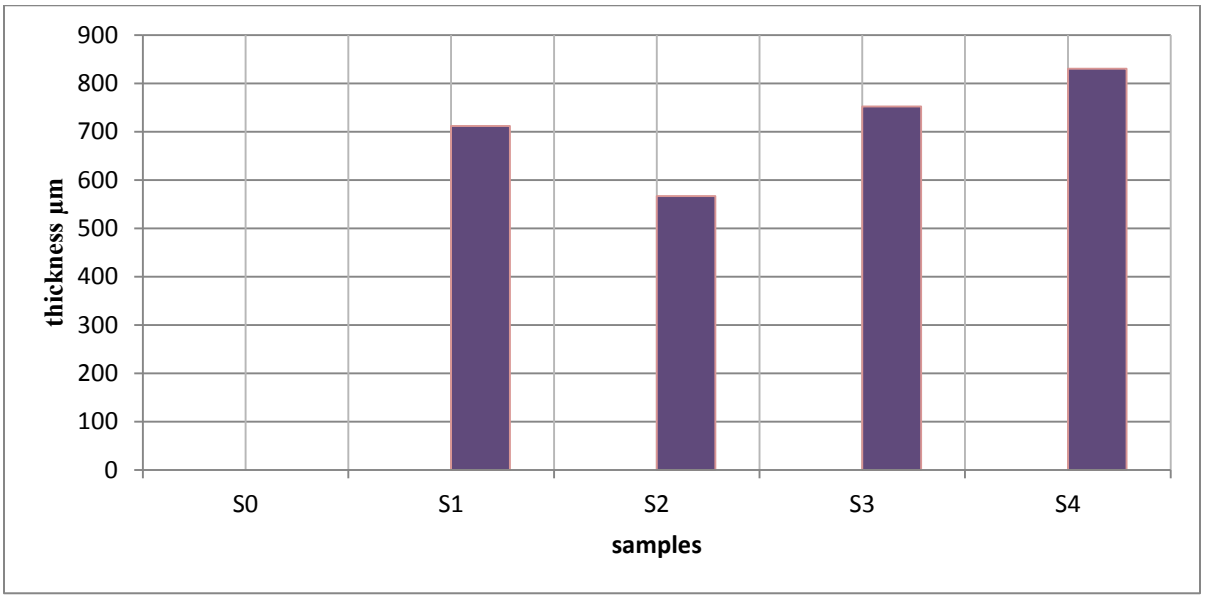

Figure (4.39) shows the coating thickness for insulation samples.

4.2.3.5 Ultra -Violent Visible (U.V) Test

The (U.V) test performed for the purpose of providing with information about the extent of absorptivity, reflectivity and transmission of the coating layer, whether it is to increase conductivity or to increase insulation. The samples used in this test are in the form of a liquid mixture of coating materials. The reflectivity

and transmission is inversely proportional to absorptivity, when reflectivity and transmission decrease the absorptivity increases and vice versa [99].

1-The (U.V) Test for Samples to Increase Thermal Conductivity

The test was performed on samples coated to increase the thermal conductivity (G1, G5). The coating mixture used to improve the conductivity of graphite materials is opaque black in color, which results in an increase in absorptivity and a decrease in reflectivity and transmission according to the base (absorptivity + reflectivity+ transmission=1) [99]. As for the sample (G5), the absorptivity is higher than the sample (G1) because its viscosity and density is higher and the correlation between the particles is stronger, and the result of the reflectivity and transmission of (G5) is less than (G1). Figure (4.40 a, b) shows the difference in absorptivity between the sample (G1) and the sample (G5). At frequency (190.00nm) the absorbance of the sample (G1) is (3.220) while the absorbance of the sample (G5) is (3.390).

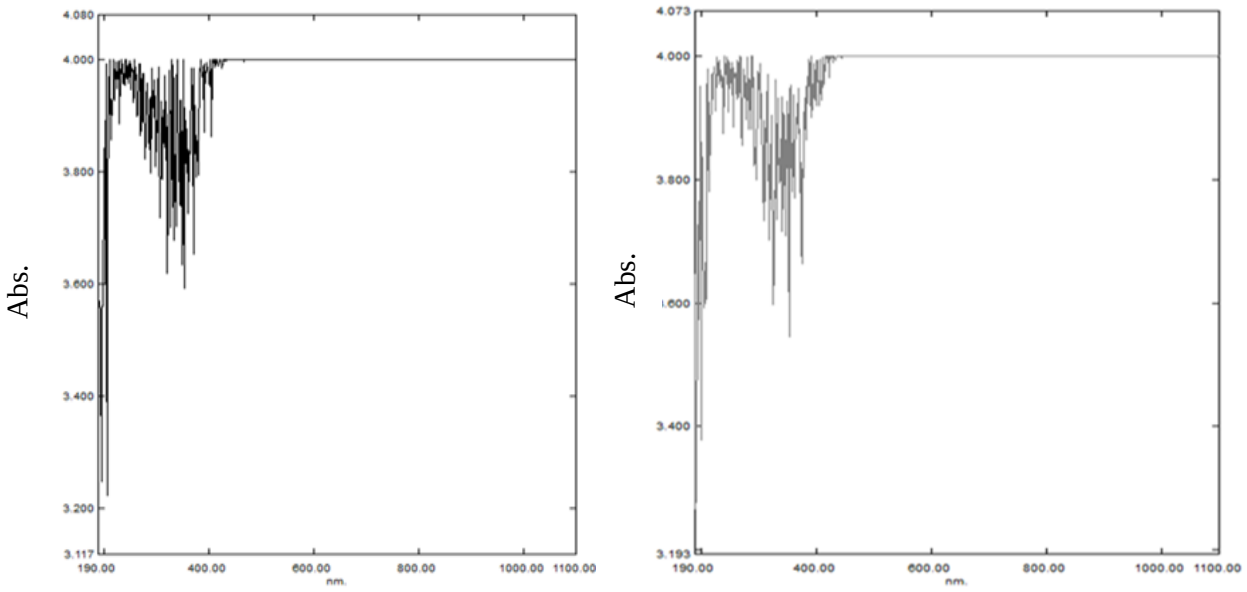

(a) **(b)**

Figure (4.40) The U.V test absorptivity for conductive samples (a) **G1** (b) **G5** .

Figure (4.41 a,b) shows the difference in reflectivity between the sample(G1) and the sample(G5). At frequency (190.00nm) the reflectivity of the sample (G1) is (-0.08) while the reflectivity of the sample (G5) is (-0.15).

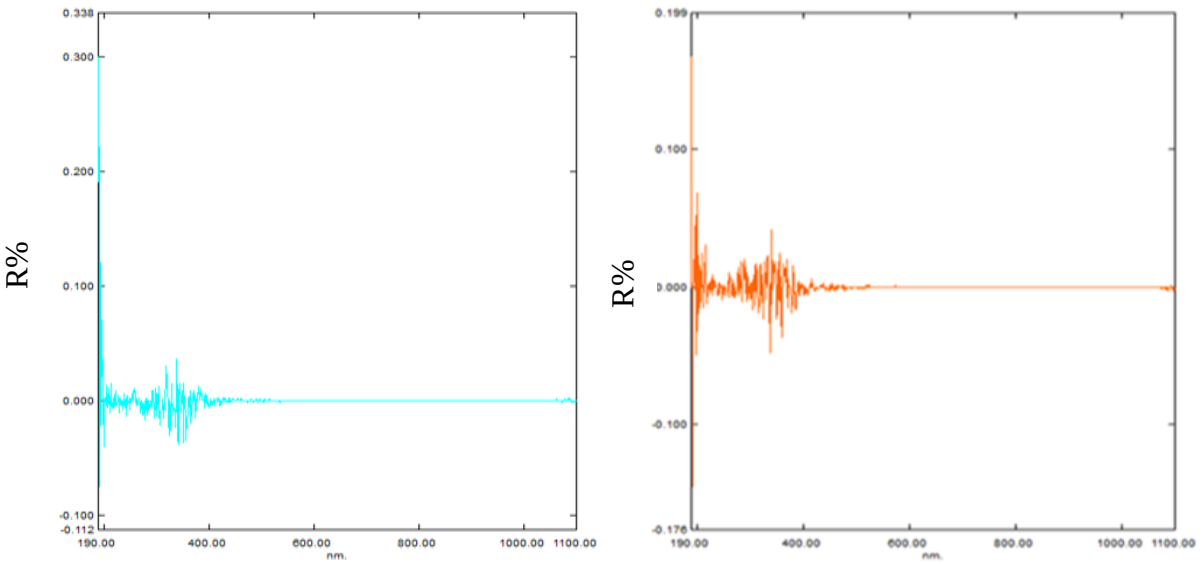

(a) **(b)**

Figure (4.41) the U.V test reflectivity for conductive samples (a) for **G1** and (b) for **G5.**

Figure (4.42 a,b) shows the difference in transmission between the sample (G1) and the sample(G5). At the frequency (190.00nm) the sample transmittance (G1) is (0.7) while the sample transmittance (G5) is (0.4).

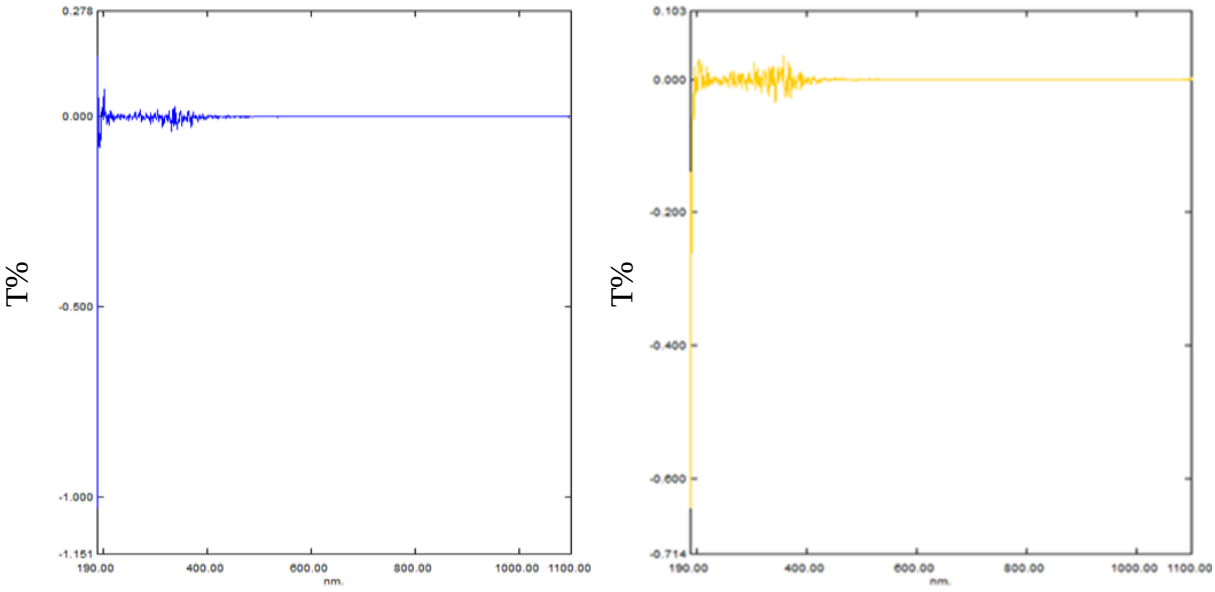

(a) **(b)**

Figure (4.42) the U.V test transmission for conductive samples (a) for **G1** and (b) for **G5.**

2-The U.V Test for Samples to Increase Thermal Insulation

The U.V test is performed on samples (S2, S4) coated to increase insulation. The samples are mixture of coating materials which contain Mullite, Titanium dioxide, and polystyrene that is dissolved in solutions (Chloroform, DMF). The color of the coating mixture in this case is translucent white. The sample (S4) has a higher reflectivity and transmission than the sample (S2) because it contains a higher percentage of Mullite and Titanium dioxide. The Titanium dioxide increases the reflectivity significantly when its quantity is increased. Absorptivity of the sample (S4) is less than the sample (S2) and according to the rule (absorptivity + reflectivity + transmission=1).

Figure (4.43 a,b) shows the difference in absorptivity between the sample(S2) and the sample (S4). At frequency (190.00nm), the absorbance of the sample (S2) is (-2.800) while the absorbance of the sample (S4) is (-3.000).

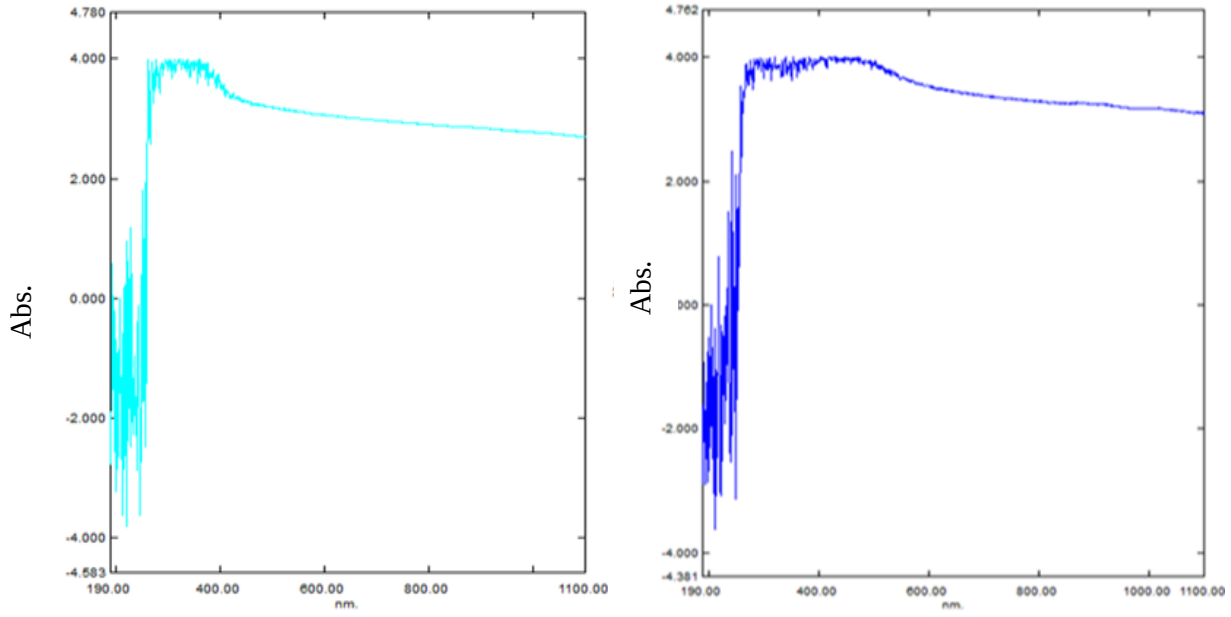

(a) **(b)**

Figure (4.43) the U.V test absorptivity (a) for **S2** and (b) for **S4** .

Figure (4.44 a,b) shows the difference in reflectivity between the sample(S2) and the sample(S4). At frequency (190.00nm) the reflectivity of the sample (S2) is (100) while the reflectivity of the sample (S4) is (180).

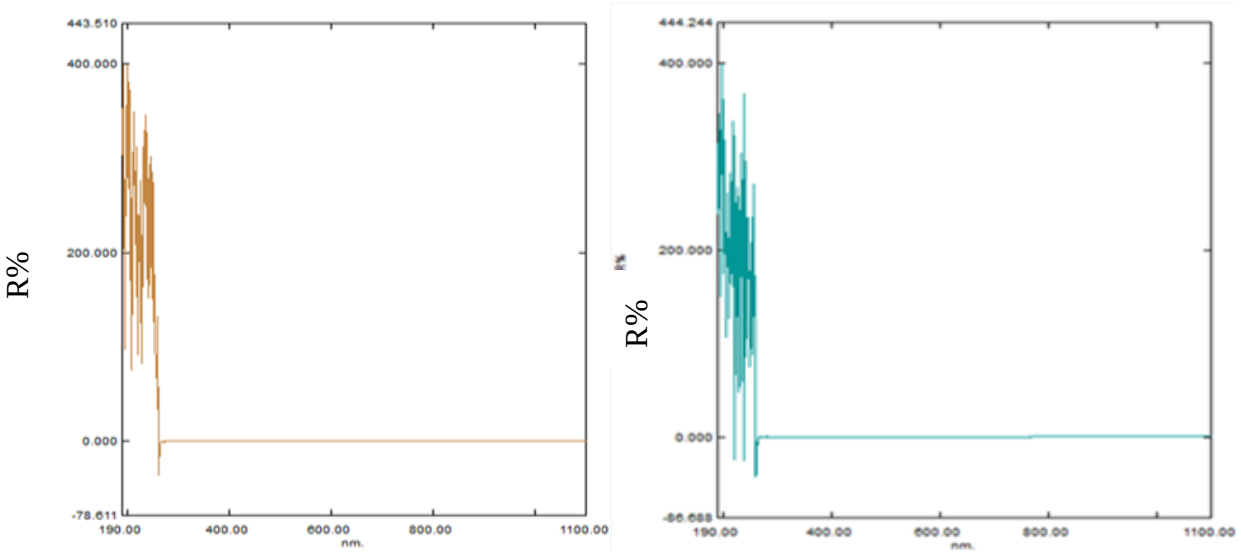

(a) **(b)**

Figure (4.44) the UV test reflectivity for insulation samples (a) **S2** (b) for **S4**.

Figure (4.45 a,b) shows the difference in transmission between the sample (S2) and the sample (S4). At the frequency (190.00nm) the sample transmittance (S2) is (130) while the sample transmittance (S4) is (180).

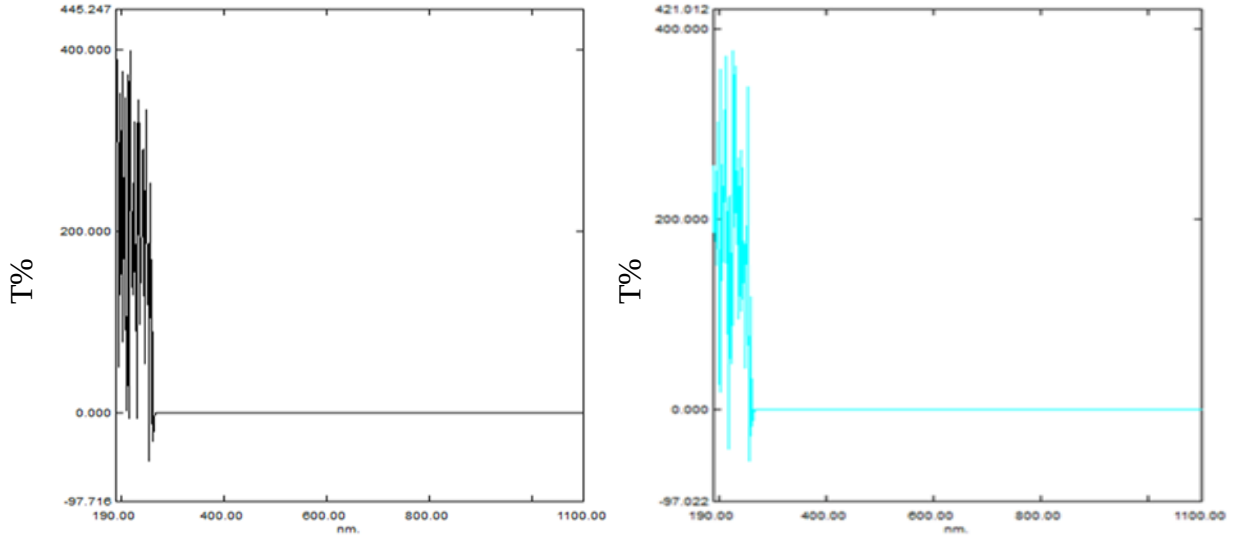

(a) **(b)**

Figure (4.45) the UV test transmission for insulation samples (a) **S2** (b) **S4**.

Figure (4.46) illustrates the difference between the conduction and insulation samples in the U.V test (a) absorptivity (b) reflectivity and (c) transmission.

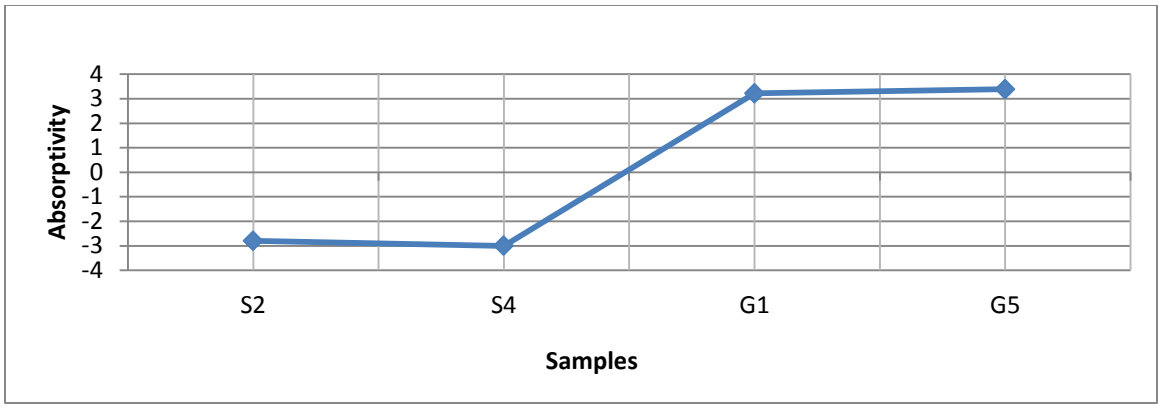

(a)Absorptivity

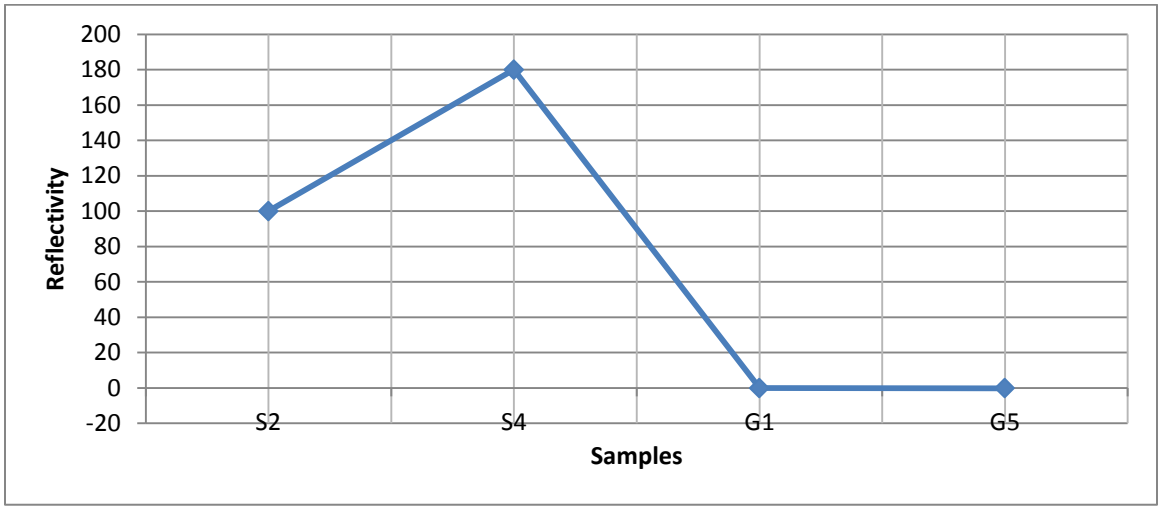

(b)Reflectivity

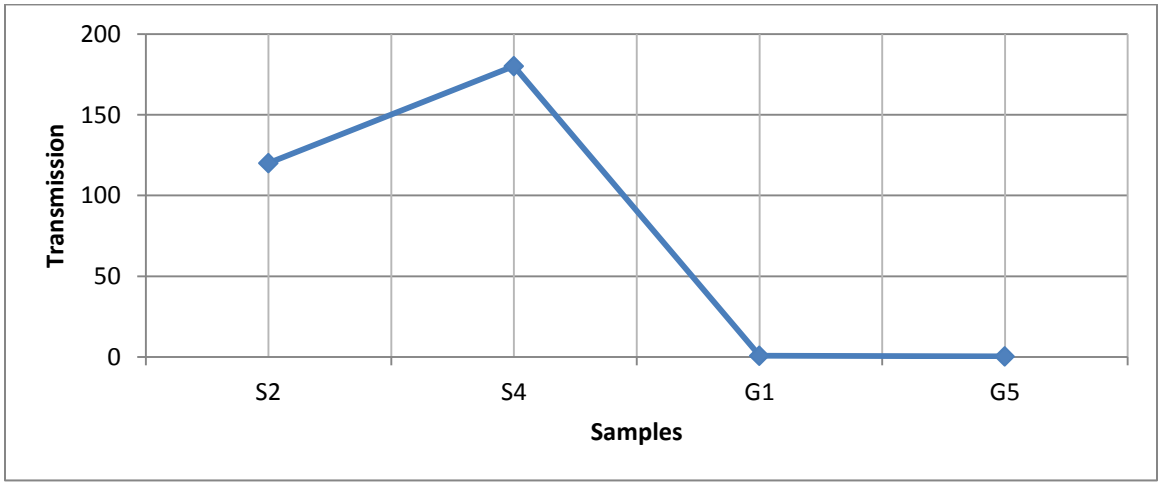

(c)Transmission

Figure (4.46) shows a comparison between the conduction and insulation samples in the U.V test (a) absorptivity (b) reflectivity and (c) transmission.

4.2.4 Thermal Properties Tests

4.2.4.1 Thermal Conductivity Test for Increasing Thermal Conductivity

Thermal conductivity test for samples to increase thermal conductivity is improved by graphite coating about (60%) in sample (G1) and when adding ratios of copper powder having micro scale the thermal conductivity increases about (80%) as in sample (G5). The thermal conductivity of the coating layer increases with increasing density and decreasing porosity, that is confirmed in the results of the density and porosity tests , this corresponds to the source [96].

The increase in thermal conductivity is due to the thermal conductivity properties of the coating materials, graphite has thermal conductivity (1500 w⁄m .k) and specific heat (707 J⁄kg .k)[7], and copper powder an ability to conduct heat about (401 w⁄m .k) and specific heat (390 J⁄kg .k)[2]. Table (4.1) shows the results in thermal conductivity test by Lee disc device for all conductive samples. The thermal conductivity value of epoxy/alumina-coated graphite composite shows a significant increase from (0.22 w/m .k) (neat epoxy) to (0.64 w/m .k) the increase in thermal conductivity is about twice and that is consistent with the results obtained [78].

Table (4.1) shows the values thermal conductivity test for all samples coated to increase thermal conductivity.

Sample No.	Thermal conductivity w⁄m. k
G0	202
G1	322.53
G2	360.22
G3	362.6
G4	364.55
G5	364.89

The G0 sample is without coating (aluminum plate only).The G1 sample coated with graphite only without added copper powder. The G2, G3, G4 and G5 samples are coated with graphite and added copper powder with different amounts.

Figure (4.47) shows the evolution of the improvement in thermal conductivity between all coated samples for the purpose of increasing thermal conductivity. It is noted that the main increase in thermal conductivity occurs in the sample (G1) coated with graphite material only. As for the increase in thermal conductivity for the rest of the samples, it will be slight and gradual due to the presence of different proportions of copper, compared to the source sample (G0), which does not contain substance coating.

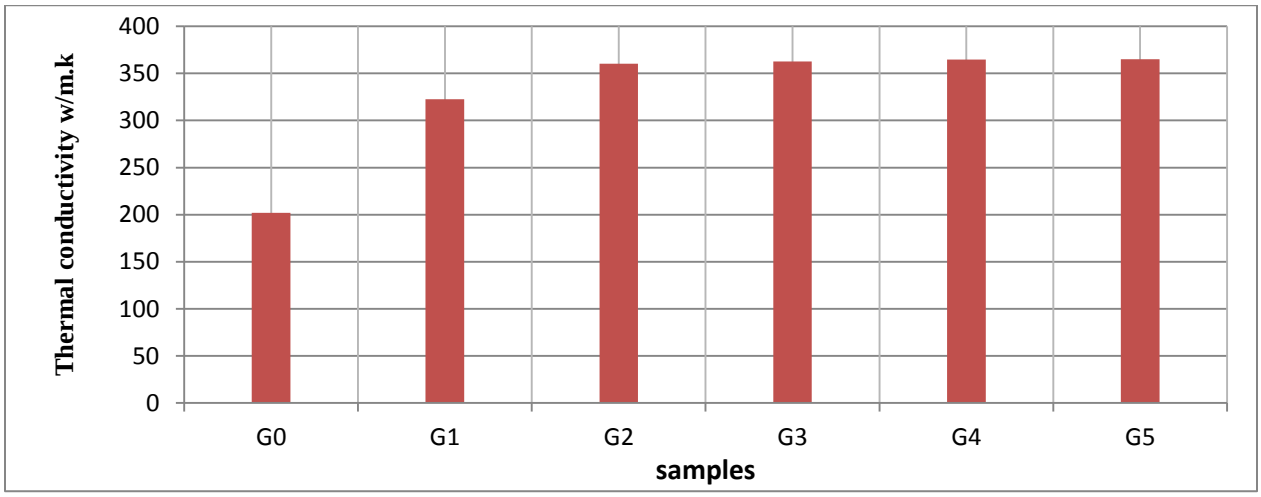

Figure (4.47) illustrates the increasing in thermal conductivity for conductive samples.

4.2.4.2 Thermal Conductivity Test for Decreasing the Thermal Conductivity

Thermal conductivity test for samples to increase insulation the improvement by using Mullite and TiO2 at percentage (1%) with polystyrene the thermal conductivity decrease about (48%) as in sample (S2). When increasing the ratios the Mullite and TiO2 to (5%), the increasing is in the insulation about (57%) as in sample (S4). The thermal insulation of the coating layer increases with decreasing density and increasing porosity, and that is confirmed in the results of the density and porosity tests , this corresponds to the source [96].

The increase in thermal insulation is due to the thermal insulation properties of the ceramic coating materials. Mullite has thermal conductivity (3.3 w/m.k) at temperature (1400k), also Titanium dioxide an ability to conduct heat about (3.3 w/m .k) at temperature (1400k) [12]. Table (4.2) shows the results in thermal conductivity test by Lee disc device for all insulation samples.

Table (4.2) shows the values thermal conductivity for all coated samples to increase thermal insulation.

Sample No.	Thermal conductivity w/m.k
S0	202
S1	164.22
S2	103.83
S3	97.93
S4	86.89

Note that the highest change in the increase in thermal insulation is in the sample (S2) coated with 1% of mullite and (TiO_2), while the highest insulation value is achieved in the sample (S4) for the presence of 5% of Mullite and (TiO_2) compared to the source sample (S0), which does not contain substance coating.

Figure (4.48) shows the evolution of the improvement in thermal insulation between all coated samples for the purpose of increasing thermal insulation.

The **S0** sample is without coating (aluminum plate only). The **S1** sample coated with polystyrene (polymer) only. The **S2**, **S3** and **S4** are coated with mixture of Mullite, Titanium dioxide and polystyrene with different amounts.

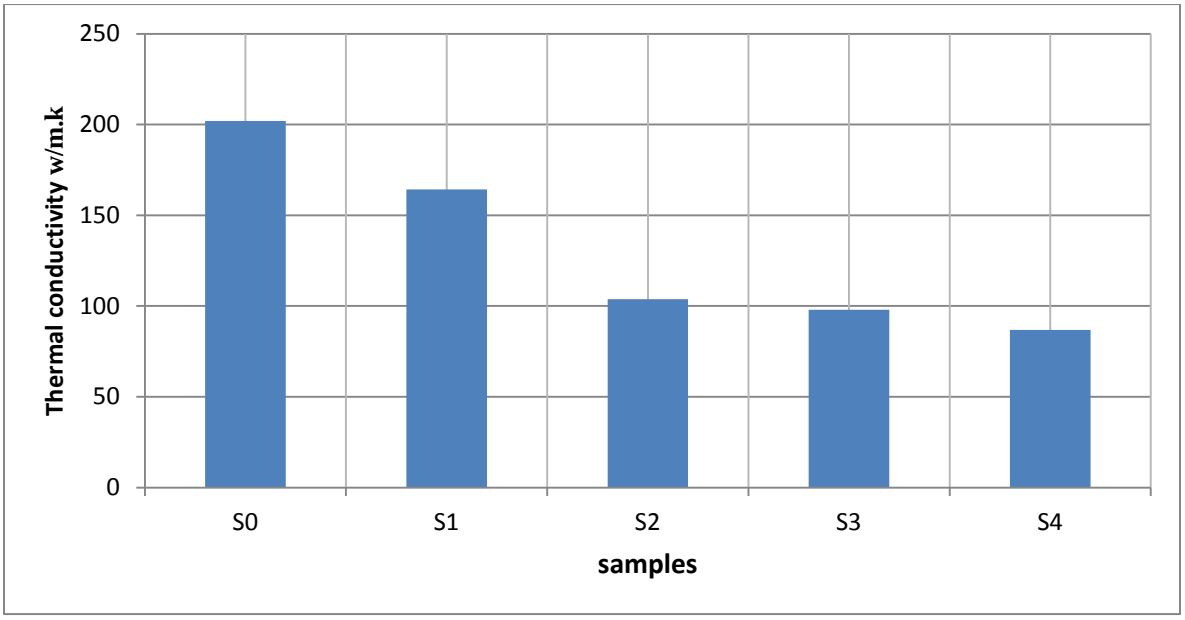

Figure (4.48) illustrates the increasing in thermal insulation for insulation samples.

4.2.4 Mechanical Properties Tests

4.2.4.1 Adhesion Strength Test

The adhesion strength test worked to ensure the adhesion force and durability the coating layer on substrate surface. The adhesion strength for conductive sample (G1) is (19.06 MPa) the coating layer contains on graphite material only. When add the copper powder the stability, and adhesion strength of the coating layer increases with the sample (G5) the adhesion strength reaches (19.82 MPa). The copper powder that added to mixture of the coating increase thermal conductivity, adhesion strength and improving stability and structure the mixture coatings [34].
The adhesion strength of samples coated with an insulating coating, when using a polystyrene layer with polyester resin in sample (S1) the adhesion value is (17.31MPa) and when adding ceramic materials from the ratios of Mullite and Titanium dioxide, the value of the adhesion strength is (17.73Mpa) for sample (S4) due to the increasing in the stability of the coating layer through reinforcement with Mullite and Titanium dioxide grains. Figure (4.49) shows both conduction and insulation samples after conducting adhesion strength tests. Figure (4.50) illustrates adhesion strength values for both conduction and insulation samples.

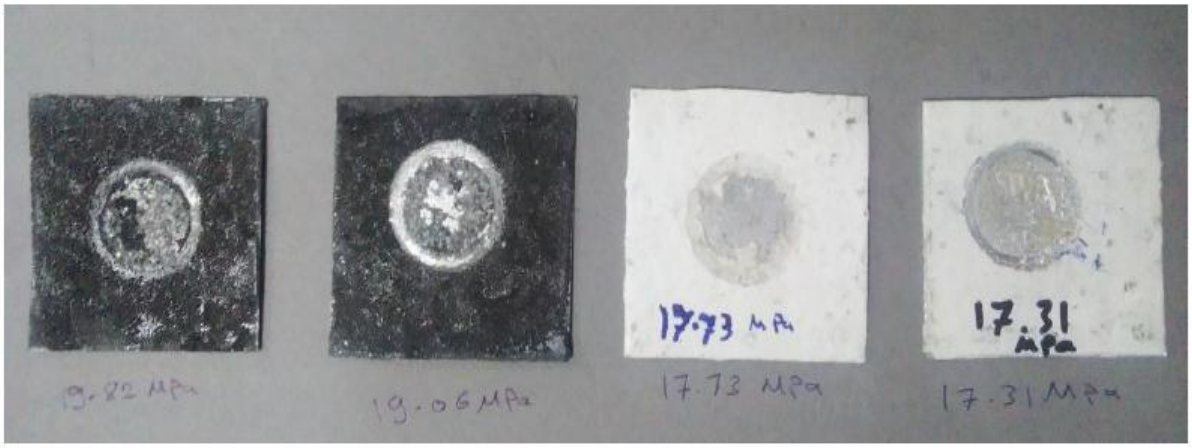

Figure (4.49) illustrate adhesion strength test for conductive and insulation samples.

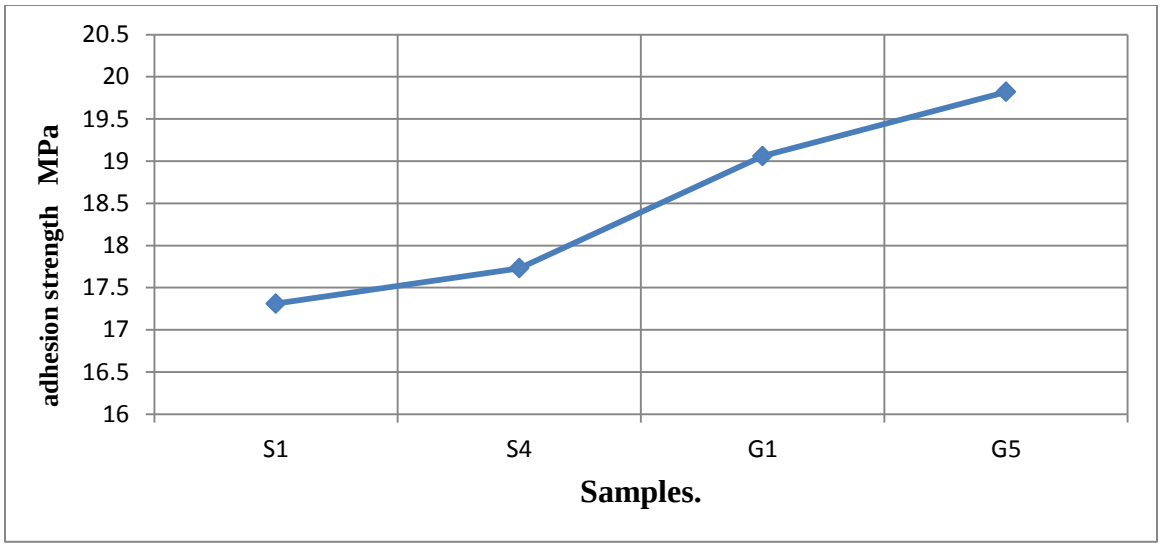

Figure (4.50) illustrates adhesion strength values for conductive and insulation samples.

4.2.5 Numerical Analysis Results

The temperature difference between the inlet and outlet temperatures of the fluid in the heat exchanger tube of the solar collector can be simulated by the ANSYS 16.1 software fluid flow (fluent). The water inlet temperature was (293k), the flow velocity was (0.2 m/s), and the mass flow rate was (0.05 kg/s). The latitude and longitude of the city of Babylon were taken to determine the intensity of the incident solar radiation [100][93]. The ratio of the absorption of infrared waves (Direct IR) (0.9) and the ratio of the absorption of visible rays (Direct visible) was also fixed (0.9) in the program settings, the absorptivity is greater than 0.9 for graphene and black paint [71]. Because of the slow flow velocity the option (k-epsilon) was used to deal with the nature of the fluid flow[93].

The difference in inlet and outlet temperatures of the heat exchanger tube is simulated before and after coating with ceramic materials that increase thermal conductivity. The results of the conductivity sample (G5), which has the highest thermal conductivity, were taken and compared with the bare aluminum metal plate. The semi-circular cross section of the aluminum heat exchanger tube using has an area in cross section (253.3mm^2). The amount of the Reynolds number is up to (2330).

Assume that the material of the coating layer is homogeneous and does not contain gaps of air, which reduces the thermal conductivity, as well as the coating layer adhesion completely with the aluminum plate metal.

Figure (4.51) shows the temperature distribution of the absorber plate of the flat plate solar collector without coating layer. The results were very good as the thermal gradient between the entrance and output of the exchanger tube without coating is (23˚C) as in the figure (4.52). While in the case of using ceramic coating that increases the thermal conductivity of the sample (G5). The difference in inlet and outlet temperatures is (57 ˚C) as in figure (4.54). When solar water heaters were tested using (ABRO) black spray, a temperature increases of (14.9) ˚C which was gained at the absorber plate outlet as in the source [5]. In the source [74] the test results showed that the north-facing room had an average temperature over (17)°C while the south-facing room was over (20) °C, which illustrated that a good heating effect was achieved in COP system . Figure (4.52) represents the thermal gradient between the entrance and output in the heat exchanger tube of the flat plate solar collector before coating (without coating). The process of absorbed radiation from the atmosphere to the absorber plate (aluminum metal plate) directly. The occurrence of conduction process between the tube walls and the absorber plate leads to a transfer of heat to the working fluid (water), as well as the occurrence of convection from the side walls of the absorber plate and the pipes of the heat exchanger leads to a percentage of the acquired heat loss and the heat transfer coefficient is (5w/m².k).

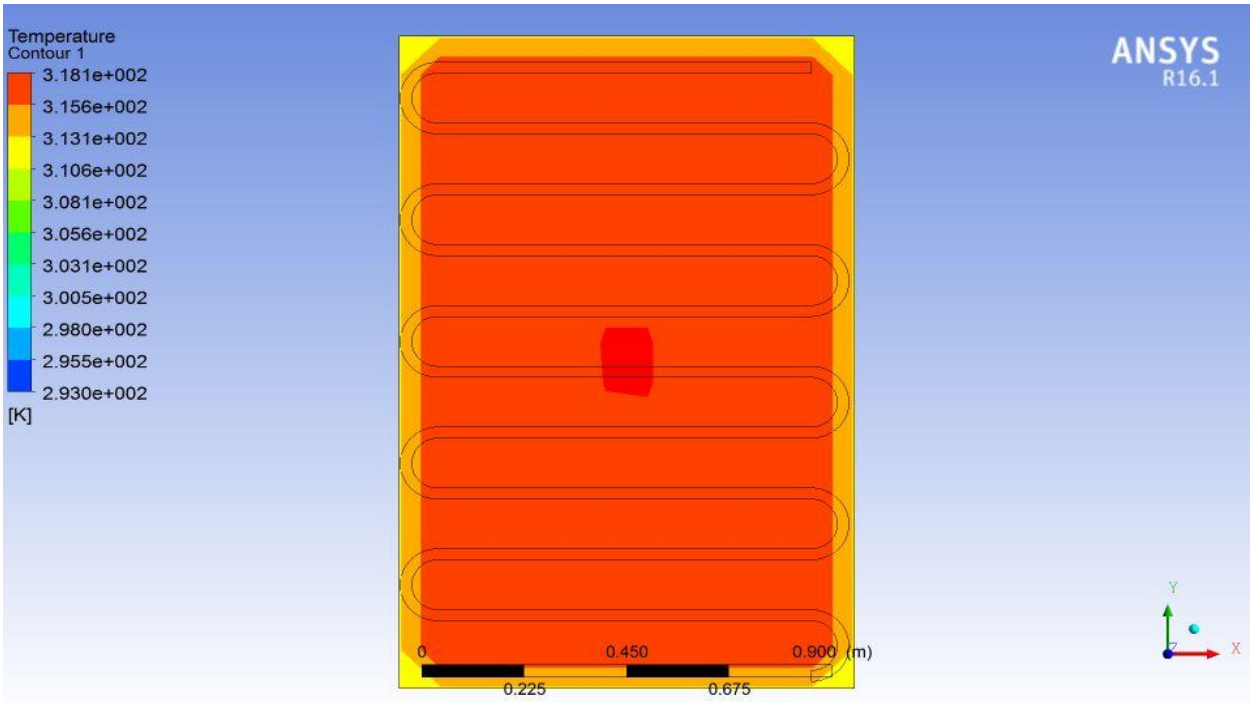

Figure (4.51) shows the temperature distribution of the absorber plate without coating layer.

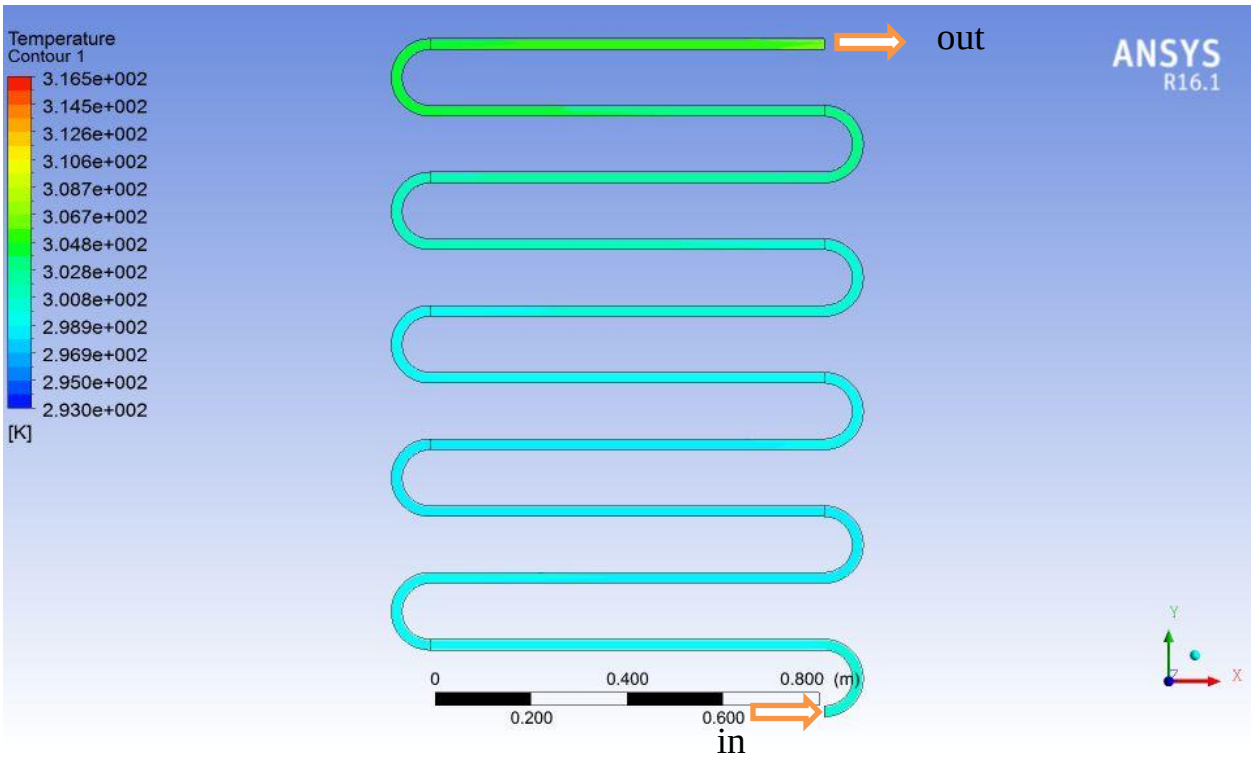

Figure (4.52) shows the temperature distribution of the heat exchanger tube of the flat plate solar collector without coating layer.

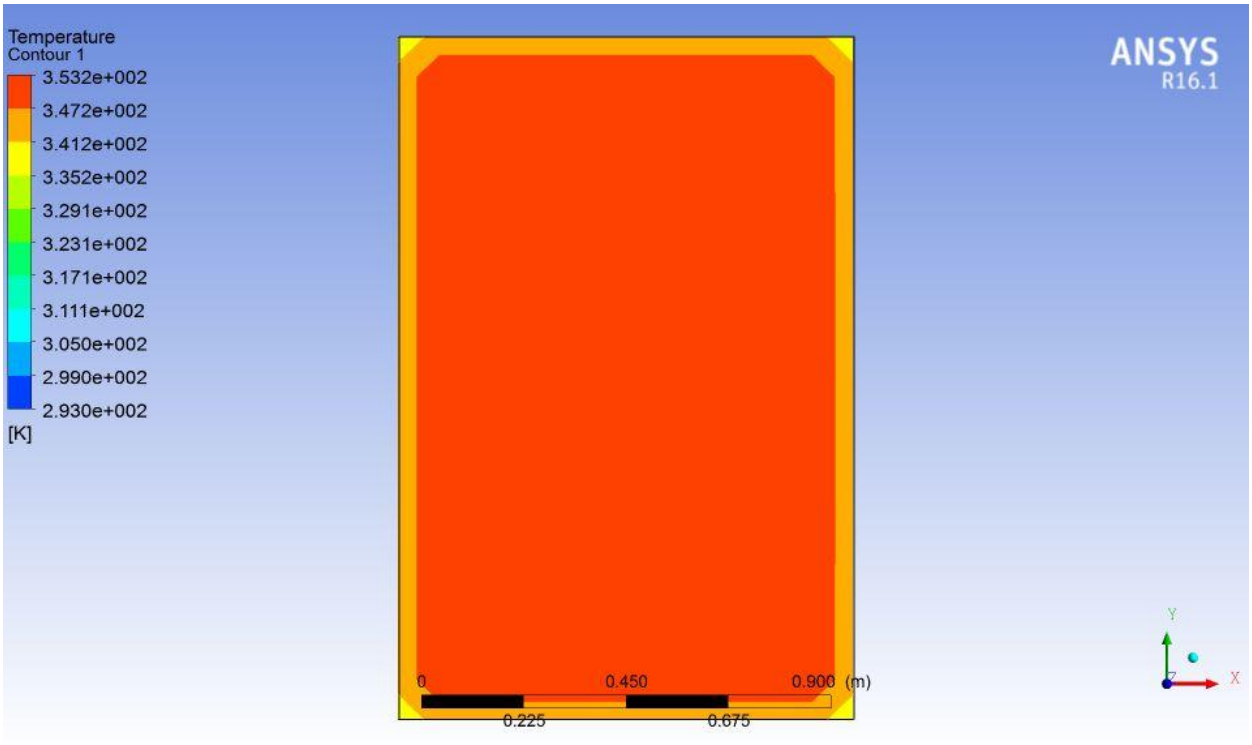

Figure (4.53) shows the temperature distribution of the absorber plate with coating layer.

Figure (4.53) represents the temperatures distribution on absorber plate of the flat plate solar collector in the case of conductive ceramic coatings. Figure (4.54) represents the temperature difference between the inlet and outlet tube heat exchanger of the flat plate solar collector with conductive ceramic coating. The process of absorbing solar radiation is through ceramic coating, and because of the properties of thermal coatings, which are thermal conductivity and specific heat, as well as the colour of black coating, which is the most absorbable colour for all lengths of the solar spectrum, all of the above properties led to an increase in the absorption of solar radiation. Conduction process occurs between the surfaces of the absorber plate (aluminum plate metal and the coating layer), as well as between the surface of the absorber plate and the wall of the heat exchanger tube, that causes water to receive heat. The presence of convection process from side walls for heat exchanger pipes, and the side absorber plate causes a portion of the acquired heat energy to be lost.

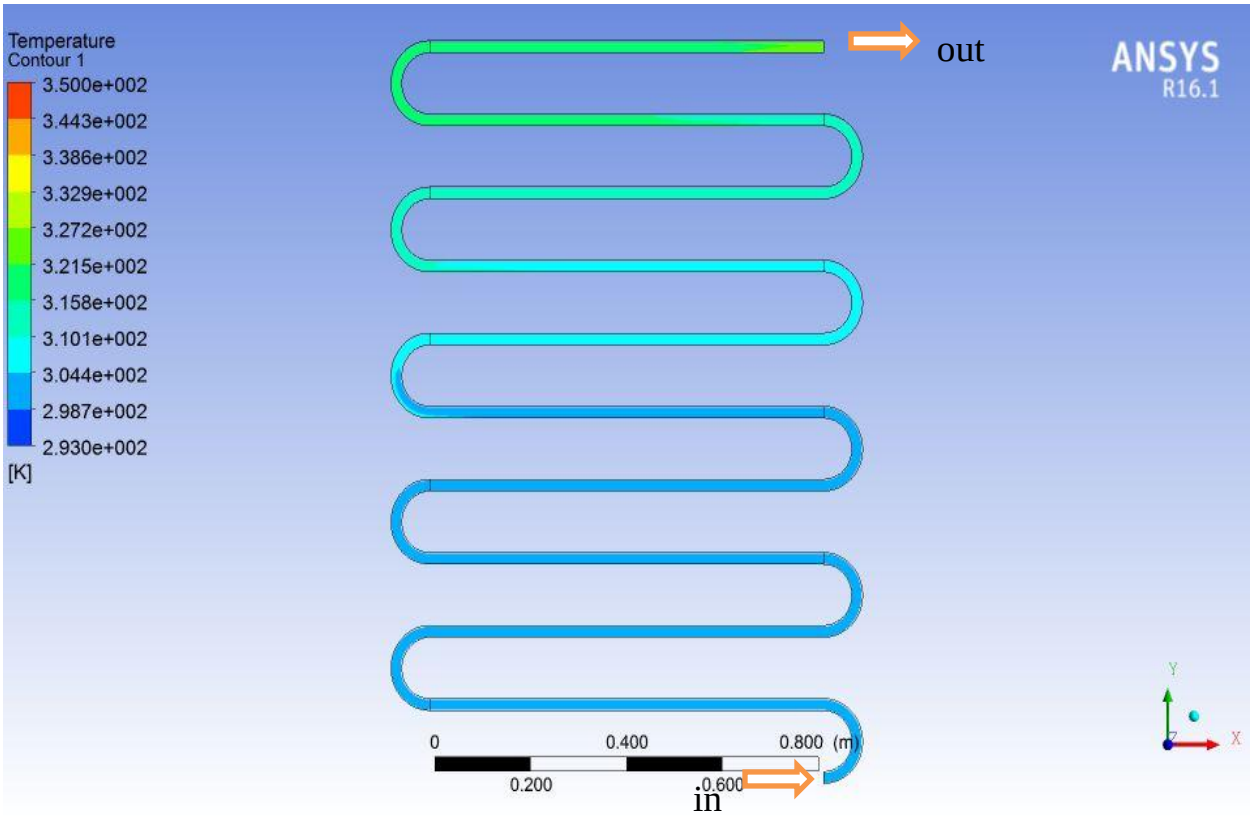

Figure (4.54) shows the temperature distribution of the heat exchanger tube of the flat plate solar collector with coating layer.

The K-epsilon turbulent model is used to present the fluid flow behaviour through the curved pipe, as shown in figures above. The sudden change in the direction of the flow will generate a kind of turbulence with the pressure distribution and the amount of losses caused by the viscosity, ready to use this equation to get an appropriate representation of the behaviour of the flows. The flow is turbulent flow at low Reynolds number and this method, with modification, can only define this problem[101][66].

CHAPTER FIVE

CONCLUSIONS, SUGGESTIONS, AND RECOMMENDATIONS FOR FUTURE WORK

Chapter Five
Conclusions, Suggestions, and Recommendations for Future Work

5.1 Conclusions

The study reaches the following conclusions:

1- This research is an experimental study and numerical analysis to develop and increase the efficiency of flat plate solar collector (FPSC) through the use of selective coatings to increase the thermal conductivity and absorptivity from the facing side of sunlight and on the other hand increase thermal insulation and reduce emissivity from the back of absorber plate.

2- Thermal conductivity test proved that the percentage of increase in thermal conductivity in the sample (G1) was (60%) that coated with graphite material only compared with the uncoated sample (G0), while the percentage of increase in the sample (G5) was (80%) coated by graphite material and percentage of copper powder (4%) compared to the thermal conductivity of the sample (G0) (bare aluminum plate).

3- Thermal conductivity test (for thermal insulation) assure that the decrease in thermal conductivity in the sample (S2) was (48%) coated by 1% of (Mullite and Titanium dioxide) compared with the uncoated sample (S0), while the percentage of decrease in the sample (S4) was (57%) coated with 5% of (Mullite and Titanium dioxide) compared to the thermal conductivity of the sample (S0) (bare aluminum plate).

4- The adhesion strength of the sample coated to increase the thermal conductivity (G1) is (19.06 MPa) containing only graphite, while the adhesion strength of the sample (G5) is (19.82 MPa), which contained graphite and percentages of copper powder.

5- The adhesion strength of the sample coated to increase the thermal insulation (S1) is (17.31 MPa), which contains polystyrene material only. While the adhesion strength of the sample (S4) is (17.73 MPa), which contains 5% coating materials (Mullite and Titanium dioxide).

6- From the measurement of the cross-sectional porosity of the conduction coating, the achieved porosity percentage is (4.62%), while the porosity ratio in the sectional view of the insulation samples coating is (68.28%).
7- The coating thickness average of the samples coated to increase the thermal conductivity is (0.405 mm), while the coating thickness average for samples coated to increase the thermal insulation is (0.715mm).
8- Simulation results ANSYS16.1 software showed the inlet and outlet temperature difference of the heat exchanger tube of the flat plate solar collector without coating was (23˚C) while after coating with ceramic materials the inlet and outlet temperature difference was (57˚C) assuming that the coating layer is homogeneous and does not contain large air gaps and perfect adhesion with substrate.

5.2 Suggestions and Recommendations for Future Work

1- Using high thermal conductivity nano-ceramic materials such as carbon nanotube, and graphene with a mixture of polymeric materials to give high thermal conductivity and a homogeneous coating.

2 - The use of ceramic materials with high thermal insulation such as Zirconia (ZrO2) and Lanthanum Zerconate (La2Zr2O7) with a suitable coating method for these materials such plasma sprays method and flame spray method.

3 - Studying the wear, corrosion resistance and oxidation of the absorber plate metals and the heat exchanger tube through the effect of the working fluid on them.

4- The use of polymeric materials such as (Polyacrylic acid (PAA), polyethylene-alt-maleic anhydride (PEMah), and polyvinyl phosphonic acid (PvPA)) with thin layers on the metal's surface and before the coating process with ceramic materials to increase the adhesion strength and the durability of the coating layer.
5- Applying the selective coatings to other types of solar collectors such as parabolic collector and evacuated tube collector to increase their efficiency.
6- Studying the increase in the development and improvement of the cross-section of the heat exchanger tube by adding internal fins or metal tapes and making a wrap for the heat exchanger tube.
8- Use ANSYS 16.1 software in numerical analysis to simulate the insulating ceramic coating from the bottom of the absorber plate.

REFERENCES

References

[1] T. Alam *et al.*, "Performance augmentation of the flat plate solar thermal collector: A review," *Energies*, vol. 14, no. 19, pp. 1–23, 2021, doi: 10.3390/en14196203.

[2] M. A. Alghoul, M. Y. Sulaiman, B. Z. Azmi, and M. abd Wahab, "Review of materials for solar thermal collectors," *Anti-Corrosion Methods Mater.*, vol. 52, no. 4, pp. 199–206, 2005, doi: 10.1108/00035590510603210.

[3] M. M. Peiravi and J. Alinejad, "Hybrid conduction, convection and radiation heat transfer simulation in a channel with rectangular cylinder," *J. Therm. Anal. Calorim.*, vol. 140, no. 6, pp. 2733–2747, 2020, doi: 10.1007/s10973-019-09010-0.

[4] M. Meikandan, P. G. Kumar, and D. Sakthivadivel, "Multi-wall carbon nanotubes coating on a copper substrate using airbrush spray coating," pp. 1–7, 2020, doi: 10.1177/0954408920959157.

[5] F. Filli, P. Gebray, and A. Kebedom, "Comparative study of antireflection coating materials for solar thermal collectors," *Momona Ethiopian Journal of Science*, vol. 10, no. 1. p. 1, 2018, doi: 10.4314/mejs.v10i1.1.

[6] V. Teixeira *et al.*, "Spectrally selective composite coatings of Cr-Cr2O3 and Mo-Al2O3 for solar energy applications," *Thin Solid Films*, vol. 392, no. 2, pp. 320–326, 2001, doi: 10.1016/S0040-6090(01)01051-3.

[7] Y. Zhang *et al.*, "Recent advanced thermal interfacial materials: A review of conducting mechanisms and parameters of carbon materials," *Carbon N. Y.*, vol. 142, pp. 445–460, 2019, doi: 10.1016/j.carbon.2018.10.077.

[8] J. Choi, W. Nakayama, N. Okimura, Y. Hirata, N. Ohtake, and H. Akasaka, "Deposition of High-Density Carbon Nanotube-Containing Nickel-Based Composite Films by Low-Pressure Cold Spray," *J. Therm. Spray Technol.*, vol. 29, no. 8, pp. 1902–1909, 2020, doi: 10.1007/s11666-020-01108-4.

[9] J. Li, J. Liang, and Y. Liu, "High-thermal conductive coating used on metal heat exchanger," *Chinese J. Chem. Eng.*, vol. 22, no. 5, pp. 596–601, 2014, doi: 10.1016/S1004-9541(14)60068-9.

[10] L. Gong, Y. Wang, X. Cheng, R. Zhang, and H. Zhang, "Porous mullite ceramics with low thermal conductivity prepared by foaming and starch consolidation," *J. Porous Mater.*, vol. 21, no. 1, pp. 15–21, 2014, doi: 10.1007/s10934-013-9741-z.

[11] A. Schüler, I. R. Videnovic, P. Oelhafen, and S. Brunold, "Titanium-containing amorphous hydrogenated silicon carbon films (a-Si:C:H/Ti) for durable solar absorber coatings," *Sol. Energy Mater. Sol. Cells*, vol. 69, no. 3, pp. 271–284, 2001, doi: 10.1016/S0927-0248(00)00396-2.

[12] X. Q. Cao, R. Vassen, and D. Stoever, "Ceramic materials for thermal barrier

coatings," *J. Eur. Ceram. Soc.*, vol. 24, no. 1, pp. 1–10, 2004, doi: 10.1016/S0955-2219(03)00129-8.

[13] Z. A. A. Majid, A. A. Razak, M. H. Ruslan, and K. Sopian, "Characteristics of solar thermal absorber materials for cross absorber design in solar air collector," *International Journal of Automotive and Mechanical Engineering*, vol. 11, no. 1. pp. 2582–2590, 2015, doi: 10.15282/ijame.11.2015.36.0217.

[14] M. N. E. A. Al Nasim and D. M. Chun, "Substrate-dependent deposition behavior of graphite particles dry-sprayed at room temperature using a nano-particle deposition system," *Surf. Coatings Technol.*, vol. 309, pp. 172–178, 2017, doi: 10.1016/j.surfcoat.2016.11.062.

[15] Y. Sohn, T. Han, and J. H. Han, "Effects of shape and alignment of reinforcing graphite phases on the thermal conductivity and the coefficient of thermal expansion of graphite/copper composites," *Carbon N. Y.*, vol. 149, pp. 152–164, 2019, doi: 10.1016/j.carbon.2019.04.055.

[16] L. Muñoz *et al.*, "Improving the interaction between aluminum surfaces and polymer coatings," *Surf. Coatings Technol.*, vol. 358, no. November 2018, pp. 435–442, 2019, doi: 10.1016/j.surfcoat.2018.11.051.

[17] K. Hanada, K. Hatsukano, K. Matsuzaki, K. Umeda, M. Ishiwata, and M. Tsukita, "Graphite coating of tool steel by pressure spraying," vol. 165, pp. 856–861, 2005, doi: 10.1016/j.jmatprotec.2005.02.171.

[18] S. K. Verma, K. Sharma, N. K. Gupta, P. Soni, and N. Upadhyay, "'Performance comparison of innovative spiral shaped solar collector design with conventional flat plate solar collector,'" *Energy*, vol. 194. 2020, doi: 10.1016/j.energy.2019.116853.

[19] E. M. Alawadhi, *Finite Element Simulations Using ANSYS*. 2015.

[20] X. Chen and Y. Liu, *Finite Element Modeling and Simulation with ANSYS Workbench*. .

[21] U. S. Ioannis Koutromanos Department of Civil and Environmental Engineering Virginia Polytechnic Intitute and State University Blacksburg, VA, *Fundamentals of Finite Element Analysis*. .

[22] S. Eiamsa-ard, K. Kiatkittipong, and W. Jedsadaratanachai, "Heat transfer enhancement of TiO2/water nanofluid in a heat exchanger tube equipped with overlapped dual twisted-tapes," *Engineering Science and Technology, an International Journal*, vol. 18, no. 3. pp. 336–350, 2015, doi: 10.1016/j.jestch.2015.01.008.

[23] M. Khoukhi, "The combined effect of heat and moisture transfer dependent thermal conductivity of polystyrene insulation material: Impact on building energy performance," *Energy Build.*, vol. 169, pp. 228–235, 2018, doi: 10.1016/j.enbuild.2018.03.055.

[24] M. S. Al-homoud, "Performance characteristics and practical applications of

common building thermal insulation materials," vol. 40, pp. 353–366, 2005, doi: 10.1016/j.buildenv.2004.05.013.

[25] K. Y. Wen, T. J. Marrow, and B. J. Marsden, "The microstructure of nuclear graphite binders," *Carbon N. Y.*, vol. 46, no. 1, pp. 62–71, 2008, doi: 10.1016/j.carbon.2007.10.025.

[26] N. Ooi, A. Rairkar, and J. B. Adams, "Density functional study of graphite bulk and surface properties," *Carbon N. Y.*, vol. 44, no. 2, pp. 231–242, 2006, doi: 10.1016/j.carbon.2005.07.036.

[27] Y. Quan, Q. Liu, S. Zhang, and S. Zhang, "Comparison of the morphology, chemical composition and microstructure of cryptocrystalline graphite and carbon black," *Appl. Surf. Sci.*, vol. 445, pp. 335–341, 2018, doi: 10.1016/j.apsusc.2018.03.182.

[28] M. Wissler, "Graphite and carbon powders for electrochemical applications," *J. Power Sources*, vol. 156, no. 2, pp. 142–150, 2006, doi: 10.1016/j.jpowsour.2006.02.064.

[29] C. Clasen and W. M. Kulicke, "Determination of viscoelastic and rheo-optical material functions of water-soluble cellulose derivatives," *Prog. Polym. Sci.*, vol. 26, no. 9, pp. 1839–1919, 2001, doi: 10.1016/S0079-6700(01)00024-7.

[30] M. S. Haahman, Md Saifursan *et al.*, "Recent developments of carboxymethyl cellulose," *Polymers (Basel).*, vol. 13, no. 8, 2021, doi: 10.3390/polym13081345.

[31] A. Benchabane and K. Bekkour, "Rheological properties of carboxymethyl cellulose (CMC) solutions," *Colloid Polym. Sci.*, vol. 286, no. 10, pp. 1173–1180, 2008, doi: 10.1007/s00396-008-1882-2.

[32] B. Z. A. and M. A. W. M.A. Alghoul, M.Y. Sulaiman, "Review of materials for solar thermal collectors." 2005.

[33] H. Che, X. Chu, P. Vo, and S. Yue, "Cold spray of mixed metal powders on carbon fibre reinforced polymers," *Surf. Coatings Technol.*, vol. 329, pp. 232–243, 2017, doi: 10.1016/j.surfcoat.2017.09.052.

[34] F. Nazeer *et al.*, "Effect of processing routes on mechanical and thermal properties of copper–graphene composites," *Mater. Sci. Technol. (United Kingdom)*, vol. 35, no. 14, pp. 1770–1774, 2019, doi: 10.1080/02670836.2019.1646962.

[35] E. Nieminen, M. Linke, M. Tobler, and B. Vander, "EU COST Action 628 : life cycle assessment (LCA) of textile products , eco-efficiency and definition of best available technology (BAT) of textile processing," vol. 15, pp. 1259–1270, 2007, doi: 10.1016/j.jclepro.2006.07.011.

[36] Y. Gao, P. romero, H. Zhang, M. Huang, and F. Lai, "Unsaturated polyester resin concrete: A review," *Constr. Build. Mater.*, vol. 228, p. 116709, 2019,

doi: 10.1016/j.conbuildmat.2019.116709.
[37] A. Chabros, B. Gawdzik, B. Podkościelna, M. Goliszek, and P. Paczkowski, "Composites of unsaturated polyester resins with microcrystalline cellulose and its derivatives," *Materials (Basel).*, vol. 13, no. 1, 2020, doi: 10.3390/ma13010062.
[38] *Ceramic and Glass Materials Structure, Properties and Processing*. 2008.
[39] H. Schneider, J. Schreuer, and B. Hildmann, "Structure and properties of mullite — A review," vol. 28, pp. 329–344, 2008, doi: 10.1016/j.jeurceramsoc.2007.03.017.
[40] J. Anggono, "Mullite Ceramics: Its Properties, Structure, and Synthesis," *J. Tek. Mesin*, vol. 7, no. 1, pp. 1–10, 2005.
[41] W. Zhou, W. Yan, N. Li, Y. Li, Y. Dai, and Z. Zhang, "Fabrication of mullite-corundum foamed ceramics for thermal insulation and effect of micro-pore-foaming agent on their properties," *J. Alloys Compd.*, vol. 785, no. 947, pp. 1030–1037, 2019, doi: 10.1016/j.jallcom.2019.01.212.
[42] J. Xiao, W. Chen, L. Wei, W. He, and H. Guo, "Mechanical properties and thermal conductivity of ytterbium-silicate-mullite composites," *Materials (Basel).*, vol. 13, no. 3, 2020, doi: 10.3390/ma13030671.
[43] K. Hashimoto, H. Irie, and A. Fujishima, "TiO 2 photocatalysis: A historical overview and future prospects," *Japanese J. Appl. Physics, Part 1 Regul. Pap. Short Notes Rev. Pap.*, vol. 44, no. 12, pp. 8269–8285, 2005, doi: 10.1143/JJAP.44.8269.
[44] A. J. Haider, Z. N. Jameel, and I. H. M. Al-Hussaini, "Review on: Titanium dioxide applications," *Energy Procedia*, vol. 157, pp. 17–29, 2019, doi: 10.1016/j.egypro.2018.11.159.
[45] A. K. Rana, S. B. Rana, A. Kumari, and V. Kiran, "Significance of Nanotechnology in Construction Engineering," *Int. J. Recent Trends Eng.*, vol. 1, no. 4, pp. 6–8, 2009, [Online]. Available: http://ijrte.academypublisher.com/vol01/no04/ijrte0104046048.pdf.
[46] S. Shamsudin *et al.*, "Hydrophobic rutile phase TiO2 nanostructure and its properties for self-cleaning application," *AIP Conf. Proc.*, vol. 1883, no. September, 2017, doi: 10.1063/1.5002048.
[47] S. Wahyuningsih, R. E. Cahyono, F. N. Aini, and A. H. Ramelan, "Preparation Titanium Dioxide Combined Hydrophobic Polymer with Photocatalytic Self-Cleaning Properties," *Bull. Chem. React. Eng. Catal.*, vol. 15, no. 3, pp. 874–884, 2020, doi: 10.9767/BCREC.15.3.9225.874-884.
[48] C. Buzea, I. I. Pacheco, K. Robbie, and C. Buzea, "Nanomaterials and nanoparticles : Sources and toxicity Nanomaterials and nanoparticles : Sources and toxicity," vol. 17, no. December 2007, 2016, doi: 10.1116/1.2815690.

[49] R. Riedel and I. Chen, *Ceramics science and technology: Materials and Properties*, vol. 2. 2008.
[50] M. Mohamad, B. Ul, R. Ahmed, A. Shaari, N. Ali, and R. Hussain, "Materials Science in Semiconductor Processing A density functional study of structural , electronic and optical properties of titanium dioxide : Characterization of rutile , anatase and brookite polymorphs," *Mater. Sci. Semicond. Process.*, vol. 31, pp. 405–414, 2015, doi: 10.1016/j.mssp.2014.12.027.
[51] J. Zheng, A. He, J. Li, J. Xu, and C. C. Han, "Studies on the controlled morphology and wettability of polystyrene surfaces by electrospinning or electrospraying," vol. 47, 2006, doi: 10.1016/j.polymer.2006.08.019.
[52] T. Roberts, B. T. Ho, T. K. Roberts, and S. Lucas, "An overview on biodegradation of polystyrene and modified polystyrene : the microbial approach An overview on biodegradation of polystyrene and modified polystyrene : the microbial approach," *Crit. Rev. Biotechnol.*, vol. 0, no. 0, pp. 308–320, 2017, doi: 10.1080/07388551.2017.1355293.
[53] M. Worzakowska, "Thermal and mechanical properties of polystyrene modified with esters derivatives of 3-phenylprop-2-en-1-ol Thermal and mechanical properties of polystyrene modified with esters derivatives of 3-phenylprop-2-en-1-ol," *J. Therm. Anal. Calorim.*, no. July, 2015, doi: 10.1007/s10973-015-4547-7.
[54] M. R. Ayer, "A Study of the Influence of Surface Roughness on Heat Transfer," pp. 1–23, 2010.
[55] S. Kuroda, J. Kawakita, M. Watanabe, and H. Katanoda, "Warm spraying - A novel coating process based on high-velocity impact of solid particles," *Science and Technology of Advanced Materials*, vol. 9, no. 3. 2008, doi: 10.1088/1468-6996/9/3/033002.
[56] B. Fotovvati, N. Namdari, and A. Dehghanghadikolaei, "On coating techniques for surface protection: A review," *J. Manuf. Mater. Process.*, vol. 3, no. 1, 2019, doi: 10.3390/jmmp3010028.
[57] A. Tabeei, A. Keikhosravani, A. Samimi, D. Mohebbi-Kalhori, and M. Zakeri, "Experimental evaluation of parameters affecting the coating performance of urea seeds in a prototype bottom external mixing spray two-fluid nozzle fluidized bed granulator," *Chem. Eng. Res. Des.*, vol. 172, pp. 242–253, 2021, doi: 10.1016/j.cherd.2021.06.014.
[58] J. Kawakita, H. Katanoda, M. Watanabe, K. Yokoyama, and S. Kuroda, "Warm Spraying: An improved spray process to deposit novel coatings," *Surf. Coatings Technol.*, vol. 202, no. 18, pp. 4369–4373, 2008, doi: 10.1016/j.surfcoat.2008.04.011.
[59] M. Winnicki, "Advanced Functional Metal-Ceramic and Ceramic Coatings,"

Coatings, vol. 11, no. i, p. 1044, 2021.
[60] S. Marx, A. Paul, A. Köhler, and G. Hüttl, "Cold Spraying : Innovative," vol. 15, no. June, pp. 177–183, 2006, doi: 10.1361/105996306X107977.
[61] H. Assadi, F. Ga, T. Stoltenhoff, and H. Kreye, "Bonding mechanism in cold gas spraying," vol. 51, pp. 4379–4394, 2003, doi: 10.1016/S1359-6454(03)00274-X.
[62] A. Srikanth, G. Mohammed Thalib Basha, and B. Venkateshwarlu, "A Brief Review on Cold Spray Coating Process," *Mater. Today Proc.*, vol. 22, pp. 1390–1397, 2019, doi: 10.1016/j.matpr.2020.01.482.
[63] C.-J. Li, W.-Y. Li, Y. Y. Wang, and H. Fukanuma, "Effect of Spray Angle on Deposition Characteristics in Cold Spraying," in *Thermal Spray 2003: Advancing the Science and Applying the Technology*, 2003, pp. 91–96.
[64] J. Peiró and S. Sherwin, "Finite Difference, Finite Element and Finite Volume Methods for Partial Differential Equations," *Handb. Mater. Model.*, vol. M, pp. 2415–2446, 2005, doi: 10.1007/978-1-4020-3286-8_127.
[65] F. G. Becker *et al.*, *THE FINITE ELEMENT METHOD AND APPLICATIONS IN ENGINEERING USING ANSYS®*, vol. 7, no. 1. 2015.
[66] M. M. Rahman and T. Siikonen, "A NEW TIME SCALE BASED LOW-Re - ¯ MODEL," no. May 2003, 2016.
[67] "CHAPTER FOUR Solar Thermal Energy Collectors 4.1," no. 4, pp. 1–30, 2019.
[68] S. A. S. · M. S. Valipour1 and Received:, "Investigation on the effect of different coated absorber plates on the thermal efficiency of the flat‐plate solar collector." .
[69] J. Long, C. Jiang, J. Zhu, Q. Song, and J. Hu, "Controlled TiO2 coating on hollow glass microspheres and their reflective thermal insulation properties," *Particuology*, pp. 3–9, 2019, doi: 10.1016/j.partic.2019.03.002.
[70] R. Liu *et al.*, "Ultralight, thermal insulating, and high-temperature-resistant mullite-based nanofibrous aerogels," *Chem. Eng. J.*, vol. 360, no. December 2018, pp. 464–472, 2019, doi: 10.1016/j.cej.2018.12.018.
[71] R. Senthil, K. Kishore Kumar, K. Rohan Rajendra, and A. Juneja, "Enhancement of absorptance of absorber surfaces of a flat plate solar collector using black coating with graphene," *Energy Sources, Part A: Recovery, Utilization and Environmental Effects*, vol. 43, no. 20. pp. 2595–2608, 2021, doi: 10.1080/15567036.2020.1826016.
[72] J. Van Den Brand, S. Van Gils, P. C. J. Beentjes, H. Terryn, V. Sivel, and J. H. W. De Wit, "Improving the adhesion between epoxy coatings and aluminium substrates," vol. 51, pp. 339–350, 2004, doi: 10.1016/j.porgcoat.2004.08.005.
[73] P. Mayer, A. Dmitruk, and J. W. Kaczmar, "Adhesion of functional layers

based on epoxy and polyurethane resins for aluminum substrate," *Int. J. Adhes. Adhes.*, vol. 109, no. May, p. 102899, 2021, doi: 10.1016/j.ijadhadh.2021.102899.

[74] X. Yang, Y. Wang, and T. Xiong, "Numerical and experimental study on a solar water heating system in lhasa," *Energies*, vol. 10, no. 7, pp. 1–12, 2017, doi: 10.3390/en10070963.

[75] A. A. Hawwash, A. K. Abdel Rahman, S. A. Nada, and S. Ookawara, "Numerical Investigation and Experimental Verification of Performance Enhancement of Flat Plate Solar Collector Using Nanofluids," *Appl. Therm. Eng.*, vol. 130, pp. 363–374, 2018, doi: 10.1016/j.applthermaleng.2017.11.027.

[76] M. E. Nakhchi, "Numerical investigation of turbulent CuO–water nanofluid inside heat exchanger enhanced with double V‐cut twisted tapes M." 2020.

[77] NORSOK STANDARD, "Surface preparation and protective coating," *M-Cr-501*, vol. Rev. 1, no. December, pp. 20–31, 1994.

[78] D. Tang *et al.*, "Preparation of alumina-coated graphite for thermally conductive and electrically insulating epoxy composites," *RSC Adv.*, vol. 5, no. 68, pp. 55170–55178, 2015, doi: 10.1039/c5ra08010j.

[79] U. N. C. Asheville, Y. Chapter, and D. Moments, "N Λ = 2 D Sin Θ," no. February, pp. 1–18, 2018.

[80] M. Dowsett, R. Wiesinger, and M. Adriaens, "X-ray diffraction," *Spectrosc. Diffr. Tomogr. Art Herit. Sci.*, pp. 161–207, 2021, doi: 10.1016/B978-0-12-818860-6.00011-8.

[81] S. Methods, "StandardTest Methods for Determining Average Grain Size 1," pp. 1–27, 2021, doi: 10.1520/E0112-12.1.4.

[82] Astm D729, "Standard Test Methods for Density and Specific Gravity (Relative Density) of Plastics by Displacement," *Am. Soc. Test. Mater.*, p. 6, 2008, doi: 10.1520/D0792-20.2.

[83] "Standared Test Mthod For Density of Liquid Coatings, Ink and Related Products." 2009.

[84] Ekele Ogwu Augustine, "Design Fabrication and Testing of a Viscometer for Testing Viscosity of Liquids," *Int. J. Eng. Res.*, vol. V8, no. 05, 2019, doi: 10.17577/ijertv8is050388.

[85] M. D. Abràmoff, P. J. Magalhães, and S. J. Ram, "Image processing with imageJ," *Biophotonics Int.*, vol. 11, no. 7, pp. 36–41, 2004, doi: 10.1201/9781420005615.ax4.

[86] J. Schindelin, C. T. Rueden, M. C. Hiner, and K. W. Eliceiri, "The ImageJ ecosystem: An open platform for biomedical image analysis," *Mol. Reprod. Dev.*, vol. 82, no. 7–8, pp. 518–529, 2015, doi: 10.1002/mrd.22489.

[87] A. D7091, "Standard Practice for Nondestructive Measurement of Dry Film

Thickness of Nonmagnetic Coatings Applied to Ferrous Metals and Nonmagnetic, Nonconductive Coatings Applied to Non-Ferrous Metals, ASTM International," pp. 1–7, 2013, doi: 10.1520/D7091-13.minimum.

[88] Z. Sun, H. Liang, J. Liu, and G. Shi, "Estimation of photosynthetically active radiation using solar radiation in the UV–visible spectral band," *Sol. Energy*, vol. 153, pp. 611–622, 2017, doi: 10.1016/j.solener.2017.06.007.

[89] "INSTRUCTION MANUAL Operation Guide UV-1800 SHIMADZU SPECTROPHOTOMETER 206-97042A," 2008.

[90] C. Whitewares, R. Products, and W. Air, "Standard Test Method for Thermal Conductivity of Whiteware Ceramics 1," *Development*, vol. 88, no. Reapproved, pp. 1–4, 1999.

[91] V. M. Barragán, J. C. Maroto, E. Pastuschuk, and S. Muñoz, "Testing a simple Lee's disc method for estimating throuh-plane thermal conductivity of polymeric ion-exchange membranes," *Int. J. Heat Mass Transf.*, vol. 184, no. xxxx, pp. 1–11, 2022, doi: 10.1016/j.ijheatmasstransfer.2021.122295.

[92] J. Fletcher and D. Barnes, "Sspc 2015," *Pull Off Adhes. Test. Coatings - Improv. Your Tech.*, vol. IIIA, no. SSPC 2015, pp. 1–12, 2015.

[93] إ. ف. الشعراني and غ. ج. الوزير, "No Title ،"التعويضات المتحركة الكاملة و التعويضات الفكية الوجهية *منشورات جامعة دمشق*, vol. 1999, no. December, pp. 1–6, 2006.

[94] A. B. D. Nandiyanto, R. Oktiani, and R. Ragadhita, "How to read and interpret ftir spectroscope of organic material," *Indones. J. Sci. Technol.*, vol. 4, no. 1, pp. 97–118, 2019, doi: 10.17509/ijost.v4i1.15806.

[95] M. G. Donoso, A. Méndez-Vilas, J. M. Bruque, and M. L. González-Martin, "On the relationship between common amplitude surface roughness parameters and surface area: Implications for the study of cell-material interactions," *Int. Biodeterior. Biodegrad.*, vol. 59, no. 3 SPEC. ISS., pp. 245–251, 2007, doi: 10.1016/j.ibiod.2006.09.011.

[96] S. C. Stacy, X. Zhang, M. Pantoya, and B. Weeks, "The effects of density on thermal conductivity and absorption coefficient for consolidated aluminum nanoparticles," *Int. J. Heat Mass Transf.*, vol. 73, pp. 595–599, 2014, doi: 10.1016/j.ijheatmasstransfer.2014.02.050.

[97] N. Phumkokrux and K. Maneeintr, "Density and viscosity measurement and correlations of aqueous solution of 2-(diethylamino)ethanol for CO2 capture," *Chem. Eng. Trans.*, vol. 72, no. July 2018, pp. 331–336, 2019, doi: 10.3303/CET1972056.

[98] R. Reddy Pinninti, "Temperature and Stress Analysis of Ceramic Coated SiC-Al Alloy Piston Used in a Diesel Engine Using FEA," *Int. J. Innov. Res. Sci. Eng. Technol. (An ISO Certif. Organ.*, vol. 3297, no. 8, 2007, doi: 10.15680/IJIRSET.2015.0408083.

[99] M. Volterrani, A. Minelli, M. Gaetani, N. Grossi, S. Magni, and L. Caturegli,

"Reflectance, absorbance and transmittance spectra of bermudagrass and manilagrass turfgrass canopies," *PLoS One*, vol. 12, no. 11, pp. 1–13, 2017, doi: 10.1371/journal.pone.0188080.

[100] I. Reda and A. Andreas, "Solar position algorithm for solar radiation applications," *Sol. Energy*, vol. 76, no. 5, pp. 577–589, 2004, doi: 10.1016/j.solener.2003.12.003.

[101] Y. Bazilevs, M. Hsu, J. Kiendl, R. Wüchner, and K. Bletzinger, "3D Simulation of Wind Turbine Rotors at Full Scale. Part II: Fluid – Structure Interaction Modeling with Composite Blades," *Int. J. Numer. Methods Fluids*, vol. 65, no. October 2010, pp. 236–253, 2011, doi: 10.1002/fld.

الخلاصة

يعتبر توفير الطاقة والحد من التلوث من اهم أهداف العالم المتطور وذلك من خلال استخدام مصادر الطاقة البديلة للوقود التقليدي (الأحفوري) ، والتي تعتبر سببًا للتلوث عند استهلاكها. تعد الطاقة الشمسية ، باعتبارها مصدرًا متجددًا ونظيفًا للطاقة ، أحد أهم الحلول والعلاجات للتلوث البيئي وزيادة تكاليف الإنتاج.
أحد الأجهزة التي تستغل الطاقة الشمسية هي مجمعات الألواح الشمسية المسطحة (FPSCs). يتكون من الغطاء شفاف واللوحة ماصة وأنبوب المبادل حراري والهيكل الخارجي. اللوح الماص مصنوع من صفيحة من معدن الألمنيوم بسمك (٠.٥ ملم) ، وكذلك أنبوب المبادل الحراري مصنوع من معدن الألمنيوم بسمك (١.٣ ملم).استخدام طريقة (الرش الهوائي) في طلاء (FPSC) والتي تعتبر من أبسط وأرخص طرق رش.
في هذا البحث تم استخدام الكرافيت مع نسب من مسحوق النحاس كطلاء لزيادة التوصيل الحراري, وتبين من اختبار التوصيلية الحرارية انه عند استخدام الكرافيت كمادة طلاء فقط كما في العينة (G1) زادت الموصلية الحرارية بحوالي ٦٠% ، وعند إضافة نسبة من مسحوق النحاس حوالي (٤%) مع الكرافيت كما في العينة (G5) زادت إلى حوالي (٨٠%). في حالة الطلاءات العازلة تم استخدام المولايت وثاني أوكسيد التيتانيوم ، حيث باستخدام نسبة مولايت حوالي (٠.٧٥%) مع ثاني أوكسيد التيتانيوم (٠.٢٥%) كما في العينة (S2) زاد العزل بنسبة (٤٨%) ، بينما بزيادة نسبة المولايت الى (٣.٧٥ %) وثاني أوكسيد التيتانيوم (١.٢٥%) كما في العينة (S4) ارتفعت نسبة العزل إلى (٥٧%).
مقاومة الالتصاقية للعينة المطلية لزيادة الموصلية الحرارية (G1) تبلغ (١٩.٠٦ميجا باسكال) التي تحتوي على الكرافيت فقط ، بينما كانت قوة الالتصاقية للعينةG5 تبلغ (19.82ميجا باسكال) والتي احتوت على الكرافيت ونسبًا من مسحوق النحاس.في حين ان مقاومة الالتصاقية للعينة المطلية لزيادة العزل الحراري (S1) تبلغ (١٧.٣١ ميجا باسكال) والتي تحتوي على مادة البوليستايرين فقط. بينما كانت قوة الالتصاق لعينة (S4) تبلغ (17.73 ميجا باسكال) والتي تحتوي على (٥%) مواد طلاء (مولايت وثاني أكسيد التيتانيوم).
بلغت نسبة المسامية المتحققة من قياس المسامية المقطعية لطلاء التوصيل (٤.٦٢٪) بينما بلغت نسبة المسامية في المقطع العرضي لطلاء عينات العزل (٦٨.٢٨٪) .
متوسط سمك الطلاء لعينات التوصيل (٤٠٥ مايكرومتر) في حين ان متوسط سمك عينات العزل (٧١٥ مايكرومتر) .
يتحقق التحليل العددي من التحسينات في التوصيل الحراري التي تزيد في كفاءة المجمع الشمسي باستخدام برنامج (ANSYS 16.1) لمحاكاة الهندسة ثلاثية الأبعاد لتدفق السوائل عبر أنابيب المبادل الحراري.
تم بناء نموذج رياضي بواسطة برنامج (ANSYS-FLUENT 16.1) باستخدام المقطع العرضي النصف دائري بدلا من المقطع الدائري لانبوب المبادل الحراري ووضعه بالابعاد الحقيقية لمحاكاة انتقال الحرارة من الصفيحة الماصة الى انبوب المبادل الحراري عن طريق الاشعاع الشمسي وذلك بتثبيت خطوط الطول والعرض لموقع مدينة بابل بعدد ساعات (١٣) ساعة باليوم.
نتائج محاكاة برنامجANSYS16.1 اظهرت الفرق في درجات حرارة المدخل والمخرج لانبوب المبادل الحراري للمجمع الشمسي ذوالصفيحة المسطحة بدون طلاء كانت (٢٣ درجة مئوية) بينما بعد الطلاء بمواد سيراميكية كان الفرق بدرجات حرارة المدخل والمخرج (٥٧ درجة مئوية).

وزارة التعليم العالي والبحث العلمي
جامعة بابل
كلية هندسة المواد
قسم السيراميك و مواد البناء

تحسين الخواص الحرارية للمجمع الشمسي باستخدام مواد طلاء سيراميكية

رسالة
مقدمة لقسم السيراميك ومواد البناء في كلية هندسة المواد / جامعة بابل في استيفاء جزئي لمتطلبات درجة الماجستير في هندسة المواد \سيراميك.

من قبل الباحث
احمد زكي هاشم حمزة
بكلوريوس هندسة مواد ٢٠٠٢.

باشراف
أ. د. الهام عبد المجيد
أ. د. حيدر كريدي راشد

١٤٤٤هـ ٢٠٢٢م

APPENDICES

Date: May 18, 2022
Paper ID: IICESAT_378

LETTER OF ACCEPTANCE

Dear Authors,

On behalf of the IICESAT | ICMAICT -22 Scientific Committee, and based on the reviewers' evaluation after double blind peer review Process and Guest Editors' Preliminary approval we are pleased to inform you that your paper entitled:

Experimental investigation of ceramic coating materials to enhance the performance of solar collectors by increasing thermal conductivity

Written By

Elham A.A. majeed, Hayder K. Rashid, Ahmed Z. Hasheem

Has been accepted and will be processed for possible publication in AIP Conference Proceedings (ISSN: 0094-243X, 1551-7616). It is our pleasure to invite you to attend 4th International Scientific Conference of Engineering Sciences and Advances Technologies (IICESAT) will be held By Iraq Academic Syndicate on 3-4 June, 2022, to present your paper. We congratulate you for your achievement, the technical details about the publication will be informed later. Remember that, the paper should follow accurately our reviewer comments, and the technical notes which has been sent earlier. The publication of the accepted paper will be provided after passing the Internal Check of AIP Editors, and the paper should not contain plagiarism till that date more than 15%, and the content also follow our conference Guidelines and template. Publication time it depends on Publisher process and we will provide to your after we held our conference.

We Will encourage more quality submissions from you and your colleagues in future

Regards

Shubham Sharma

Prof. Dr. Shubham Sh. Sharma
IICESAT | ICMAICT Conference Guest Editor

CAUTION: This Acceptance Letter Made by IICESAT / ICMAICT Conference Guest Editors, All Approval and other Inquiries Should be addressed to Conference Editorial Board and Patrons Committee, as all Accepted Papers will Process for Possible Publication in AIP Conference Proceedings, and Final Decision upon Publish of your/s Paper will be Made by AIP Publication Editors Only after Review the Paper Contents and Writing Quality.

Date: May 24 2022
Paper ID: IICESAT_438

LETTER OF ACCEPTANCE

Dear Authors,

On behalf of the IICESAT | ICMAICT -22 Scientific Committee, and based on the reviewers' evaluation after double blind peer review Process and Guest Editors' Preliminary approval we are pleased to inform you that your paper entitled:

Review of using ceramic coatings to increase the performance of solar collectors with air brush spray method on aluminium substrate

Written By

Ahmed Z. Hasheem, Elham A. majeed, and Hayder K. Rashid

Has been accepted and will be processed for possible publication in AIP Conference Proceedings (ISSN: 0094-243X, 1551-7616). It is our pleasure to invite you to attend 4th International Scientific Conference of Engineering Sciences and Advances Technologies (IICESAT) will be held By Iraq Academic Syndicate on 7–8 May, 2022, to present your paper. We congratulate you for your achievement, the technical details about the publication will be informed later. Remember that, the paper should follow accurately our reviewer comments, and the technical notes which has been sent earlier. The publication of the accepted paper will be provided after passing the Internal Check of AIP Editors, and the paper should not contain plagiarism till that date more than 15%, and the content also follow our conference Guidelines and template. Publication time it depends on Publisher process and we will provide to your after we held our conference.

Regards

Shubham Sharma

Prof. Dr. Shubham Sh. Sharma
IICESAT || ICMAICT Conference Guest Editor

CAUTION: This Acceptance Letter Made by IICESAT / ICMAICT Conference Guest Editors, All Approval and other Inquiries Should be addressed to Conference Editorial Board and Patrons Committee, as all Accepted Papers will Process for Possible Publication in AIP Conference Proceedings, and Final Decision upon Publish of your/s Paper will be Made by AIP Publication Editors Only after Review the Paper Contents and Writing Quality.

The 3rd International Conference on Electromechanical Engineering & its Applications

ICEMEA-2022

ACCEPTANCE LETTER

Dear, [Elham A.A. majeed, Hayder K. Rashid, and Ahmed Z. Hasheem]

We are pleased to inform you that your manuscript entitled (Experimental investigation by coatings ceramic materials for thermal insulation to increase the performance of flat plate solar collector) has been accepted for oral presentation at the 3rd International Conference on Electromechanical Engineering and its Applications (ICEMEA-2022) to be held on July 19th – 20th, 2022 at the University of Technology, Baghdad, Iraq. Decision was made upon double-blind review process. The exact date, time and place of your presentation will be posted at the conference website.

On behalf of the organizing committee of ICEMEA 2022, we are looking forward to seeing you at the University of Technology, Baghdad, Iraq. If you have any further questions, please do not hesitate to contact us.

Sincerely,

The Chairman of ICEMEA-2022
Professor Dr. Hosham Salim

+964-7736-833726
eme.icemea@uotechnology.edu.iq
https://eme.uotechnology.edu.iq/icemea

جمهورية العراق

وزارة التخطيط
الجهاز المركزي للتقييس والسيطرة النوعية

العدد : ٢٢٨٢
التاريخ م : ٢٠٢٢/١٠/٥
هـ : / /

رئاسة الجهاز
مديرية براءات الاختراع والنماذج الصناعية
القسم الاداري/ شعبة التدقيق

الى / جامعة بابل / كلية هندسة المواد / قسم السيراميك ومواد البناء

م/ تـــأييـد

يهدي الجهاز أطيب تحياته .....

نؤيـــد استلام طلب براءة الاختـــراع المرقم (٥٦٨/ ٢٠٢٢) في ٢٠٢٢/٨/٢٩

والموســـوم : (**زيادة أداء المجمع الشمسي بأستخدام مواد طلاء سيراميكية جديدة لتعزيز التوصيل الحراري والعزل)**

والمودع من قبل السادة المدرجة اسمائهم في ادناه :

١- ا٠د٠ ألهام عبد المجيد
جامعة بابل / كلية هندسة المواد / قسم السيراميك ومواد البناء

٢- ا٠د٠ حيدر كريدي راشد
جامعة بابل / كلية هندسة المواد / قسم السيراميك ومواد البناء

٣- ر٠مهندسين أحمد زكي هاشم
وزارة الصحة / دائرة صحة كربلاء المقدسة

وحالياً قيد اجراءات الفحص والتقييم، وبناء على طلبهم زودناهم بهذا التأييد

مـــع التقـــدير

نعيم أحمد آسماعيل
مدير القسم الاداري
ع/ مسجل براءات الاختراع والنماذج الصناعية
٢٠٢٢/١٠/٥

صورة عنه الى /
- ر٠مهندسين أحمد زكي هاشم / وزارة الصحة / دائرة صحة كربلاء المقدسة ٠٠٠مع التقدير
- مديرية براءات الاختراع والنماذج الصناعية/ القسم الفني / للحفظ في اضبارة الطلب اعلاه

العراق - بغداد - الجادرية - ص . ب (١٣٠٣٢) - البريد الالكتروني : www.cosqc.gov.iq
هاتف ٨٤ / ٨٣ / ٨٢ / ٨١ / ٧٧٨٥١٨٠ تليفاكس ٧٧٦١٩٨١ cosqc@cosqc.gov.iq